

**Key Points:**

- The Tunisian Tell hosts High-Pressure Low-Temperature (HP/LT) domes underlying late Miocene extensional detachments, driven by slab delamination
- Metamorphic and rutile U-Pb data shows that rocks in Northern Tunisia reached HP/LT conditions in the early Eocene and early Miocene
- Halokinetic structures in Northern Tunisia are rooted in the Mejerda detachment and related to late Miocene extension

**Supporting Information:**

Supporting Information may be found in the online version of this article.

**Correspondence to:**

G. Booth Rea,  
[gbooth@go.ugr.es](mailto:gbooth@go.ugr.es)

**Citation:**

Booth Rea, G., Gaidi, S., Melki, F., Marzougui, W., Ruano, P., Nieto, F., et al. (2023). Metamorphic domes in Northern Tunisia: Exhuming the roots of nappe belts by widespread post-subduction delamination in the Western Mediterranean. *Tectonics*, 42, e2022TC007467. <https://doi.org/10.1029/2022TC007467>

Received 22 JUN 2022

Accepted 12 MAY 2023

**Author Contributions:**

**Conceptualization:** G. Booth Rea, S. Gaidi, F. Melki, J. M. Azañón


**Data curation:** G. Booth Rea, S. Gaidi, P. Ruano

**Formal analysis:** S. Gaidi, F. Nieto, J. M. Azañón, C. J. Garrido

**Funding acquisition:** G. Booth Rea, W. Marzougui, P. Ruano, J. M. Azañón, J. P. Galvé

© 2023. The Authors. Tectonics published by Wiley Periodicals LLC on behalf of American Geophysical Union. This is an open access article under the terms of the [Creative Commons Attribution License](https://creativecommons.org/licenses/by/4.0/), which permits use, distribution and reproduction in any medium, provided the original work is properly cited.

## Metamorphic Domes in Northern Tunisia: Exhuming the Roots of Nappe Belts by Widespread Post-Subduction Delamination in the Western Mediterranean

G. Booth Rea<sup>1,2</sup> , S. Gaidi<sup>1,3</sup> , F. Melki<sup>3</sup> , W. Marzougui<sup>4</sup>, P. Ruano<sup>1</sup>, F. Nieto<sup>5</sup> , J. M. Azañón<sup>1,2</sup>, J. P. Galvé<sup>1</sup>, K. Hidas<sup>6</sup>, and C. J. Garrido<sup>2</sup>

<sup>1</sup>Department of Geodynamics, University of Granada, Granada, Spain, <sup>2</sup>Instituto Andaluz de Ciencias de la Tierra, CSIC-UGR, Granada, Spain, <sup>3</sup>Faculté des Sciences de Tunis, Université de Tunis El Manar, Tunis, Tunisia, <sup>4</sup>Office National de Mines, Tunis, Tunisia, <sup>5</sup>Department of Mineralogy and Petrology, University of Granada, Granada, Spain, <sup>6</sup>Departamento de Geología y Subsuelo, Centro Nacional Instituto Geológico y Minero de España del CSIC, Project Office of Granada, Granada, Spain

**Abstract** Cenozoic extension in the Western Mediterranean has been related to the dynamics of back-arc domains. Although, in most of its orogenic belts extension propagated into the fore-arc nappe domains. Here we revisit the structure, metamorphism and radiometric ages of the Tunisian Tell, where HP/LT rocks (350°C at 0.8 GPa), were exhumed by the sequential activity of extensional detachments after heating and decompression (410°C–440°C at 0.6–0.3 GPa) in a plate convergent setting. Normal faults thinning the Tunisian Tell detached at two different crustal levels. The shallower one cuts down into the Atlas Mesozoic sequence, involving Tellian Triassic evaporites in the hanging-wall forming halokinetic structures in the Mejerda basin late Miocene. The deeper-detachment bounds metamorphic domes formed by marbles and metapsammites from the Atlas domain. Illite crystallinity on Triassic rocks shows epizonal to anchizonal values, at deep and intermediate structural depths of the Tell-Atlas nappe belt, respectively. New U-Pb 49.78 ± 1.28 Ma rutile ages from Tellian metabasites, together with existing phlogopite 23–17 Ma K-Ar ages in Atlas marbles from the footwall of the deepest detachment, indicate a polymetamorphic evolution. The Tell rocks underthrust the Kabylie flysch in the early Eocene. Further, early Miocene shortening thrust the metabasites over lower-grade sediments, producing HP/LT metamorphism and ductile stretching at the base of the Atlas belt. The exhumation of midcrustal roots of Western Mediterranean nappe belts after tectonic shortening is a common feature related to tearing at the edges of the subduction systems and inboard delamination of their subcontinental lithospheric mantle.

**Plain Language Summary** Mountain belts are formed by shortened sedimentary rocks. The Tell cordillera in Northern Tunisia is interpreted as a classic mountain belt developed through protracted shortening from the late Cretaceous until Present, formed by folded and overthrust rocks, and intruded by salt bodies. However, we show here that conversely, some of the supposed salt bodies are formed by metamorphic rocks that were originally buried at depths of approximately 26 km. Moreover, the remaining salt structures in the Tunisian Tell formed in relation to the late-stage thinning and collapse of the mountain belt, as they intrude through extensional faults into late Miocene sediments. We characterize the temperature and pressure conditions reached by the metamorphic rocks and obtain a 49 Ma age of an early metamorphic event by radiometric dating of rutile. Metamorphic rocks were also exhumed in other Western Mediterranean mountain belts like the Betics, Rif, Algerian Tell after the main shortening stage. We relate this process to delamination, a deep mantle tectonic mechanism, which strips the nappe belt crustal domain from its underlying mantle root.

### 1. Introduction

Certain orogenic nappe belt domains surrounding the Western Mediterranean, in the Betics, Mallorca, Tell, Rif, and Apennines occur over relatively thin continental crust and lithosphere, below 30 and 70 km, respectively (e.g., Agostinetti et al., 2008; de Lis Mancilla and Díaz, 2015; El-Sharkawy et al., 2020; Miller & Agostinetti, 2012; Palomeras et al., 2014; Piana Agostinetti et al., 2002; Research Group for Lithospheric Structure in Tunisia, 1992). In some cases contrasting with nearby domains where the crust reaches up to 50 km thickness, forming part of thick 150–200 km lithosphere (e.g., de Lis Mancilla et al., 2015; El-Sharkawy et al., 2020; Li et al., 2021). This feature is explained by two contrasting hypothesis, proposing either that the nappe belt domains preserve the

**Investigation:** G. Booth Rea, S. Gaidi, F. Melki, W. Marzougui, P. Ruano, F. Nieto, J. M. Azañón, J. P. Galvé, K. Hidas, C. J. Garrido  
**Methodology:** G. Booth Rea, S. Gaidi, W. Marzougui, P. Ruano, F. Nieto, K. Hidas, C. J. Garrido  
**Project Administration:** P. Ruano, J. P. Galvé  
**Resources:** G. Booth Rea  
**Software:** S. Gaidi, P. Ruano  
**Supervision:** G. Booth Rea, F. Melki, J. M. Azañón  
**Validation:** C. J. Garrido  
**Visualization:** G. Booth Rea, S. Gaidi, P. Ruano, J. P. Galvé  
**Writing – original draft:** G. Booth Rea, S. Gaidi, C. J. Garrido  
**Writing – review & editing:** F. Melki, W. Marzougui, P. Ruano, F. Nieto, J. M. Azañón, J. P. Galvé, K. Hidas, C. J. Garrido

original thrust-stack structure with only minor, later extension, and with existing extensional structures being mostly inherited from Mesozoic rifting (e.g., Crespo-Blanc & Frizon de Lamotte, 2006; Frizon de Lamotte et al., 1991; Gelabert et al., 1992; Gimeno-Vives et al., 2019; Khomsi et al., 2016; Pedrera et al., 2020; Platt, Allerton, et al., 2003; Sabat et al., 2011). Or, other work suggests that these nappe belts were extended, with their lithosphere rejuvenated in relation to several deep-mantle tectonic mechanisms, including slab roll back, delamination, detachment and by lithospheric tearing along Subduction Transfer Edge Propagator faults (STEP) (Govers & Wortel, 2005; Lonergan & White, 1997; Wortel & Spakman, 2000). These tectonic mechanisms drove lithosphere thinning of the Western Mediterranean nappe belt domains during and after tectonic shortening, in the Miocene, or younger in the Apennines-Tyrrhenian (Booth-Rea et al., 2012, 2018; Caby et al., 2001; Carmignani & Kligfield, 1990; Carminati et al., 1998; Cohen et al., 1980; Crespo-Blanc & Campos, 2001; de Ruig, 1995; Faccenna et al., 2004; L. G. Gómez de la Peña, Ranero, et al., 2020; Jolivet et al., 1998; Jolivet et al., 2009; Lonergan & White, 1997; Molli et al., 2018; Moragues et al., 2021; Rodríguez-Fernández, Azor, & Azañón, 2011; Roure et al., 2012; Saadallah & Caby, 1996) (Figure 1).

These contrasting views of the Western Mediterranean nappe domains imply differences in crustal and lithospheric structure, age of extension, hydrocarbon prospectivity, amount and age of shortening, role of tectonic inversion, age and position of orogenic boundaries and tectonic mechanisms driving deformation in the region, among other features. For example, stratigraphic omissions observed in the lithological series of these nappe belt domains are related to erosion or salt welds according to the first hypothesis (e.g., Daudet et al., 2020; Khelil et al., 2021) or to extensional tectonic omissions by the latter (Booth-Rea et al., 2012, 2018; Brogi, 2008; Crespo-Blanc & Campos, 2001; García-Dueñas et al., 1992; Moragues et al., 2021; Rodríguez-Fernández, Azor, & Azañón, 2011). Extensional faults cut down into the previous structure toward the sense of hanging-wall displacement producing lithological omissions in the stratigraphic sequence, including metamorphic gaps, with less metamorphic over higher-grade rocks, along crustal-scale extensional shear zones (e.g., Caby et al., 2001; Lonergan & Platt, 1995; Martínez-Martínez et al., 2002; Platt, 1986; Wernicke, 1981; Wernicke & Burchfiel, 1982). Metamorphic gaps across shear zones are also described in relation to out of sequence thrusts affecting previously folded sequences (Morley, 1988; Sani et al., 2004). Syn-orogenic extensional shear zones frequently unroof metamorphic domes, coeval to metamorphism and shortening structures in the footwall (e.g., Booth-Rea et al., 2015; Jolivet et al., 2010; Lamont et al., 2020; Searle & Lamont, 2020). This process contributes to the extrusion of HP units in subduction settings (e.g., Ring et al., 2007, 2010; Ryan et al., 2021). Syn-orogenic extension in the Mediterranean orogens is followed by later post-orogenic extension, leading to the development of back arc basins, generally associated with magmatism (e.g., Jolivet et al., 2003; Platt, Whitehouse, et al., 2003; Rossetti et al., 1999; Vignaroli et al., 2009). The geometry of extensional systems in extended nappe belts is further determined by the rheological structure developed during the previous thrust stacking (e.g., Booth-Rea et al., 2004; Brogi, 2008; Gartrell, 1997). Extension with pre-rift evaporites can further promote halokinetic features like diapirs, salt walls and minibasins (e.g., de Ruig, 1995; Granado et al., 2021; Roca et al., 2006).

The Tunisian Tell and Atlas belts are interpreted as external foreland nappe and fold belts comprising only sediments, despite the presence of the Giallo Antico marbles, well known since Roman times (e.g., Bugini et al., 2019; Röder, 1988), outcropping in the Hairech massif at the supposed boundary between the two orogenic belts (e.g., Khelil et al., 2019; Figure 2). Equivalent marbles with thin intercalated calcschist layers also crop out in Jebel Ichkeul and the Oued Belif domes, representing the structurally deepest rocks in the Tell belt (Booth-Rea et al., 2018; Khelil et al., 2019; Figure 2, cross-sections A-A' and B-B'). Greenschist metamorphism affecting Mesozoic Tellian and Kabylian flysch sediments, metabasites and serpentinites is also described in the nearby Algerian Tell (e.g., Boukaoud et al., 2021; Caby et al., 2001; Durand-Delga, 1971; Wildi, 1983). However, the origin, modes of exhumation, age, nature and implications that these metamorphic rocks have for the tectonic evolution of the region, and at a larger scale, for the evolution of the Western Mediterranean nappe belts, have not been satisfactorily explained.

Here, we study the structure, metamorphism and timing of geological processes in Northern Tunisia using a multidisciplinary approach. We use fieldwork and the analysis of industry multichannel seismic reflection lines to study the structure of the Mejerda basin and Kroumerie massif to the Northwest, with a special emphasis in determining the relationships between polyphasic late Miocene extension, the development of halokinetic structures, synrift basin and metamorphic rocks exhumation. Moreover, we determine illite crystallinity for Triassic metapelite intercalations cropping out in the Tell nappe belt of Northern Tunisia and analyze the metamorphic mineral parageneses, including multiequilibrium thermobarometric results for the Ichkeul calcschist. Furthermore, we

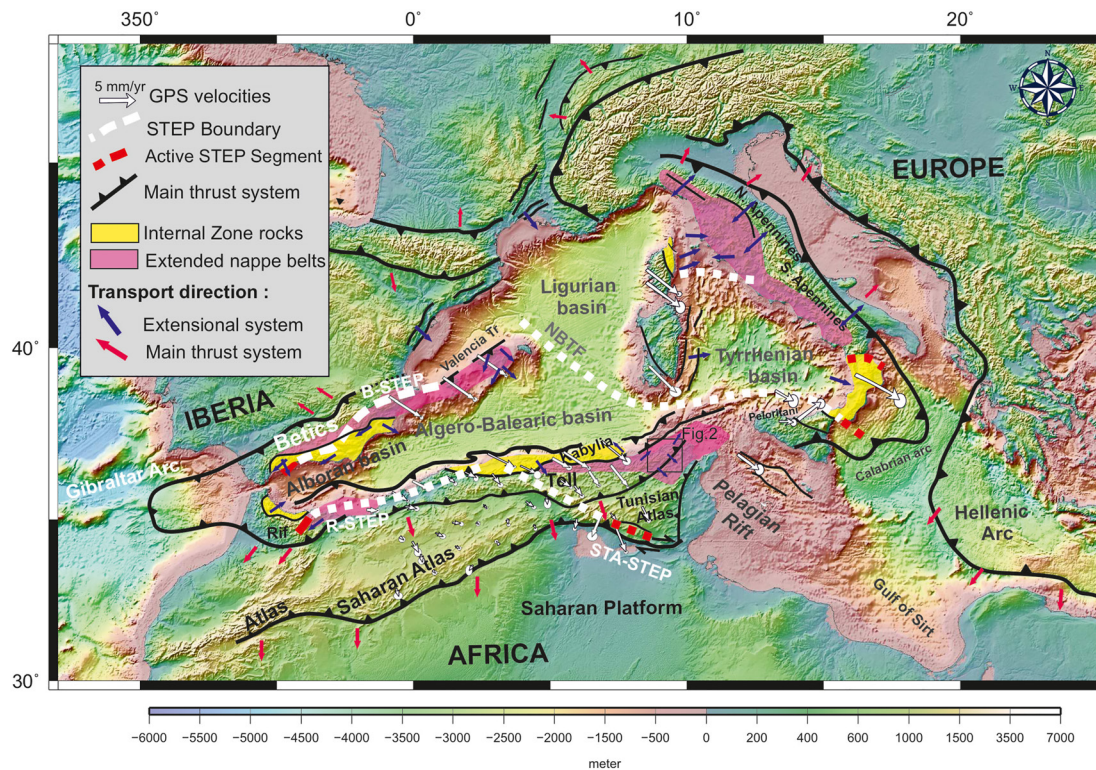


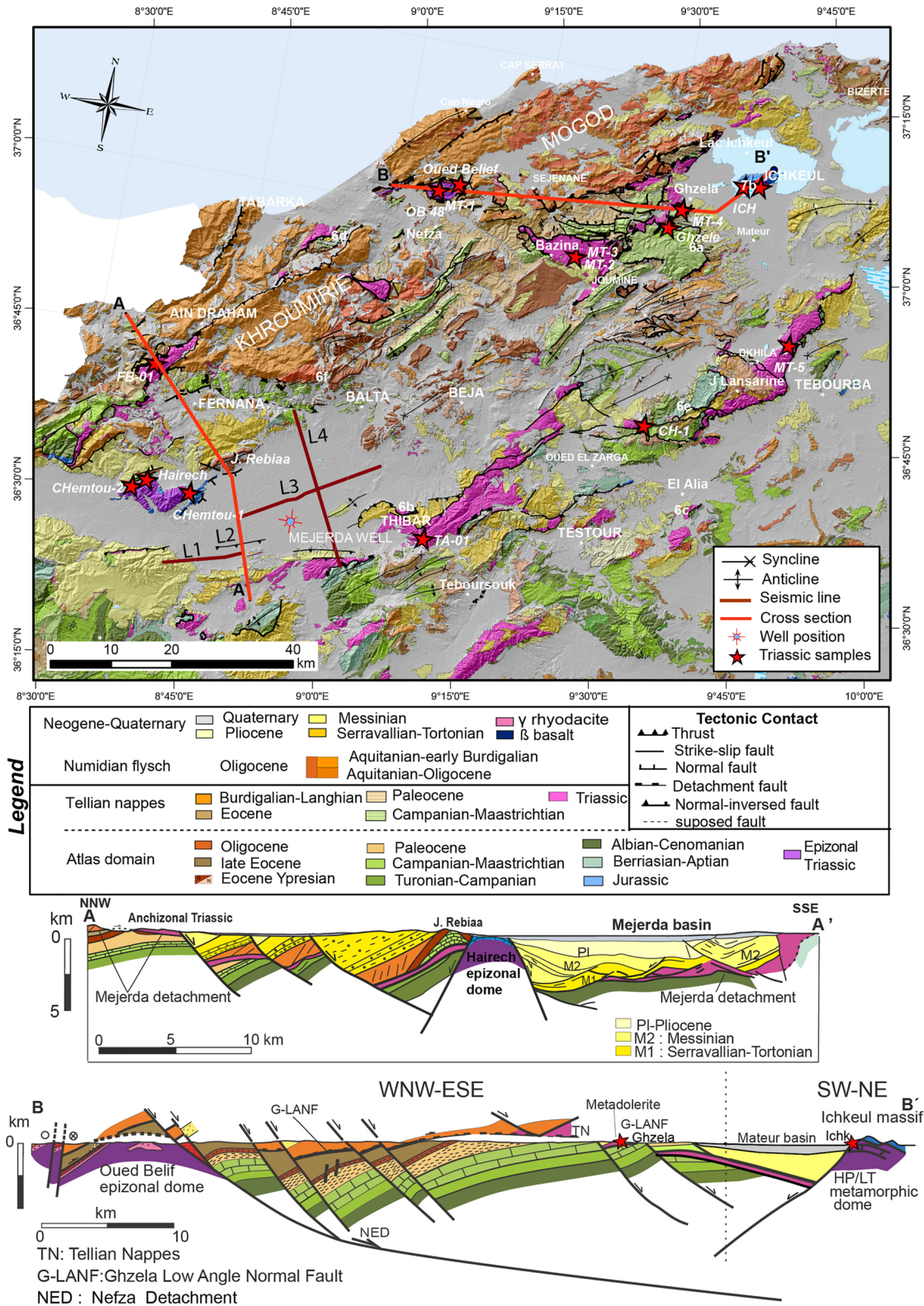
**Figure 1.** Tectonic boundaries, orogenic arcs and basins of the Western Mediterranean. Figure modified from Booth-Rea et al. (2007, 2018) and Gaidi et al. (2020). GPS movement toward fixed Africa from Bougrine et al. (2019) and Nocquet (2012). Fault pattern along Algeria-Tunisia based on Kherroubi et al. (2009), Rabaute and Chamot-Rooke (2014), and (Aïdi et al., 2018). Extended nappe belt domains from Carmignani and Kligfield (1990), Ghisetti and Vezzani (2002), Booth-Rea et al. (2012, 2018), Molli et al. (2018), Rodríguez-Fernández et al. (2013), and Moragues et al. (2021).

use rutile U-Pb laser-ablation ion-probe dating to determine the age of metamorphism in metabasites. These data, together with other previously published K-Ar data suggest a polymetamorphic evolution in the Tell-Atlas domain, between the Cretaceous and early Miocene. Favoring a model of Eocene and early Miocene crustal thickening and High-Pressure Low-Temperature (HP/LT) metamorphism followed by extensional exhumation and crustal thinning. Driving late Miocene basin development, halokinesis of overthrust evaporite-rich layers in the upper crust and ductile flow below the brittle-ductile transition. Finally, we integrate these findings in a new tectonic evolution for the Algerian-Tunisian orogenic belt and evaluate their significance for other nappe belts of the Western Mediterranean.

## 2. Geological Setting

The Tell nappe belt in Northern Tunisia is part of the Alpine orogenic system that surrounds the Western Mediterranean Liguro-Provençal, Algero-Balearic, Tyrrhenian and Alboran basins, formed in a context of Nubia-Eurasia convergence since late Cretaceous times (Dewey et al., 1989; Figure 1). This convergent setting favored the action of other tectonic mechanisms related to subduction, like slab roll back accompanied by slab tearing and detachment at the edges of the Western Mediterranean orogenic arcs, which contributed to the development of these basins and their surrounding mountain belts (e.g., Booth-Rea et al., 2007; Carminati et al., 1998; Chertova et al., 2014; Govers & Wortel, 2005; Lonergan & White, 1997; Moragues et al., 2021; Romagny et al., 2020; Van Hinsbergen et al., 2014; Wortel & Spakman, 2000). Furthermore, delamination of the subcontinental lithospheric mantle driving crustal thinning, magmatism and topographic uplift, has also been proposed beneath continental domains like the South Eastern Betics, Northern Tunisia, the Rif or the Central Apennines (Booth-Rea et al., 2018; Camafort et al., 2020; de Lis Mancilla et al., 2015; Di Luzio et al., 2009; Duggen et al., 2003; Levander et al., 2014; Martínez-Martínez et al., 2006; Negrodo et al., 2020; Petit et al., 2015; Roure et al., 2012) (Figure 1). The present crustal thickness of northern Tunisia decreases from 30 km at the southern margin of the Mejerda basin to approximately 20 km at the coast along the EGT'85 N-S seismic refraction Line 1 (Research Group for Lithospheric Structure in Tunisia, 1992).







The Tell nappe belt in Tunisia is represented by the overthrust Mesozoic to Tertiary Tellian nappes and overlying Numidian Flysch, together with the underlying Atlasic domain that deposited along the North Maghrebian passive margin during the Mesozoic and Cenozoic (Belayouni et al., 2013; Khomsi et al., 2009; Riahi et al., 2010; Riahi et al., 2021) (Figure 2). The Oligocene to early Miocene Numidian Flysch is interpreted to have formed over the previously shortened and eroded underlying Tellian sequence, in order to explain the stratigraphic omissions found along its basal contact (Khomsi et al., 2021; Khomsi et al., 2022). On the other hand, other authors, propose its deposition in the Tethys oceanic realm (e.g., Guerrero et al., 2005).

The Tellian nappes are formed by up to four imbricated allochthonous units that include mostly Cretaceous to Aquitanian sediments (Belayouni et al., 2013; Khomsi et al., 2009; Rouvier, 1992, 1993). Triassic evaporites occur at the base of the Tellian nappes that are interpreted either as autochthonous Triassic piercing the nappe structure (Khelil et al., 2019; Rouvier, 1992, 1993) or as part of the Tellian overthrusting series (Booth-Rea et al., 2018; Troudi et al., 2017). The Atlas series are formed by Triassic to early Miocene sediments, interpreted as autochthonous (Khomsi et al., 2009, 2016) (Figures 2 and 3).

The hinterland domain of the Tell is found to the NW in the Kabylies in Algeria, where polymetamorphic rocks derived from the AlKaPeCa European margin, overthrusting the Kabylia Flysch and Tellian domain rocks, crop out showing both Hercynian and Alpine metamorphic ages (e.g., Bouillin et al., 1986; Monie et al., 1988; Peucat et al., 1996). Furthermore, a tectonic window below the Maghrebian Flysch and greenschist Mesozoic Tellian rocks, forming the Edough massif, offers outcrops of exhumed African lower crust (e.g., Caby et al., 2001; Vila, 1970; Wildi, 1983) with UHP metamorphic slivers and peridotite (Caby et al., 2014) giving  $32.4 \pm 3.3$  Ma U-Pb rutile ages (Bruguier et al., 2017). The HT exhumation path of the Edough massif dome was dated by UPb in zircon and Ar-Ar in biotite and muscovite between 20.7 and 17 Ma (Fernandez et al., 2016) (Figure 3). This exhumation was followed by felsic magmatism (Chazot et al., 2017) and related Cu-Pb-Zn mineralizations (Boutaleb et al., 2000; Marignac et al., 2016), basin subsidence onshore (Arab et al., 2016) and oceanic spreading of the easternmost Algerian basin between 17 and 11 Ma (Haidar et al., 2022; Figure 3).

Metamorphic rocks also occur in Northern Tunisia. These are described as Permo-Triassic epizonal rocks that reached temperatures between 300°C and 400°C in the core of the Oued Belif dome (Mahdi et al., 2013). Furthermore, at intermediate structural positions within the Tell nappe stack, metabasites derived from early Mesozoic intraplate basalts, included in the Triassic evaporitic sequence show a polymetamorphic evolution (Kurtz, 1983). Metamorphic minerals have been dated in the Tunisian Tell and Atlas. K-Ar ages on K-feldspar and phlogopite in metabasites and marbles give different age populations (Figure 3), including late Cretaceous to Paleocene ages (97–64 Ma) in Le Kef diapir, younger late Oligocene to early Miocene (25–18 Ma) ages in more internal Triassic outcrops, and only early Miocene ages (23–17 Ma) in the deeper Ichkeul massif (Bellon & Perthuisot, 1977). This age disparity has been interpreted as mixed Cretaceous rifting ages with late Miocene magmatic or hydrothermal-related thermal resetting by Bellon and Perthuisot (1977).

The Tunisian Tell and Atlas has been considered for decades as a paradigmatic region for the study of diapiric structures in an external foreland thrust belt (e.g., Amri et al., 2020; Ayed-Khaled et al., 2015; Bedir et al., 2001; Ben Chelbi et al., 2006; Melki et al., 2010; Perthuisot, 1981; Troudi et al., 2017; Vila, 1995). Diapiric intrusions of Triassic evaporites are interpreted as related to Cretaceous rifting of the North Maghrebian passive margin, extruding to the surface as thousand km<sup>2</sup> large salt glaciers or canopies (Amri et al., 2020; Ayed-Khaled et al., 2015; Ghanmi et al., 2001; Masrouhi & Koyi, 2012; Masrouhi et al., 2014; Vila, 1995; Vila et al., 1996; Zouaghi et al., 2013). This Mesozoic extensional-diapiric structure would have evolved later in a convergent to transcurrent setting during the Cenozoic development of the Tell and Atlas nappe and thrust belts (Amri et al., 2020; Bouaziz et al., 2002; Melki et al., 2010, 2011) (Figures 1 and 3). Salt tectonics is interpreted to have played an important role during thrusting, with the main décollements being located within the Triassic evaporites at the base of the main Tellian thrust sheets (Booth-Rea et al., 2018; Khomsi et al., 2009, 2016). Thus, some authors interpret the proposed salt canopies, alternatively, as overthrust Triassic evaporites at the base of the Tellian nappes (Khomsi et al., 2009; Troudi et al., 2017).

**Figure 2.** Geological map of Northern Tunisia and cross-sections through the studied region. Map of the Tunisian Tell with the location of the analyzed Triassic samples, interpreted reflection seismic lines, Mejerda well and location of outcrop photographs. OB 48 locality corresponds to bore hole where Mahdi et al. (2013) analyzed epizonal samples. Location in Figure 1. Cross section A-A' across the Kroumerie massif and the Mejerda basin. The structure across the Mejerda basin is based on reflection seismic line 2. Cross section B-B' from the Oued Belief epizonal dome, through the Mogods massif, reaching the Ichkeul High-Pressure Low-Temperature massif. Notice the two extensional detachment levels, with the Ghzela Low-Angle Normal Faults cutting above the Atlas Cenozoic and Cretaceous series and the Nefza detachment and associated listric fan cutting the previous structure and exhuming the Oued Belif and Ichkeul metamorphic domes.

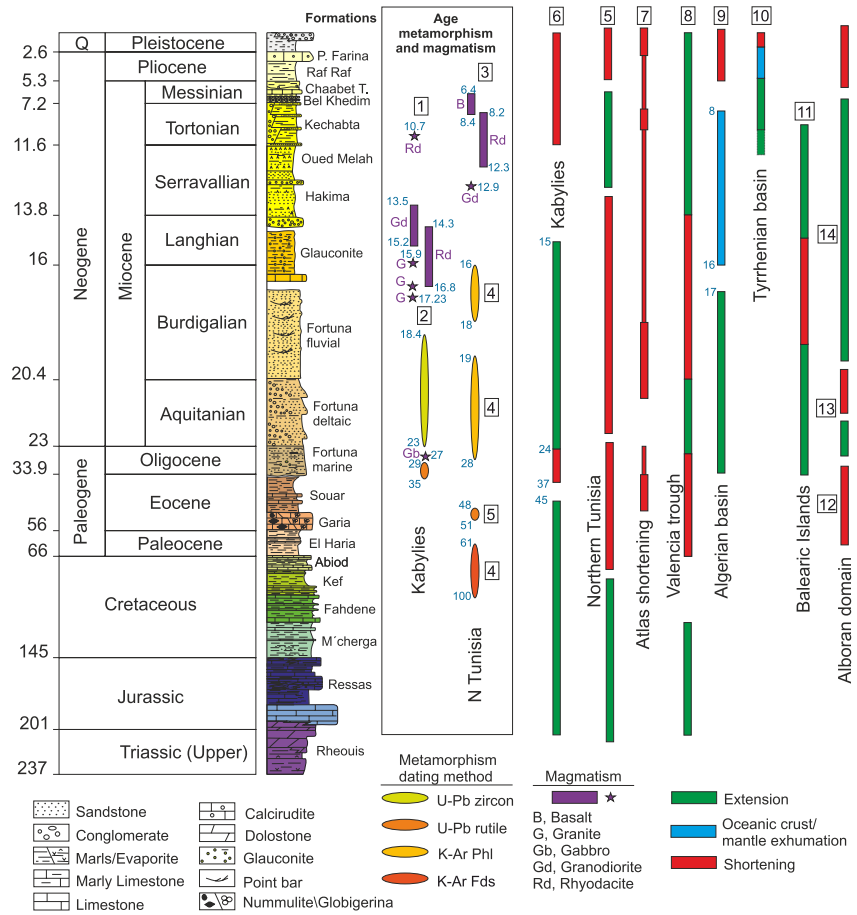


**Figure 3.** Tectonic events in selected regions of the Western Mediterranean together with the magmatic and metamorphic evolution of Northeastern Algeria and Northern Tunisia. We include the stratigraphic sequence of the Atlas domain in Northern Tunisia (Triassic-Eocene from Melki et al. (2012); Oligocene-Langhian from Riahi et al. (2021); Post Langhian from Alyahyaoui and Zouari (2014)). Ages (blue numbers) of metamorphism and magmatism of Kabyliques and N Tunisia and tectonic events over time of Western Mediterranean domains based on: 1. Abbassene et al. (2016) and Chazot et al. (2017); 2. Bruguier et al. (2017); 3. Decrée et al. (2014); 4. Bellon and Perthuisot (1977); 5. present work; 6. Caby et al. (2001); 7. Frizon de Lamotte et al. (2009) and Marmi and Guiraud (2006); 8. Fontboté et al. (1990); 9. Aidi et al. (2018); 10. Faccenna et al. (2004); 11. Moragues et al. (2021); 12. Platt et al. (2005); 13. Hidas et al. (2013) and Balanyá et al. (1997); 14. García-Dueñas et al. (1992) and Lonergan and Platt (1995).

Tectonic shortening initiated in the late Cretaceous to Palaeogene producing angular and erosive unconformities sealing folds in different regions of the Tunisian and Algerian Tell and Atlas, together with olistostromic sedimentary formations (El Ghali et al., 2003; Khomsi et al., 2009; Marmi & Guiraud, 2006; Masrouhi et al., 2008; Saadi et al., 2023; Wildi, 1983). During this period, special emphasis is given to a middle to late Eocene “Atlas event” (Benaouali-Mebarek et al., 2006; Bracène & Frizon de Lamotte, 2002; Frizon de Lamotte et al., 2000; Khomsi et al., 2009, 2021; Leprêtre et al., 2018) (Figure 3). The Atlas event was followed by later overthrusting of Oligocene to late Burdigalian Numidian Flysch series and the underlying Tellian substrate over early Miocene foredeep glauconitic sediments of Burdigalian to Langhian age in the Tunisian Tell (Belayouni et al., 2013; Belhajtaher et al., 2023; Boukhalfa et al., 2020; Khomsi et al., 2009, 2016; Riahi et al., 2010) (Figure 3). Most authors consider continuous shortening and folding in Northern Tunisia throughout the late Miocene (Melki et al., 2010, 2011; Ramzi & Lassaad, 2017). However, recent work has reinterpreted the related folds as being extensional fault-bend roll-over anticlines and hanging-wall synclines produced during Tortonian to Messinian extensional collapse of the Tell nappe belt, coeval to the development of sedimentary basins (Booth-Rea et al., 2018, 2020; Gaidi et al., 2020) (Figure 3). This extension was coeval to felsic magmatism and polymetallic mineralizations in Northern Tunisia (Ben Aïssa et al., 2018; Decrée et al., 2008, 2014, 2016), dated between the early Tortonian and the Messinian (Jemmali et al., 2014; Yans et al., 2021). Continental semigrabens in Northern



Tunisia were dated as late Serravallian to early Tortonian (11.6–10 Ma) by mammalian biostratigraphy and U-Th/He dating of supergene iron oxide mineralizations in the Nefza mining district area (Yans et al., 2021).

Renewed shortening and tectonic inversion in Northern Tunisia occurred since the Pliocene-Quaternary, marked by a prominent post-rift angular unconformity in reflection seismic lines. This phase developed new basin depocenters over the footwall of reverse faults and oblique strike-slip faults (e.g., Ayed-Khaled et al., 2015; Booth-Rea et al., 2018; Camafort et al., 2020; Gaidi et al., 2020; Melki et al., 2010, 2011) (Figure 3). Many of the reverse fault segments formed by tectonic inversion of late Miocene normal faults, especially those bounding sedimentary depocenters, such as the Mejerda and Mateur basins (Booth-Rea et al., 2018; Gaidi et al., 2020). The main fault system accommodating this late Pliocene to Present-day convergence across Northern Tunisia is the Alia-Thibar dextral reverse fault zone (Gaidi et al., 2020). Extension propagated southward, affecting large areas of central Tunisia and the Pelagian platform between the Messinian-Zanclean and Quaternary (Arab et al., 2020; Belguith et al., 2011, 2013; Bouaziz et al., 2002; Dhifaoui et al., 2021; Saïd et al., 2011).

### 3. Methods

In order to analyze the structure of Northern Tunisia and the metamorphism undergone by the Triassic rocks, we used a multidisciplinary approach. We carried out field work to analyze the structure and sample different Triassic evaporite bodies in the region. Our work is based on 1:50,000 geological maps of Northern Tunisia published by the Office National des Mines (ONM), which we digitized and revised (Booth-Rea et al., 2018; Gaidi et al., 2020). Furthermore, we interpreted several industry multichannel reflection seismic lines from the Tunisian Company of Petroleum Activities (ETAP) that cross through the Mejerda basin in Northwestern Tunisia. We analyzed Triassic metapelite, calcschist and metabasite samples from different massifs in Northern Tunisia, using X-ray diffraction techniques, Scanning Electron Microscopy (SEM), Raman spectroscopy, Electron Backscatter Diffraction (EBSD) and electron microprobe (EPMA) for determining illite crystallinity in metapelites, existing mineral paragenesis, crystallographic preferred orientation (CPO) and their chemical composition. Greenschist mineral parageneses were tested for local equilibria using mineral compositions and TWQ thermobarometry software (Berman, 1991). Finally, we used Laser Ablation Inductively Coupled Plasma Mass Spectrometry (LA-ICP-MS) measurements for the radiometric U-Pb dating of metamorphic rutile in the metabasites. Further, methodological details and related figures, and compositional data are exposed in Supporting Information S1.

## 4. Structure of Northern Tunisia

### 4.1. Extensional Detachments and Halokinetic Structures in Reflection Seismics

Seismic lines across the Mejerda basin show a prominent reflector that dips southwards at a low angle, cutting downwards into the Atlas Cretaceous sediments, which we name the Mejerda detachment (Seismic lines Mejerda 1, 2, 3, and 4, Figures 2, 4 and 5). This reflector has been cored in the Mejerda 1 drill hole and it separates Triassic evaporites above from underlying middle Cretaceous marly limestones (Troudi et al., 2017; Figure 2). The Triassic is overlain by a discontinuous and incomplete section of Mesozoic to Cenozoic sediments, mostly Eocene limestones (Troudi et al., 2017). These rocks are covered by the middle-late Miocene syn-rift and Pliocene to Quaternary post-rift sediments of the Mejerda basin (Gaidi et al., 2020) (Figures 4 and 5). High-angle normal faults cut the middle-late Miocene sediments, detaching at the base of the Triassic evaporites. These sediments show progressive angular unconformities and are intruded by salt walls and diapirs. Northward tilting of the middle-late Miocene sediments along line L4 (Figure 5) is compatible with mostly southward-directed transport along the underlying Mejerda detachment.

Overall, the Mejerda detachment separates two crustal wedges, an overlying one, thickening toward the South, formed by Telliian nappe rocks and overlying late Miocene sediments, and an underlying one, thinning southwards formed by Atlas Cretaceous sediments (Figure 4). The extensional structures are overlain by an angular post-rift unconformity, sealed by folded Pliocene to Quaternary sediments. Along lines 1, 2, and 3, the Mejerda detachment deepens toward the SW from 500 to 1,800 ms at the SW border of the basin (Figure 4).

Triassic evaporites form discontinuous bodies together with overlying high-amplitude packages, interpreted as Eocene limestones, cropping out nearby, above the detachment and below the late Miocene sediments (Ayed-Khaled et al., 2015) (Figure 4). Normal faults overlying the Mejerda detachment show listric geometry,

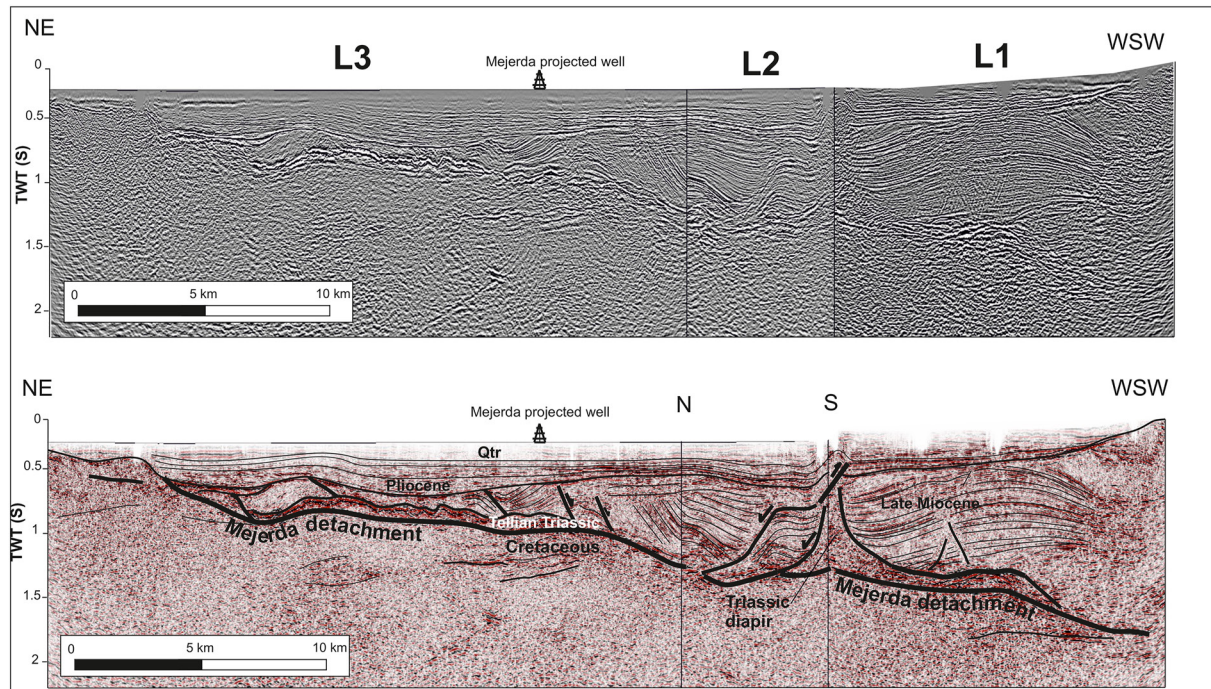


**Figure 4.** Seismic cross-section composition using multichannel reflection seismic lines L1, L2, and L3 through the Mejerda basin, showing normal fault listric fan cutting through Late Miocene sediments and rooting in the Mejerda detachment. Notice low-angle footwall ramp cutting through Cretaceous sediments sampled in the Mejerda well. The hanging-wall structure is pierced by several halokinetic structures rooted in the Telliian Triassic.

with both SW- and NE-directed kinematics (Figure 4). Overall, the normal faults cutting the late Miocene sediments form a listric fan structure that roots into the Mejerda detachment. Few reflectors dipping smoothly toward the NE occur in the footwall, indicating a low-angle ramp geometry below the detachment (Figure 4).

#### 4.2. Structure Derived From Field Outcrops

Low-grade metamorphic rocks occur in the Hairech, Ichkeul and Oued Belif massifs in Northern Tunisia (map and cross-sections in Figure 2). These massifs consist of marbles, metapsammites and metabasites, which resulted from the metamorphism of Jurassic limestone and underlying Triassic continental red-beds, dolostone and limestone with intercalated early Mesozoic basalts (Kurtz, 1983). Metabasite lenses occur also within structurally-higher Triassic rocks located at the base of the Telliian nappes within the fault zones of the Mejerda and Ghzele detachments (cross-section B-B' and Figure 6a).

The Mejerda detachment crops out extensively in the region along the northern and southern margins of the Mejerda basin, for example, to the E-SE of Fernana, in the region around Thibar, and also further East along the southern margin of the Mejerda valley (Figure 2). The detachment is directly overlain by extensional riders of diverse rocks like the Numidian Flysch, Eocene limestones or Cretaceous-Palaeocene marls, and also by tilted late-Miocene sediments (see geological map and cross-section A-A', Figure 2).

The Telliian Triassic sequence in the hanging wall of the Mejerda detachment crops out largely along the Thibar anticline, detached over early Cretaceous marls (Mcherga Formation) in the footwall, which form the core of the anticline (see Geological map in Figure 2). These features coincide with those observed in the seismic lines crossing the Mejerda basin (Figures 4 and 5). To the northwest of Fernana, the Mejerda detachment shows a low-angle footwall ramp, cutting down southwards from Eocene to Turonian-Santonian sediments (cross-section A-A', Figure 2). Thus, combining information from the geological map, seismic lines and the Mejerda drill hole, the Mejerda detachment cuts down into the Atlas sedimentary sequence, having late Eocene sediments in its footwall to the NW and reaching early Cretaceous to the SE, in the core of the Thibar anticline (cross-section A-A', Figure 2).

The detachment is defined by a low-angle foliated cataclastic breccia, affecting different Triassic lithologies, including red beds, dolostone and gypsum (Figure 6b) and overlying Cenozoic sediments. Gypsum forms



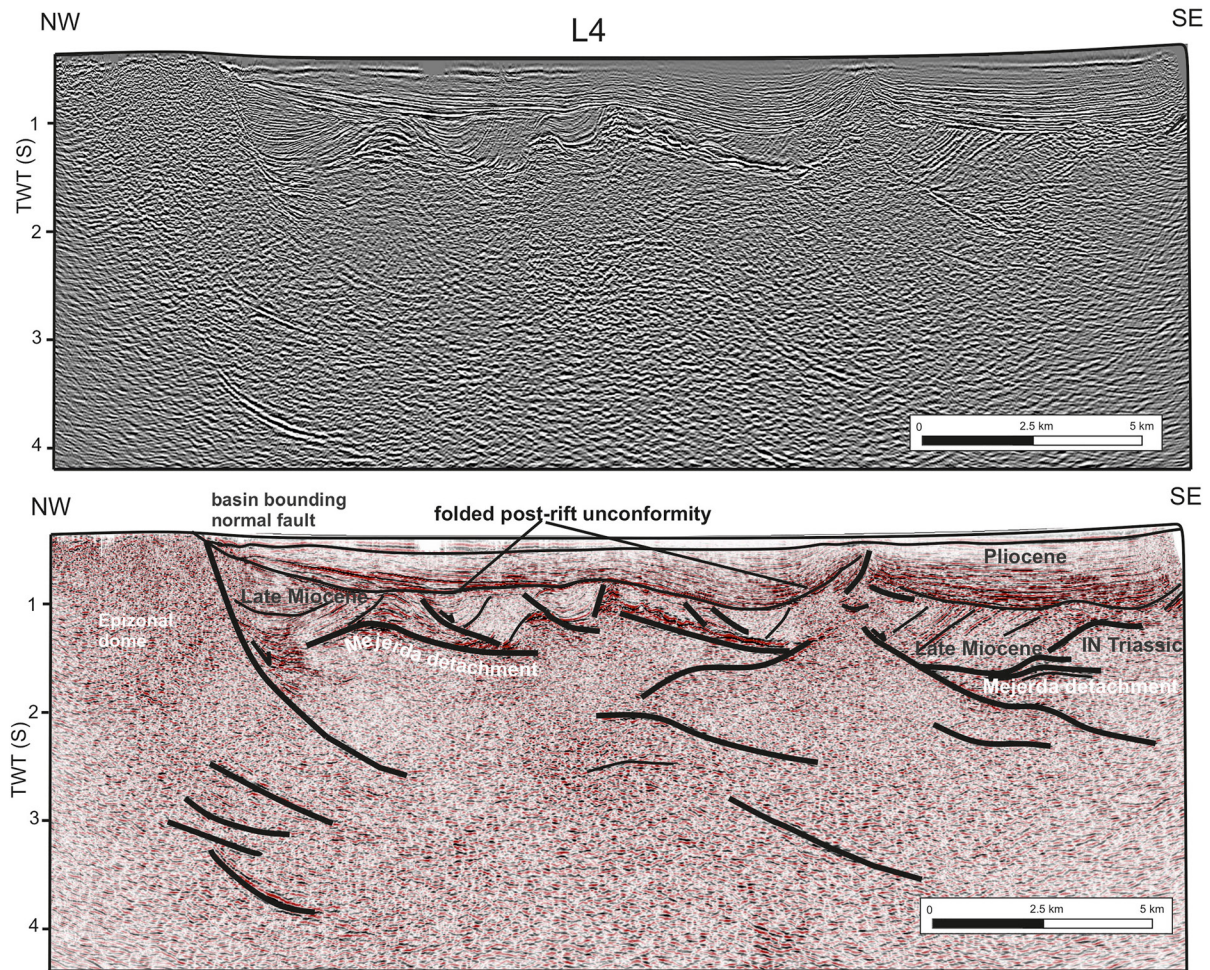


**Figure 5.** Seismic reflection line L4 across the Mejerda basin, showing high-angle faults cutting the Mejerda detachment and exhuming the autochthonous Atlas rocks to the NW and tilted Late Miocene sediments overlying the Mejerda detachment. Late Plio-Quaternary folding the post-rift unconformity is also evident in this line. This seismic line has been published before down to 2sTWT, with different interpretations by Ayed-Khaled et al. (2015), Khelil et al. (2019), and Frifita et al. (2020).

mylonitic bands within the cataclastic breccia. Gypsum mylonites include dolomite porphyroclasts indicating southward-directed transport (Figure 6c).

High-angle normal faults cutting into the Numidian Flysch sequence define semigrabens filled by late Miocene conglomerates in the Kroumerie massif (Figures 2 and 6d). These faults cut and exhume the Mejerda detachment at their footwall, exposing Triassic evaporites and overlying Telliian tectonic units, below the Numidian Flysch. Furthermore, they define the main valleys within the Kroumerie massif. We show the prolongation of these faults toward the SW in section A-A' (Figure 2). We observe similar high-angle faults toward the East in the Lansarine ridge, which cut through the low-angle Ghzele detachment and show tilted late Miocene sediments in their hanging wall (Figures 2 and 6e).

The Mejerda detachment and overlying Triassic rocks are folded and thrust over the whole sedimentary sequence of the Mejerda basin along its southern border. This tectonic inversion also affected the northern margin of the basin, along the Balta-Fernana thrust, a process that uplifted the Mejerda detachment in the hanging wall of the thrust during the Plio-Quaternary (Gaidi et al., 2020). Here, the detachment forms the southern contact of the Kroumerie Numidian Flysch outcrops on its Telliian substrate (Kasseb unit), over the Atlas Cretaceous (Figure 6f). The Kasseb unit includes Eocene limestones that form prominent discontinuous extensional horses, tilted toward the NW and detached over the Mejerda detachment (landscape photo in Figure 6f). Triassic evaporites crop out locally between the Eocene limestones and underlying Paleocene to Cretaceous series to the West of the landscape photo in Figure 6f. The Eocene limestones are interpreted also as highly-reflective bodies overlying the Mejerda detachment in the seismic lines crossing the Mejerda basin (Figures 4 and 5).



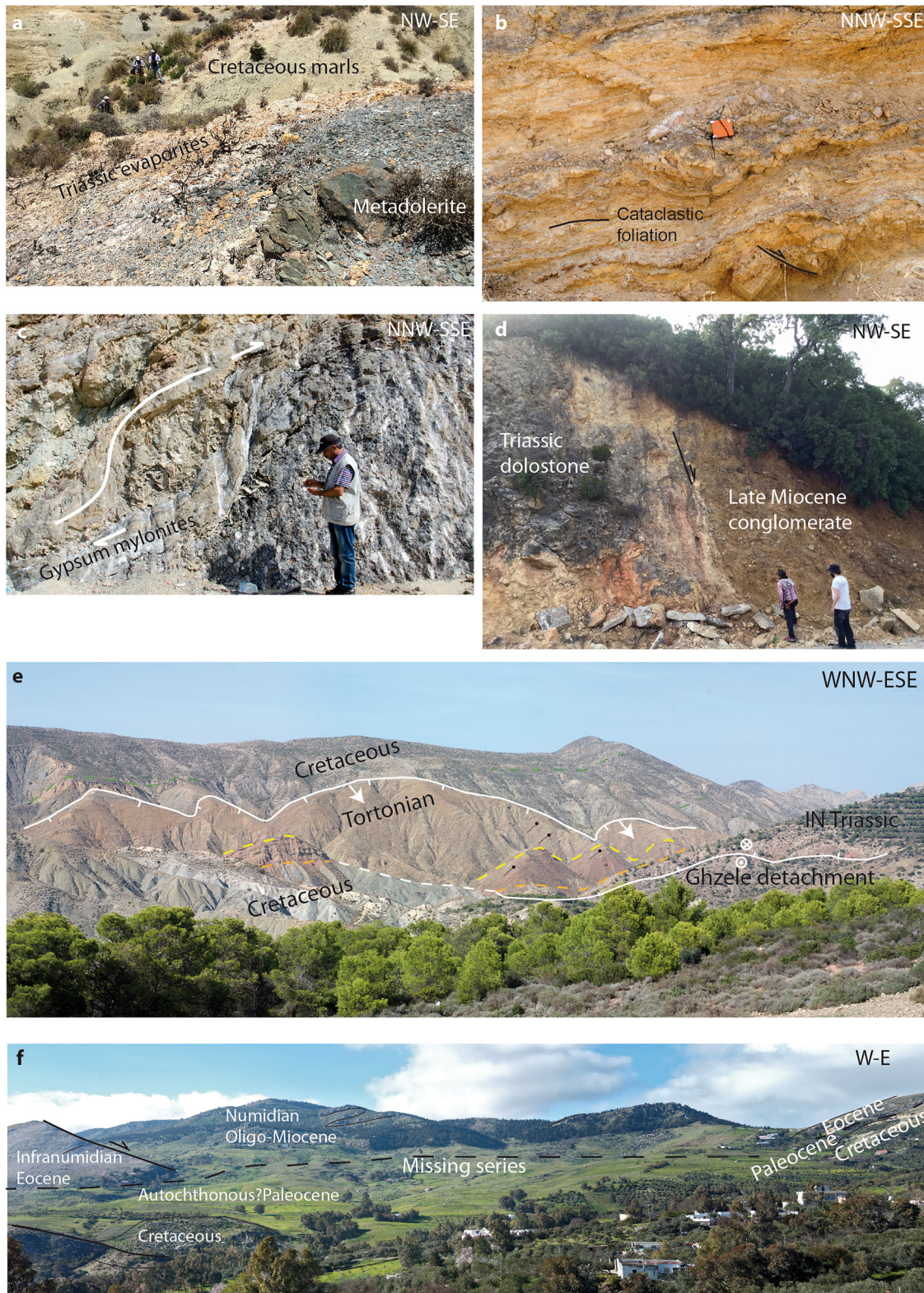


Figure 6.



Deep rocks from the footwall of the Mejerda detachment crop out in the Hairech massif along the northern border of the Mejerda basin. The Hairech massif shows an open antiformal WSW-ENE trending structure with its northern and southern limbs cut by high-angle normal faults with NW- and SE-directed transport, respectively (Khelil et al., 2019; Khomsi et al., 2022; Rouvier, 1977) (cross-section A-A', Figure 2). These normal faults bound the Messinian sediments of the Mejerda basin, both to the North and South of the massif, and also cut mineralized outcrops of Eocene allochthonous Tellian rocks (cross-section A-A', Figure 2). The massif is formed by the Chemtou marbles (e.g., Fant, 2001), and underlying Triassic metapsammites. This antiformal structure produces a prominent WSW-ENE oriented ridge with a positive gravimetric anomaly all along the northern border of the Mejerda basin, coinciding with the Hairech and Rebiaa massifs (Amiri et al., 2011; Frifita et al., 2020) (See cross-section A-A' in Figure 2). Cretaceous low-grade metasediments and mylonites are described along the normal fault bounding the northern limb of the Hairech massif (Ben Aïssa et al., 2021). The fault bounding the southeastern border of the massif is imaged in seismic line L4 (Figure 5). This normal fault cuts through the whole structure described above, rooting in low-angle reflectors at a depth of approximately 3 s TWT (Figure 5).

Marbles and metapsammites from the Hairech massif show a penetrative foliation, marked by white mica grains oriented parallel to the lithological banding (Figure 7a). These rocks contain a magnetic fabric, which has been related to a preferred crystallographic orientation in phyllosilicates, interpreted as a probable syn-metamorphic stretching lineation, with WNW-ESE to WSW-ENE orientation (Ghorabi & Henry, 1992).

Outcrops of Triassic metapelites in the Oued Belif dome are strongly overprinted by mineralizations and intruded by Serravallian granodiorites and Tortonian rhyodacites (Decrée et al., 2013, 2014; Mahdi et al., 2013). These metamorphic rocks that reached temperatures up to 540°C (Decrée et al., 2013) contrast with the overlying diagenetic Oligocene Numidian sediments, marking a metamorphic gap of at least 350°C (cross section B-B', Figure 2). Exhumation-related structures in this region are particularly clear and intimately related to magmatic processes, with a well-defined brittle-ductile shear zone between the Triassic metapelites and overlying sediments, namely, the Nefza detachment (Booth-Rea et al., 2018). The main extensional detachment produced E- to NE-directed extension during the extrusion of rhyodacites that show a magmatic foliation parallel to an overlying mylonitic foliation in marbles from the footwall of the Nefza detachment. These rocks are cut by a late Miocene fault breccia hosting a Iron Oxide, Copper, Gold-type mineralization (Booth-Rea et al., 2018; Decrée et al., 2013). This exhumation trend, with ductile structures evolving toward brittle breccias is also followed by magmatism in the region that evolves from plutonic intrusion of granodiorites in the Serravallian (12 Ma) to the shallower extrusion of volcanic rocks in the Tortonian (8–9 Ma) (Decrée et al., 2014; Halloul & Gourgaud, 2012) (Figure 3).

The Ichkeul massif in Northeastern Tunisia is formed by marbles and calcschists derived from Jurassic and late Triassic protoliths (cross section B-B', Figure 2). This massif occurs isolated by Quaternary sediments to the north of the Mateur basin (Figure 2). The marbles are presently folded in the core of a moderately inclined, moderately plunging SE-vergent anticline with a WSW-ENE oriented axis (Figure 7b). The fold hinge is cut by a NW-dipping thrust with SSE-directed transport, including a several meter-thick breccia in its footwall (Figure 7b, and inset photo). The southern limb of the anticline is cut by two sets of E-W and N-S trending high and Low-Angle Normal Faults (LANF) with mostly S-SE- and E-NE-directed transport, respectively (Figures 7c–7f, with faults and striae projected in stereoplot). Marbles in the Ichkeul massif show a L-S type fabric, containing a SW-NE trending calcite-quartz object lineation, also marked by stretched fossils, which in turn is cut by a penetrative system of NW-SE trending calcite veins (Figures 7g and 7h, including stereoplot of foliation and lineation). The main metamorphic foliation is parallel to the bedding.

**Figure 6.** Field outcrop photographs with location in Figure 2. (a) Metabasite outcrop within evaporitic breccia of the Ghzela detachment, with Cretaceous Tellian marls above. (b) Foliated breccia affecting Triassic evaporitic rocks in the Mejerda detachment. Notice cataclastic foliation and rotated porphyroclasts in the fault zone. (c) Breccias and gypsum mylonites from the Mejerda detachment. Notice large dolomitic porphyroclast indicating southwards tectonic transport. (d) High-angle fault cutting through Tellian Triassic dolostones in the footwall and with late Miocene conglomerates in the hangingwall. These faults with SE-directed transport exhume the Mejerda detachment and bound several grabens in the Khroumirie massif, see cross-section A-A', Figure 2. (e) Panoramic view of a southward transport normal fault cutting the Lansarine ridge. Notice NW-dipping Cretaceous sediments in the footwall and the overlying tilted late Miocene sequence. The normal fault zone is defined by a Triassic evaporitic breccia, probably reworking the Ghzele detachment that crops out below the Neogene sediments in the hangingwall. (f) Panoramic view of the Tell-Atlas contact near Balta. Notice the lateral omission of Tellian Eocene limestones, cut by a normal fault, along the supposed thrust contact between the Numidian Flysch and the underlying autochthonous series. Laterally, toward the West, this contact also has Tellian Triassic evaporites, which are omitted in this section. We relate the missing series along this contact to extensional reworking of the original thrust contact by the activity of the Mejerda detachment. The stratigraphic sequence overlying the detachment shows systematic tilting toward the NW.



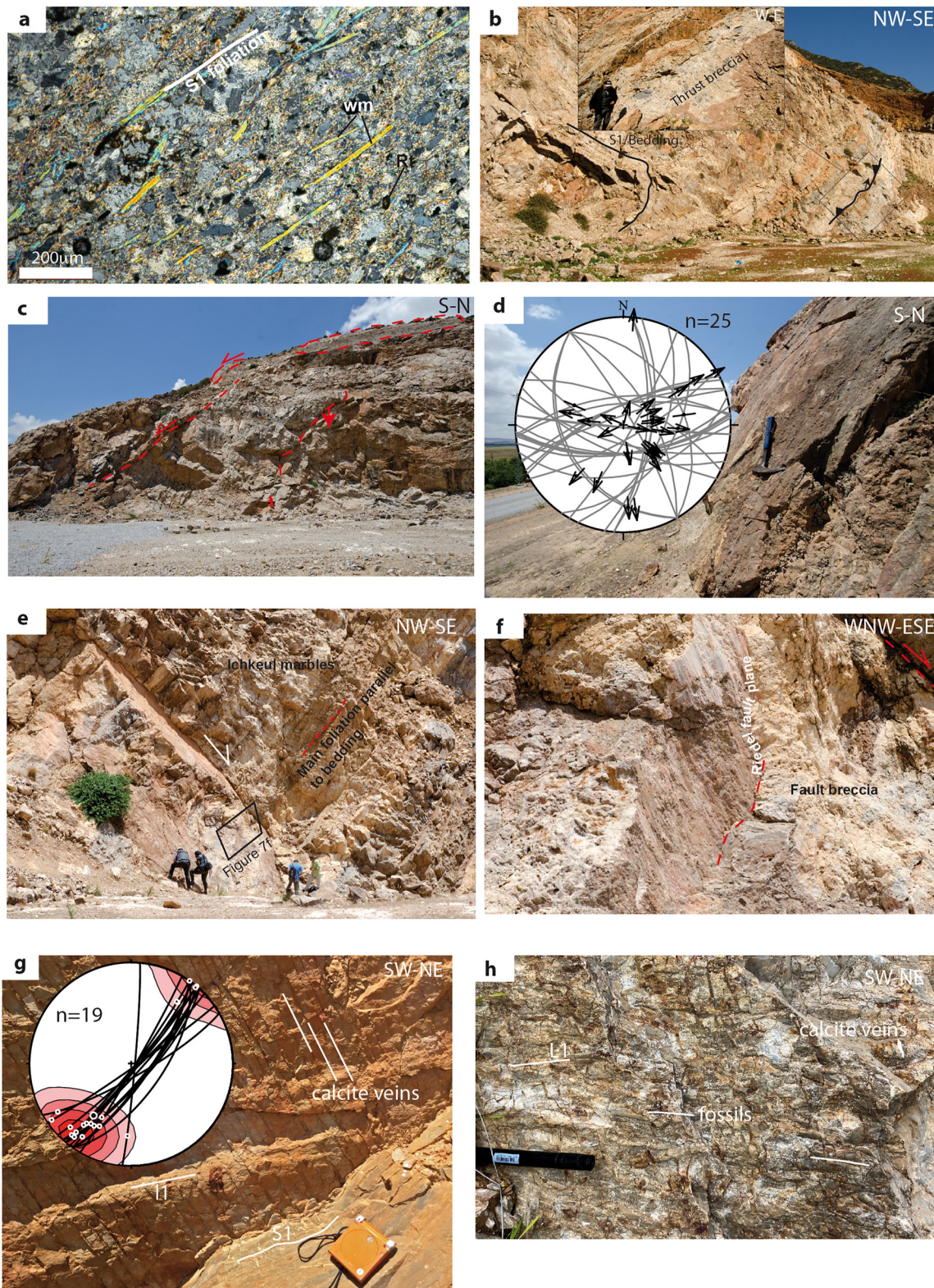
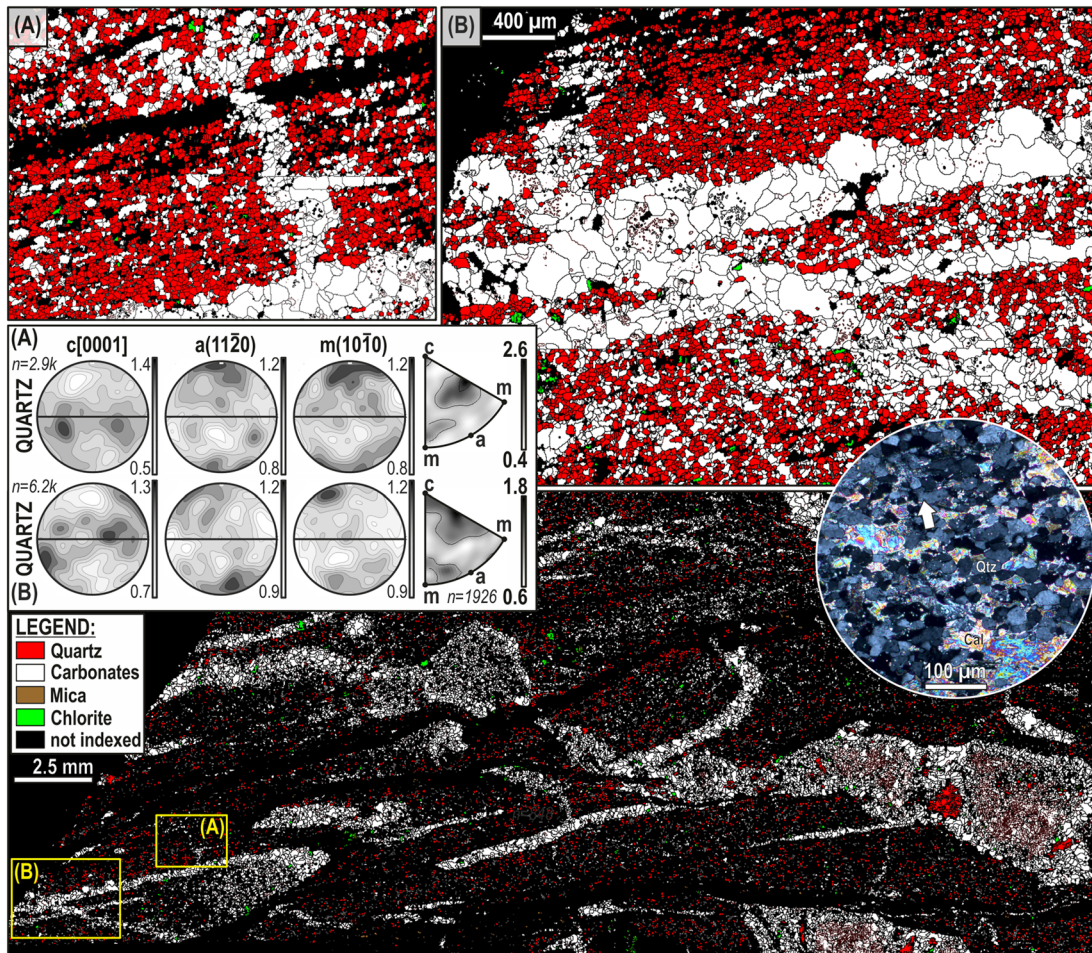


Figure 7.





**Figure 8.** Electron Backscatter Diffraction (EBSD) phase map showing the microstructure of the Ichkeul calcschist with the position of high-resolution maps (a, b). Inset in the overview map shows a photomicrograph of the quartz-rich fine-grained rock matrix in which  $S_1$  foliation develops (horizontal in the image); cross-polarized light photomicrograph. Labels—Cal: calcite; Qtz: quartz; the white arrow indicates an elongated quartz crystal in the plane of the  $S_1$  foliation with shape-preferred orientation being parallel to the macroscopic mineral lineation. Note the undulose extinction of several quartz grains. (a, b) EBSD phase maps (top) and crystallographic orientation of quartz (in the center) in the two selected areas highlighted in the overview map. The same scalebar applies to (a, b). Pole figures show the crystallographic preferred orientation of quartz and inverse pole figures in the quartz crystal reference frame display the rotation axes accommodating low-angle ( $2^\circ$ – $12^\circ$ ) misorientations. Pole figures are lower hemisphere, equal-area stereographic projections; contours are multiples of a uniform distribution with minimum and maximum density values shown beside the gray bars. Pole figures are plotted using the average orientation of each grain (“one point per grain”), horizontal full lines indicate the trace of the  $S_1$  foliation; macroscopic mineral lineation is approximately at  $90^\circ$  (and  $270^\circ$ ) of the pole figures. Labels— $n$ : number of measured grains in the pole figures and number of points in the inverse pole figures. For the interpretation of inverse pole figures and the crystal directions in quartz, see chapter 3.4 in Supporting Information S1.

### 4.3. Microstructural Analysis of the Ichkeul Calcschist

At the thin section scale, the texture of the calcschist is characterized by a penetrative  $S_1$  foliation that disrupts or wraps carbonate-rich mineral aggregates and veins (Figure 8, overview map). Within the foliated rock matrix,

**Figure 7.** Metamorphic greenschist foliation in the Hairech massif and folds, faults and stretching fabrics in the Ickeul massif. (a) Main foliation in a metapsammite from the Hairech massif defined by long K-white mica flakes. Crossed polars image. (b) Moderately inclined anticline in the core of the Ichkeul massif folding the  $S_1$  foliation. The reverse limb is cut by a south-transport thrust with a thick fault breccia in the footwall, shown in inset photograph. (c) Normal faults cutting the southern limb of the Ichkeul dome, with SE-directed extension. These faults form an extensional system that includes low-angle normal faults that separate the Ichkeul massif from the late Miocene to Present Mateur basin. (d) Striated fault scarp cutting the Ichkeul marbles in its footwall and the Mateur basin plain toward the South. The equal area stereoplots show measured faults and striae along the southern margin of the Ichkeul massif. Lower hemisphere projection. (e) Normal fault cutting the Ichkeul marbles foliation with SE-directed transport. (f) Detail of a Riedel fault plane cutting into the main fault plane shown in “e” that indicates normal fault kinematics. (g) Ichkeul marbles showing NW-SE oriented stretching lineation (L1) and L- $S_1$  fabric, later cut by calcite veins.  $S_1$  foliation and stretching lineation measured along the southern limb of the Ichkeul massif, represented in equal-area lower-hemisphere stereoplots. (h) Outcrop example of the L- $S_1$  fabric in the Ichkeul marbles marked by oriented fossils indicating SW-NE directed stretching.



**Table 1**  
Illite Crystallinity Results and Mineralogy of Triassic Pelitic Samples

Samples	Minerals	10 Å		5 Å		$d_{001}$		
		<2 $\mu^*$	WF	<2 $\mu$	WF	<i>b</i> mica	Mica	Chlorite
CHemtou-1	Quartz, mica, Kfds, hematite, smectite $\uparrow$ , kaolinite	0.26	0.26	0.26	0.26	9.032	9.978	
CHemtou-2	Quartz, mica, plagioclase, hematite	0.30	0.28	0.28	0.27	9.038	9.971	
MT-1	Mica, Kfds, quartz $\downarrow$ , jarosite	0.27	0.27	0.25	0.26			
ICH-04	Calcite $\uparrow$ , kaolinite, mica, Kfds	0.29	0.26	0.30	0.25			
ICH-05	Quartz, calcite, mica $\downarrow$ , plagioclase, smectite							
MT-2	Quartz, mica, dolomite, cristobalite	0.32	0.32	0.32	0.29			
MT-3	Quartz, mica, dolomite, cristobalite, Kfds $\downarrow$	0.34	0.31	0.32	0.28			
MT-4	Quartz, mica, smectite, Kaolinite, dolomite $\uparrow$	0.31	0.32	0.32	0.28			
MT-5	Quartz, mica, chlorite, gypsum	0.57	0.46	0.56	0.43			
CH1	Quartz, mica, chlorite, hematite $\downarrow$ , Kfds $\downarrow\downarrow$	0.47	0.46	0.41	0.38	9.029	9.971	14.19
FB-01	Dolomite $\uparrow$ , mica, chlorite, quartz $\downarrow$	0.37	0.37	0.35				14.19
TA-01	Quartz, mica, chlorite, Kfds, plagioclase	0.42	0.42	0.39	0.36	9.024	9.945	14.21
						9.044		
	$\uparrow, \downarrow, \downarrow\downarrow$ = qualitative indication of amount							
	*Anchizone limits (Warr & Ferreiro-Mahlmann, 2015) =	0.52	–	0.32				
	WF—Whole Fraction							

Note. Samples located in the geological map of Figure 2. X-ray diffraction diagrams in Figures S1–S12 in Supporting Information S1.

the major constituent phases are fine- to very fine-grained (<40  $\mu\text{m}$  in diameter) homogeneously intermixed, equidimensional or moderately elongated, anhedral carbonate (mostly calcite) and quartz, but mica, chlorite, clay minerals and opaque accessory phases are also abundant (see inset in Figure 8). The elongated crystals, with aspect ratios up to 3, are distributed in the plane of the  $S_1$  foliation marking a weak mineral lineation (see inset in Figure 8). Quartz grain interiors are usually strain-free accompanied by straight or moderately curved grain boundaries but, particularly in the larger and/or in the elongated grains, undulose extinction, development of subgrain boundaries and serrated grain boundaries are also observed (white arrow in the inset of Figure 8). Calcite shows twinning and displays curvilinear or straight grain boundaries (Figure 8). The veins and mineral aggregates are essentially composed of carbonates that have coarser grain size than the matrix (200–500  $\mu\text{m}$  in diameter) and are interlocking, mostly strain-free grains characterized by straight or moderately curved grain boundaries (Figures 8a and 8b).

In this manuscript we focus only on the microstructural analysis of quartz, because (a) this is the most abundant mineral phase in the  $S_1$  foliation of the studied sample, and (b) it is only present in the rock matrix, that is, unlike calcite, unaffected by the formation of various generations of carbonate-rich aggregates and veins. Quartz in the Ichkeul calcschist has a weak yet non-random CPO characterized by a dominantly girdle-like distribution of [0001]-axes (i.e., *c*-axis) subparallel to the  $S_1$  foliation with maximum density displaying a double-maxima at high angle to the mineral lineation, and a more dispersed appearance of [10–10]-axes (i.e., *a*-axis) along a plane perpendicular to the foliation and subparallel to the mineral lineation with maximum density at high angle to the foliation (Figures 8a and 8b). This CPO is associated with a weak quartz fabric strength (*J*-index: 1.1). The rotation axes accommodating low-angle ( $2^\circ$ – $12^\circ$ ) misorientations are typically observed at *c*(0001), and  $\pi^*$ (01–12) and, less commonly, spread at intermediate crystal directions between *a*(11–20) and *z*(01–11) (Figures 8a and 8b).

## 5. Metamorphic Petrology

We sampled three different types of rocks to investigate the metamorphism of the Permo-Triassic series of the Tell nappe belt in Northern Tunisia. First, we picked metapelites and metapsammites intercalated in Triassic evaporitic series from different outcrops to analyze their illite crystallinity. These samples come from at least two different structural levels, corresponding to deeper Triassic outcrops in the core of the Hairech, Oued Belif, and

Ichkeul massifs and to shallower samples from Tellian Triassic rocks overlying Cretaceous Atlas marls (Figure 2) (samples in Table 1). Second, we sampled metabasite lenses included in the Tellian Triassic, which show a low-temperature polymetamorphic evolution described by Kurtz (1983) (samples Ghzela-a and b, Figure 2). Third, we studied and obtained thermobarometric results from biotite-bearing calcschist layers intercalated in marbles from the Ichkeul massif (sample Ichkeul, Figure 2).

We determined the mineral assemblage and analyzed the composition of different minerals within metabasites, metapsammites and calcschists from both the deeper metamorphic domes and from metabasites at intermediate depths in the Tell nappe stack, using multiple tools including electron microprobe, SEM and RAMAN spectra analysis. The compositions of K-white mica, biotite, paragonite, plagioclase and chlorite were determined using a Camebax electron microprobe from the Granada University. Structural formulae were calculated based on 14 (anhydrous) oxygens for chlorite, 11 for micas and 8 for plagioclase. Rutile was identified with the aid of SEM images, EDX-Spectra (e.g., Figures S13 and S14 in Supporting Information S1) and MicroRaman (Figure S15 in Supporting Information S1).

### 5.1. Illite Crystallinity

X-Ray diffraction results indicates quartz, white mica  $\pm$  K-feldspar  $\pm$  plagioclase  $\pm$  hematite  $\pm$  dolomite  $\pm$  calcite (Table 1). Some of the samples from the Tellian Triassic also contain chlorite or cristobalite and one sample gypsum. Moreover, minerals usually linked to low-temperature alteration processes, like smectite, kaolinite or jarosite exist in the samples in very variable proportions (see X-Ray diffraction results in Supporting Information S1).

Illite crystallinity (KI, e.g., Kübler and Jaberiedoff, 2000) of Triassic metapelites and metapsammites cropping out in the Tunisian Tell indicate variable degrees of low-temperature metamorphism, from epizonal to diagenetic conditions (Table 1, see location in Figure 2). Samples (Chemtou01, Chemtou02, MT-1, ICH-04) picked from the deep autochthonous Triassic outcrops from Oued Belif, Hairech and Ichkeul anticlinal domes are characterized by typical epizonal values between 0.26 and 0.30 (Table 1). The allochthonous Triassic located at the base of the Tellian nappes is characterized by a range between diagenetic values (0.57, MT-5) and mostly anchizonal values between 0.33 and 0.47 (MT-2, MT-3, CH1, FB-01, and TA-01), together with an epizonal value of 0.31 in sample MT-4.

The value of mica *b* parameters in the metamorphic Triassic outcrops is between 9.032 and 9.038 Å, which would be characteristic of orogenic micas grown under an intermediate *P/T* metamorphic gradient (Guidotti & Sassi, 1986). Basal spacing of chlorites obtained in some samples is considerably high (14.19–14.20), which indicates high-Si content (Nieto, 1997), which, in turn, suggests low-temperature chlorites or high-Si bulk rock composition (Vidal et al. (2016) and references therein).

### 5.2. Metamorphic Mineral Assemblages in Metabasites, Impure Marbles and Metapsammites

Impure marble samples from the Ichkeul dome, representing the structurally deepest rocks in Northern Tunisia show a greenschist mineral association defined by chlorite + K-white mica + biotite + quartz + calcite + talc (Figures 9a–9d). The samples from Ichkeul show a L-S metamorphic foliation parallel to the compositional banding ( $S_1$ ) defined by biotite + K-white mica + chlorite + calcite + quartz in Si-Al-Mg-Fe-K-Ca marbles, surrounding domains defined by chlorite + K-white mica + quartz + calcite or by a talc + calcite + dolomite + quartz assemblage in Si-Mg-Fe-Ca marble domains (Figures 9a–9d). Talc shows fibrous intergrowths with quartz and fibrous calcite (Figure 9d). The older calcite-quartz domains are further characterized by showing contrasting calcite fabrics, including fibrous aggregates, growing perpendicular to the main  $S_1$  foliation that are surrounded by a later reaction rim of annealed calcite and ilmenite fabric showing 120° boundaries (Figure 9a). Some K-white mica + chlorite crystals seem transformed to biotite, which forms the most abundant phyllosilicate defining the  $S_1$  L-S fabric. Although, chlorite is also observed growing over previous biotite. Biotite also grows as a later phase, postkinematic to the  $S_1$  foliation and within cracks and calcite veins cutting the main foliation (Figure 9c).

Metabasite blocks occur within the Ghzele detachment at the base of the Tellian Triassic sequence at intermediate depths within the Tunisian Tell nappe belt. These rocks also occur at other Triassic outcrops in Northern Tunisia, near Bazina and in Jebel Baoula, overlying the Atlas Cretaceous rocks (Kurtz, 1983) (Cross-section



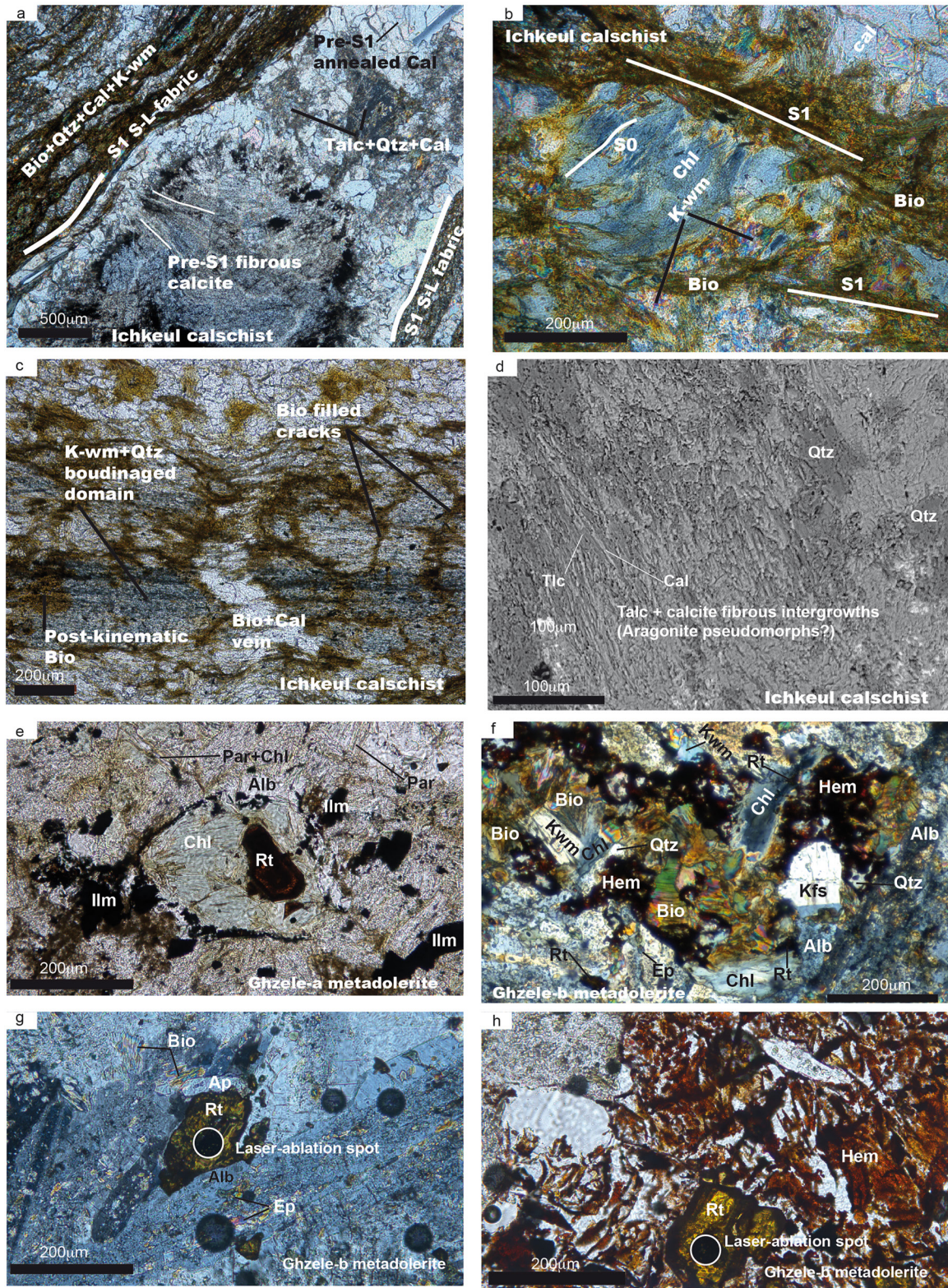


Figure 9.



B-B', Figure 2). Moreover, they are described further south in the Le Kef diapir (Kurtz, 1983). We have studied two metabasite samples from the same outcrop in the Ghzele detachment breccia (Ghzele-a and -b). Metabasite Ghzele-a shows a metamorphic association replacing the original magmatic texture, defined by albite + chlorite + epidote + paragonite + quartz + ilmenite + minor rutile (Figure 9e). Chlorite + rutile replace a previous ferromagnesian mineral, which is outlined by an ilmenite corona (Figure 9e). The original magmatic assemblage may be represented by relic anorthoclase inclusions within albite. Kurtz (1983) describes relic titanomagnetite. However, in sample Ghzele-a the original magmatic iron-titanium phase appears as pseudomorphs.

Metabasite Ghzele-b also preserves its original magmatic texture without developing a metamorphic foliation. Anorthoclase occurs as inclusions in albite with epidote. Ferromagnesian minerals appear as pseudomorphs defined by a chlorite + biotite + rutile + hemo-ilmenite association (Figures 9e–9g). Quartz and K-white mica are also present. Moreover, this sample shows a further transformation where K-rich minerals replace the metamorphic assemblage described in Ghzele-a. These include potassium-feldspar that is later replaced by biotite and minor K-white mica (Figure 9f). Large rutile crystals (200  $\mu\text{m}$ ) are abundant in Ghzele-b sample and appear replacing a previous magmatic iron-titanium phase together with chlorite (Figures 9g and 9h). Large pseudomorphs of ferromagnesian magmatic minerals are presently replaced by biotite + chlorite + K-wm + Qtz + hematite (Figure 9f). Rutile is locally replaced at a later stage by hematite in the above biotite-rich domains (Figure 9f). Hematite and calcite also grow as a late-phase mantle surrounding ferromagnesian- biotite-rich domains, or completely replacing them (Figures 9f and 9h).

Metapsammities of the Hairech massif crop out below the Chemtou marbles of Jurassic protholith. They show a mineral association defined by K-white mica + quartz + albite + rutile, with mica beards growing around quartz detrital grains and long micas parallel to the main foliation (Figure 7a).

### 5.3. Mineral Chemistry

#### 5.3.1. White Mica

White mica in the studied samples is mostly represented by K-white micas that show variable amounts of Si and interlayer cation content both within individual rock samples and between epizonal rock massifs. Paragonite was found in metabasite samples. Tchernomak ( $2\text{Al}^{\text{IV}} = \text{Si}^{\text{IV}} + (\text{Fe} + \text{Mg}^{\text{VI}})$ ) substitution in K-white micas between the celadonite and muscovite end members is strongly influenced by pressure (Massonne & Schreyer, 1987; Massonne & Szpurka, 1997), whilst interlayer cation deficiency between the muscovite and pyrophyllite end member ( $\text{K}^{\text{XII}} - 1\text{Al}^{\text{IV}} - 1\text{Si}^{\text{IV}} \square^{\text{XII}}$ ) is sensitive to a decrease of temperature (Agard et al., 2001; Leoni et al., 1998; Vidal & Parra, 2000). K-white mica from the Ichkeul Massif show Si contents between 3.26 and 3.0 apfu and Interlayer Cation content (IC) between 0.81 and 0.98 apfu (Table S1 in Supporting Information S1 and Figure 10a). K-white mica from the Hairech Massif show strongly variable compositions with Si contents ranging between 3.52 and 3.12 apfu and IC between 0.83 and 0.98 apfu (Figure 10b). K-wm also occurs in Ghzele-b sample, but its presence has been determined using SEM Energy Dispersive X-ray Spectroscopy (EDS).

Paragonite in sample Ghzele-a has variable compositions shown in Table S2. Si content calculated over 11 oxygens ranges between 3.12 and 3.64 apfu. Na content ranges between 0.66 and 0.96 apfu.

#### 5.3.2. Chlorite

Chlorite analysis in the Ichkeul calcschists give Si contents ranging between 2.94 and 2.65 apfu,  $X_{\text{Mg}}$  ( $\text{Mg}/(\text{Fe}^{2+} + \text{Mg} + \text{Mn})$ ) between 0.50 and 0.64 and octahedral summation between 5.77 and 5.90 apfu (Table S2).

**Figure 9.** Metamorphic parageneses and textures in thin sections. (a) Calcschist sample Ichkeul showing the main S-L  $S_1$  biotite-rich fabric overprinting previous vein domains. The earlier domains include quartz-calcite veins with talc, minor dolomite, chlorite and hematite. Calcite shows two contrasting fabrics, with an older fibrous texture oriented perpendicular to the main foliation, overprinted by a later granular mantle of calcite and Fe-oxides, characterized by an annealed texture with calcite forming  $120^\circ$  contacts. (b) Ichkeul calcschist showing the main  $S_1$  S-L fabric, mostly defined by biotite growth affecting a previous domain defined by chlorite + K-white mica. Crossed nicols image. (c) Boudinaged K-white mica and quartz domains with calcite + biotite veins from the Ichkeul sample. Biotite shows late growth also as postkinematic crystals and filling cracks perpendicular to the main  $S_1$  foliation. (d) Backscattered electron image of talc + calcite + quartz fibrous domains in the Ichkeul sample. (e) Mineral association in metabasite Ghzele-a showing the magmatic fabric represented by a ferromagnesian mineral pseudomorph replaced by chlorite + rutile and surrounded by an ilmenite corona. Albite + paragonite + chlorite + ilmenite + quartz grow in the matrix. (f) Biotite rich domain, surrounded by an hematite mantle, in sample Ghzele-b probably replacing a previous magmatic ferromagnesian mineral. Notice biotite and K-white mica form after a previous K-feldspar + chlorite + rutile paragenesis. Rutile occurs as inclusions in chlorite and also out of the biotite domain together with albite and epidote. Crossed nicols. (g) Example of analyzed rutile in sample Ghzele-b among albite with epidote inclusions. Also present biotite and apatite. Crossed-nicols image. (h) Large rutile crystal from Ghzele-b sample surrounded by late growth of hematite and calcite.



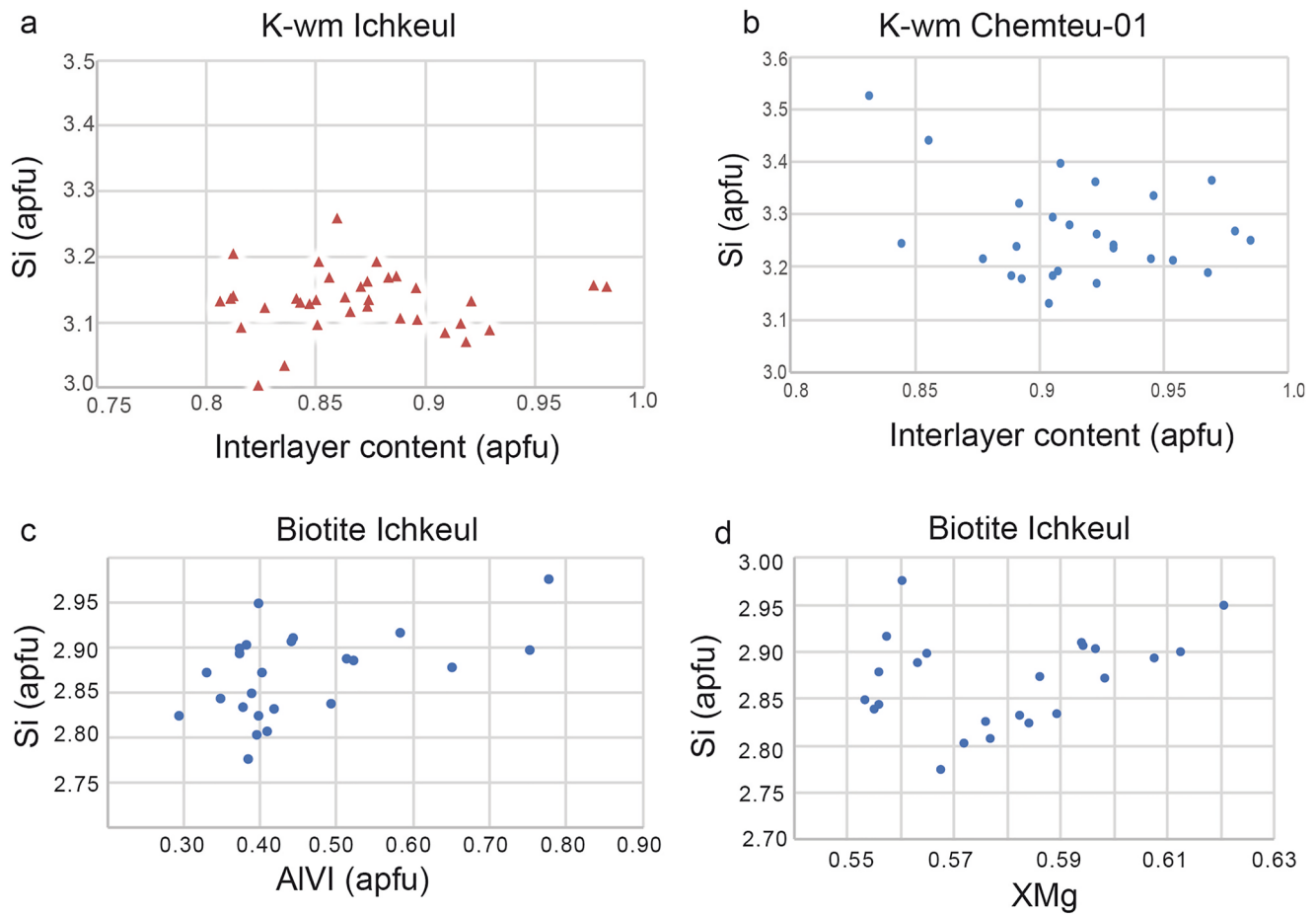


**Figure 10.** Mica composition diagrams. (a) Si-Interlayer cation content of K-white micas from the Ichkeul dome and (b) from metapsammites underlying the Chemteu marbles, from the Hairech massif. (c) Si and  $Al^{VI}$  content in biotite from the Ichkeul sample. (d) Si and  $X_{Mg}$  content in biotite from Ichkeul sample.

$Fe^{3+}$  content in chlorite cannot be determined using the electron microprobe. However, its value is important for thermobarometric calculations in the KFMAS system. We estimate  $Fe^{3+}$  in chlorite by minimizing the differences between P-T conditions resulting from two different equilibrium calculations using thermodynamic properties published by Vidal et al. (2005). The first only involves chlorite end members (Daphnite, Clinochlore, Fe-Amesite, and Mg-Amesite). Since only three of these four end members are independent, this equilibrium must be satisfied to obtain the same solid-solution free energy calculated with either clinochlore, daphnite, Fe-, or Mg-amesite (Vidal et al., 2005). The second equilibrium involves Qtz and  $H_2O$ , within the KMAS system ( $Clin + Sud = Mg-Am + Qtz + H_2O$ ). We obtain values of  $X_{Fe^{3+}}$  between 0.3 and 0.41, below maximum values actually measured in chlorite (Lanari et al., 2014; Trincal et al., 2015). Chlorite in the Ghzele metabasite shows high Si contents ranging between 2.96 and 3.00 apfu,  $X_{Mg}$  from 0.72 to 0.73 and octahedral summation between 5.90 and 5.99 apfu (Table S2).

### 5.3.3. Biotite

Biotite in the Ichkeul calcschists shows variable compositions with Si content between 2.77 and 2.97 apfu,  $X_{Mg}$  from 0.55 to 0.62 considering total Fe as  $Fe^{2+}$  (Table S3 in Supporting Information S1 and Figures 10c and 10d).  $Al^{VI}$  also shows variable content between 0.3 and 0.77 apfu. It is the most abundant mineral in the calcschist intercalations of the Ichkeul marbles growing together with K-white mica and chlorite.

### 5.3.4. Alkali Feldspar

Alkali feldspar in sample Ghzele-a shows two different populations, an older formed by anorthoclase (Na between 0.8 and 0.82 apfu, K between 0.11 and 0.19 apfu and with up to 0.1 apfu of Ca) and younger albite (Na-0.95,

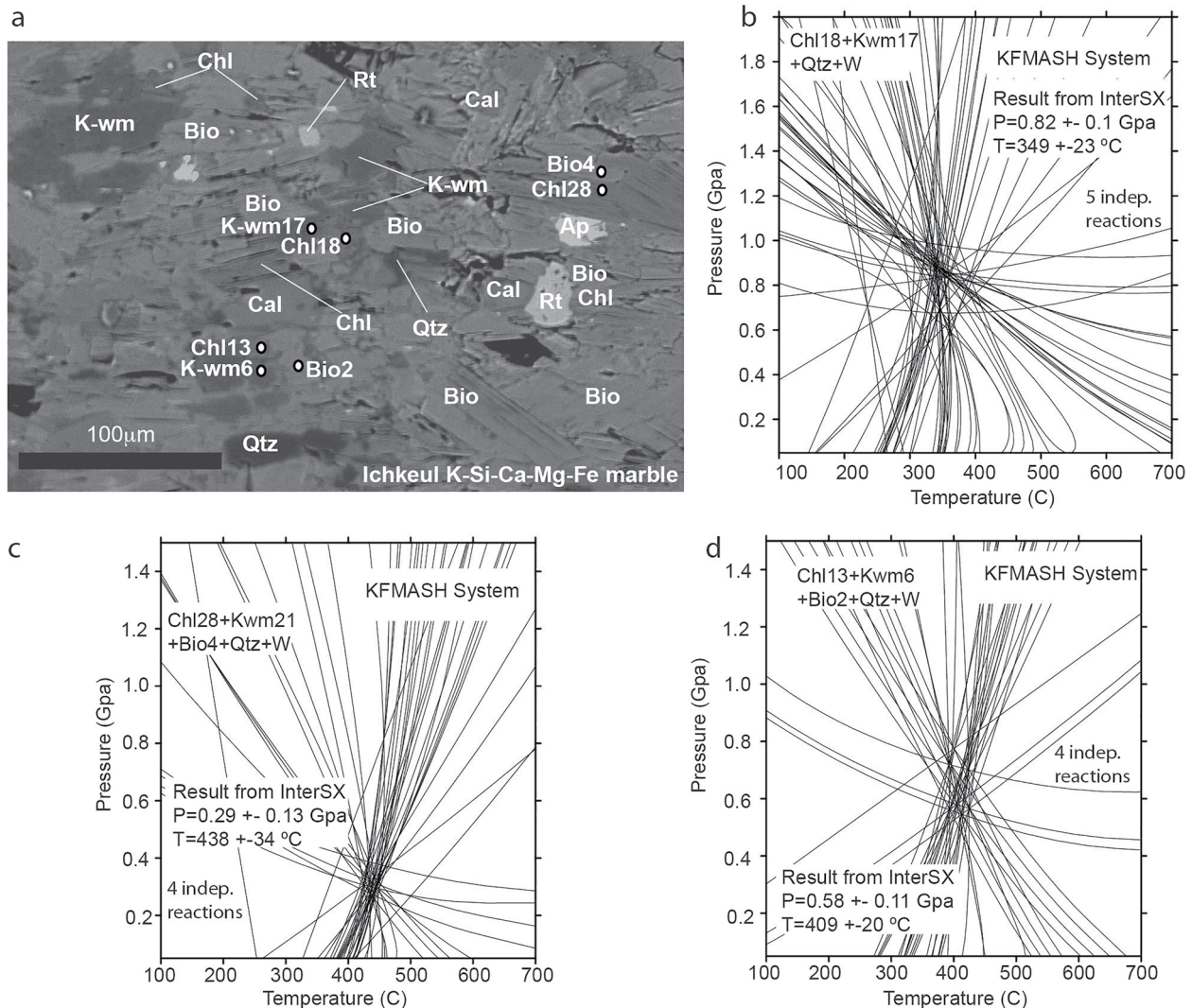


**Figure 11.** TWQ (Berman, 1991) thermobarometric results for the Ichkeul calcschist. (a) Back-scattered electron image with examples of analyzed mineral assemblages from the Ichkeul calcschist. (b) High-Pressure Low-Temperature thermobarometric results obtained for a chlorite + K-white mica + quartz assemblage in the KFMASH system with five independent reactions. (c, d) thermobarometric results for the assemblage biotite + chlorite + K-white mica + quartz + water defining the S<sub>1</sub>, S-L foliation.

K-0.02 and Ca-0.01 apfu) (Table S2). Sample Ghzele-b contains albite and K-feldspar, probably corresponding to microcline that was analyzed only by SEM-EDS (Figure 9f).

#### 5.4. Multiequilibrium P-T Results

We obtained preliminary multiequilibrium P-T data for mineral parageneses defining two metamorphic domains in the Ichkeul marbles (Figures 9a and 9b). The older one is formed by chlorite + K-white mica + quartz within vein domains pre-kinematic to the main L-S fabric and the younger one defining the main S-L fabric includes chlorite + K-white mica + biotite + quartz. Multiequilibrium results were calculated using TWQ 1.02 software (Berman, 1991) and its associated database JUN92, updated with more recent thermodynamic properties and solid solution models for chlorite and K-white mica (Parra et al., 2002; Vidal et al., 1992, 1999, 2001, 2005). Fe<sup>3+</sup> in chlorite was obtained as described in the chlorite mineral chemistry section, above. Calculations were done assuming a water activity of 1.0, which, may be unprecise, although, the presence of talc in these rocks implies high water activity (e.g., Bucher & Grapes, 2011; Eggert & Kerrick, 1981).

Obtained P-T equilibria, with five independent reactions for the pre-S<sub>1</sub> assemblage, show that the Ichkeul rocks reached HP-LT conditions of  $0.82 \pm 0.10$  GPa at  $349^\circ\text{C} \pm 23^\circ\text{C}$  during the growth of phengite-rich K-white micas



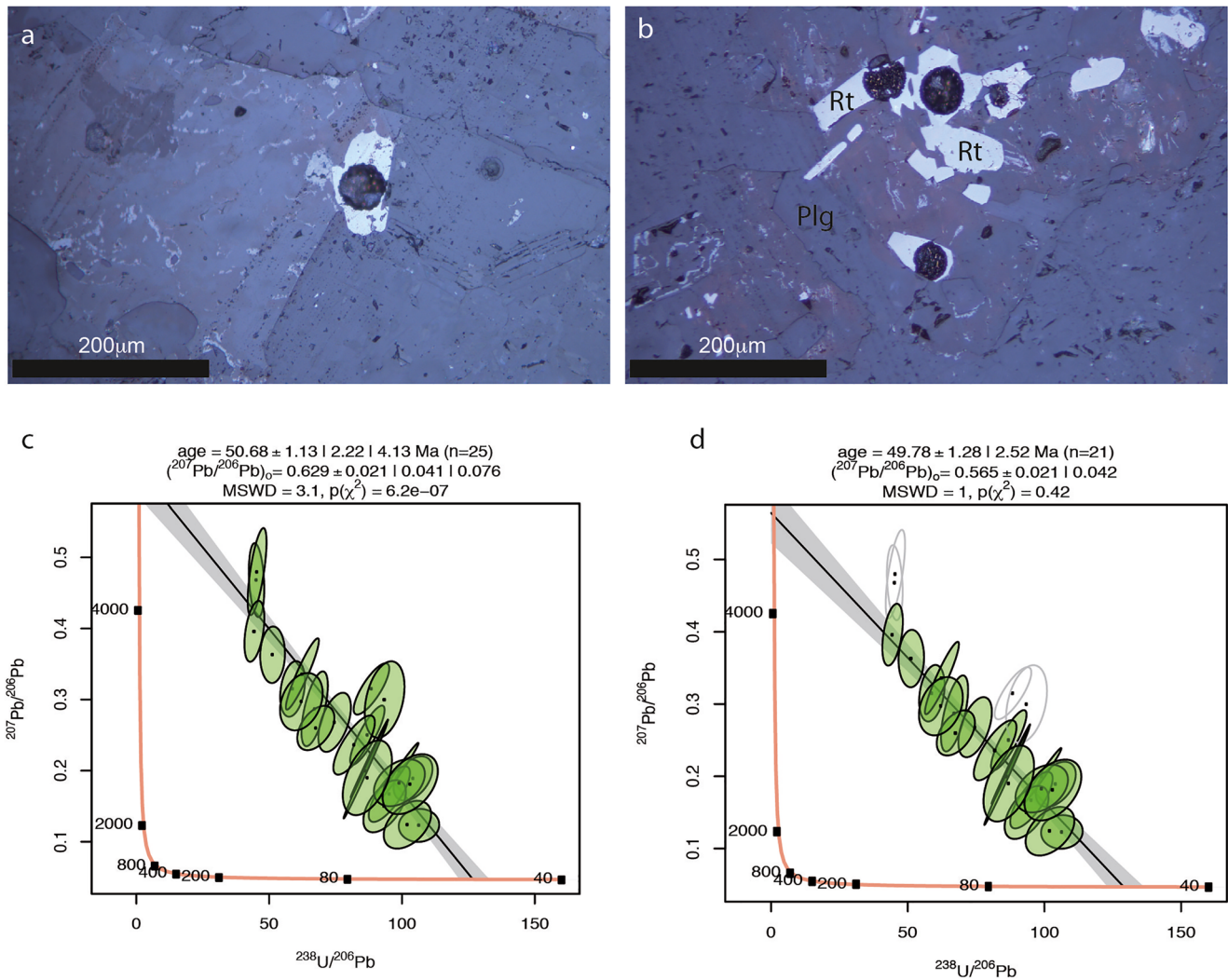


**Figure 12.** Examples of U-Pb dated rutiles and resulting Tera-Wasserburg diagrams. Discordia isochron ages were calculated with IsoplotR (Vermeesch, 2018) using the least-square “York” method without anchored common  $^{207}\text{Pb}/^{206}\text{Pb}$ . Error ellipses in Tera-Wasserburg diagrams are displayed with 95%-confidence level. (a, b) reflected light microscope images of analyzed rutile. (c) Results with all analysis. (d) Results excluding selected analysis shown as gray ellipses.

(Si = 3.26 apfu, Figure 11b). Chlorite, biotite and K-white mica growth defining the later  $S_1$  foliation developed during lower pressure at higher temperature with equilibria using four independent reactions, for example, at  $0.58 \pm 0.11$  GPa at  $409^\circ\text{C} \pm 20^\circ\text{C}$  and  $0.29 \pm 0.13$  GPa at  $438^\circ\text{C} \pm 34^\circ\text{C}$  (Figures 11c and 11d). These conditions would correspond to the  $S_1$  L-S fabric development and deformation under NE-SW stretching in the Ichkeul marbles (Figures 7g, 7h, 8, and 9a).

## 6. Rutile Geochronology

Rutile in thin sections of sample Ghzele-b was searched using SEM (Figure S13 in Supporting Information S1) with energy dispersive X-Ray analysis detectors (Figure S14 in Supporting Information S1) and its nature, instead of anatase, was corroborated using RAMAN spectra (Figure S15 in Supporting Information S1). We show the analysis and dating procedure in Text S1 in Supporting Information S1. Metamorphic rutile crystals were analyzed by LA-ICP-MS both in the albite + epidote matrix of the metabasites (Figure 9g) and within ferromagnesian rich retrograded domains (Figure 9h). The analyses are provided in Table S4.

Rutile have sufficient U and Pb content to be accurately dated. Rutile compositions suffer from a variable proportion of common Pb as reflected by the spread of the discordant data points in the Tera-Wasserburg  $(^{207}\text{Pb}/^{206}\text{Pb})$

vs.  $^{238}\text{U}/^{206}\text{Pb}$ ) diagram in Figures 12c and 12d. The observed spread in Tera-Wasserburg diagrams is commonly thought to result from a combination of common and radiogenic lead in varying proportions. In this scenario, the Concordia lower intercept is the estimated age of the crystallization of the rutile populations, as determined by the regression analysis. Figure 12c shows the results with all 25 analysis yielding a Tera–Wasserburg lower intercept date of  $50.68 \pm 1.13$  Ma (2 SE,  $n = 25$ , MSWD = 13.1). Excluding the four analysis with the largest error (plotting slightly away from the regression line and shown as gray ellipses) yields a lower-intercept date of  $49.78 \pm 1.28$  Ma (2SE,  $n = 21$ , MSWD = 1.0) (Figure 12d). These U-Pb dates likely reflect the age of the crystallization event of rutile between *c.* 51 and 48 Ma.

## 7. Discussion

### 7.1. Low-Temperature Metamorphism in the Tunisian Tell

The new illite crystallinity data and metamorphic assemblages we show in this study together with previous data in the region (Mahdi et al., 2013) manifests the presence of lower-greenschist epizonal rocks in the core of the structurally-deepest Triassic outcrops of Northern Tunisia (Table 1, cross-sections and samples in Figure 2). These Permo-Triassic rocks have been interpreted as forming the outcropping base of the Mesozoic Atlasic sedimentary cover, deposited in the North Maghrebian passive margin (Booth-Rea et al., 2018; Rouvier, 1992, 1993). The fact that these minerals show clear metamorphic textures and illite crystallinity values below the limit between anchizone and epizone imply they underwent temperatures above 300°C characteristic of mid-crustal depths (Frey, 1987; Merriman & Peacor, 1998; Merriman & Roberts, 1985). Some samples contain variable proportions of smectite, kaolinite and jarosite, which are low-temperature minerals probably resulting from fluid-mediated retrograde processes occurring under diagenetic conditions (Abad et al., 2003; Nieto et al., 2005).

The scattering of KI values for the Tellian Triassic metapelites and metapsammities that crop out, intercalated within evaporites, in a large area all along Northern Tunisia may represent original depth differences within the Tell orogenic wedge. The diagenetic value in sample MT-5 is located to the SE, theoretically, close to the Tell deformation front, where the Triassic is directly covered by early Miocene fore-deep olistostromic sediments at the Lansarine ridge (Figure 2). Most of the samples further toward the W or NW give anchizonal values, reflecting an original deeper position within the orogenic wedge. Sample MT-4 with epizone values is located at the footwall of the Ghzela extensional detachment a few meters below the fault zone, in the Jalta Pb-Zn mine, coexisting with the studied metabasites, which underwent greenschist facies metamorphism (Figures 9e and 9f).

The illite crystallinity data are further supported by the mineral associations we found in the Ichkeul calcschist and marbles, including biotite + K-wm + chlorite + quartz + calcite (Figure 9a) and calcite + dolomite + talc + chlorite + hematite (Figures 9b and 9d), respectively, which would require temperatures between 300°C and 470°C, in the stability of talc and biotite and below the stability of tremolite (Bucher & Grapes, 2011; Letargo et al., 1995). Epizonal conditions obtained in the Hairech massif are supported by a lower-greenschist mineral assemblage found in metapsammities including K-white mica + albite. However, analyzed K-white micas in these rocks show strongly variable compositions in the Si-Interlayer Cation diagram that may indicate a mixture of metamorphic and detrital micas (Figure 10b), suggesting this massif reached lower temperatures than the biotite bearing rocks in Ichkeul.

Multiequilibrium thermobarometric results for the deepest outcrops of the Tunisian Tell, corresponding to the Ichkeul marbles, indicate that the main foliation in these rocks developed between HP-LT blueschist facies at approximately 0.8 GPa and 350°C, and greenschist conditions of 0.6–0.3 GPa and 400°C–440°C (Figure 11). Given that large K-mica Si-rich crystals show biotite reaction rims and are overgrown by biotite, which also grows as a later phase in calcite veins or postkinematic to the  $S_1$  foliation (Figure 9c), our results indicate that most of the biotite and the  $S_1$  L-S fabric developed under higher temperature than the pressure peak conditions. Chlorite grew together with early K-white mica in pre- $S_1$  vein domains (Figure 9b) and also overgrowing biotite (Figure 11a).

EBSD data from the Ichkeul calcschist show that the  $S_1$  fabric has an associated quartz CPO, also evidenced by a NE-SW trending object lineation at outcrop scale (Figures 7g and 7h). The fine-grained quartz forming the rock matrix is exclusively distributed in the plane of the  $S_1$  foliation. It develops a shape preferred orientation parallel to the macroscopic mineral lineation, often having undulose extinction accompanied by straight subgrain boundaries and serrated grain boundaries, and it exhibits a penetrative, non-random CPO correlated to the structural elements of the rock (Figure 8). Altogether, these observations indicate that—associated to the development of



$S_1$  foliation—dynamic recrystallization processes (subgrain rotation and strain-induced grain-boundary migration) and crystalplastic deformation by dislocation creep were active in quartz. These processes are proposed to play an increasing role in the deformation of quartz as a function of temperature above ca. 300°C (e.g., Hirth & Tullis, 1992). Moreover, the CPO and the distribution of rotation axes accommodating subgrain-level (2°–12°) misorientations in quartz from the Ichkeul calcschist (Figures 8a and 8b) are consistent with the activation of Rhomb $\langle a \rangle$ , Prism $\langle a \rangle$  and, of minor importance, Rhomb $\langle c + a \rangle$  slip systems in this mineral phase (cf. Figure S16 in Supporting Information S1). Although, the slip system activity and the development of CPO symmetries in quartz depend on many additional variables—such as, for example, water content, strain rate and/or grain size—temperature is considered to be an important one (see Law (2014) for a review). Based on the results of Stipp et al. (2002) the slip systems proposed to be responsible for the intracrystalline deformation of quartz—hence the formation of  $S_1$  foliation in the Ichkeul calcschist—would preferentially develop at moderate temperatures (ca. 350°C–550°C). Alternatively, the very weak CPO of the Ichkeul calcschist and the minor parallelism of the quartz  $c$ -axis to the deformation flow (without the activation of the high-temperature Prism $\langle c \rangle$  slip) may be the result of dissolution-precipitation processes accompanying or overprinting the intracrystalline deformation of the fine-grained quartz assemblage (e.g., Bons & den Brok, 2000; Hippertt, 1994; Kilian et al., 2011). The overall weak quartz fabric, the straight grain boundaries and the strain-free appearance of some quartz crystals (as well as carbonate minerals in the veins, Figure 8) may be affected by a later thermally-induced annealing coeval to post-kinematic biotite growth in the calcschist. Significant quartz grain growth during this static recrystallization stage was probably impeded by pinning due to the abundance of second phase particles dispersed in the rock texture.

The Triassic rocks cropping out above the Ghzela and Mejerda extensional detachments, at the base of the Tellian nappes, reached anchizonal to diagenetic conditions below 300°C. Although, locally, sample MT-04 reached epizonal conditions above 300°C. These higher metamorphic conditions would explain the growth of biotite, paragonite, K-feldspar and rutile in metabasites included in these rocks (samples Ghzele a and b). Global composition of the metabasites indicates largely differentiated rocks with up to 52%–55% SiO<sub>2</sub> and 6%–13% K<sub>2</sub>O (Kurtz, 1983), containing a large proportion of magmatic anorthoclase. Mineral associations in samples Ghzele-a and b indicate a prograde metamorphic evolution with the initial breakdown of igneous anorthoclase to produce albite with epidote inclusions + Kfcs, whilst ferromagnesian minerals react to produce ilmenite + chlorite ± rutile. Rutile may have been initially in equilibrium with ilmenite, although, in sample Ghzele-b, rutile is abundant and ilmenite is rare, indicating the HP-replacement of ilmenite + silicate + H<sub>2</sub>O by rutile + chlorite (e.g., Luvizotto et al., 2009). The growth of K-feldspar and biotite in the metabasites was interpreted initially as related to a metasomatic phase (Kurtz, 1983). However, the presence of magmatic anorthoclase in these rocks offers a primary magmatic source for K and thus, the growth of microcline, which is later replaced by biotite can be related to successive prograde metamorphic reactions (Simpson et al., 2000).

The HP/LT thermobarometric results in the Ichkeul marbles indicate that the epizonal dome reached a typical orogenic P-T gradient of approximately 13°C/km during a HP-LT metamorphic event and was exhumed from under approximately 26 km overburden provided by the Tell-Flysch nappe stack. The exhumation path of the Ichkeul marbles is marked by the growth of biotite defining the main S-L  $S_1$  fabric and dated between 23 and 17 Ma (Bellon & Perthuisot, 1977). Thus, this process may reflect early Miocene syn-orogenic exhumation in the subduction channel as proposed for other Western Mediterranean nappe belts (Booth-Rea et al., 2015; Ryan et al., 2021). This evolution parallels the one observed in the Betics and external Rif (e.g., Azañón et al., 1998; Booth-Rea et al., 2002; Jabaloy-Sánchez et al., 2015; Negro et al., 2007). Coeval ductile early Miocene exhumation is also registered nearby in the Edough core complex in northeastern Algeria where UHP late Eocene metamorphic rocks and diatexites, including part of the subducted African lower crust, are exhumed by a mylonitic shear zone below greenschist Tellian rocks (Bruguier et al., 2017; Caby et al., 2014; Caby et al., 2001), comparable to the ones in the Ichkeul massif. A later post-orogenic extensional phase is evidenced by the present structure of the Tell belt that shows extensional listric fans overlying LANF at least at two different structural levels, corresponding to the Ghzela and Mejerda detachments, and the deeper Nefza detachment that flattens around 3s TWT (Booth-Rea et al., 2018). The younger Nefza detachment and overlying normal faults finally exhumed the mid-crustal rocks.

## 7.2. Late Cretaceous, Eocene and Early Miocene Orogenic Metamorphism in Northern Tunisia

Rutile grew together with chlorite and paragonite in the Ghzele samples (Figure 9e). Given that these rocks underwent temperatures below the Pb closure temperature in rutile, estimated between 490 and 650°C (Cherniak, 2000; Gao et al., 2014; Kooijman et al., 2010), we interpret the U-Pb c. 51 to 48 Ma age obtained for rutile in sample

Ghzele-b as a peak pressure metamorphic growth age (Figure 12). Integrating our new rutile results with previously published radiometric dating indicates a polymetamorphic evolution for the Tunisian Tell, similar to the one observed at the opposite end of the Maghrebic Alpine chain, in the Rif (Jabaloy et al., 2015; Vázquez et al., 2013). The only existing radiometric ages in metamorphic minerals of the Tunisian Tell are K-feldspar and phlogopite K-Ar ages from metabasites and marbles from different outcrops that give late Cretaceous ( $97 \pm 5$  to  $67 \pm 3$  Ma), Palaeocene ( $65 \pm 3$  Ma), Oligocene ( $27 \pm 1$  to  $25 \pm 1$  Ma) and Miocene ages ( $23 \pm 1.2$  to  $17.6 \pm 0.9$  Ma) (Bellon & Perthuisot, 1977) (Figure 3). Although, this age dispersion was interpreted as a result of Cretaceous extensional-sedimentary load related metamorphism, mixed with radiometric resetting by late Neogene magmatic heating in the region (Bellon & Perthuisot, 1977), we provide a new alternative scenario.

Although, the validity of the Bellon and Perthuisot (1977) ages need testing using more reliable Ar-Ar ages, most of these ages may represent distinct metamorphic events, related to the geodynamic evolution of the Western Mediterranean. Older late Cretaceous K-feldspar K-Ar ages, between 97 and 69 Ma, were obtained toward the South in more external outcrops (Bellon & Perthuisot, 1977) and may correspond to an early phase of greenschist metamorphism. This early metamorphic evolution may be related to the sedimentary-related overburden during crustal extension or even with shortening along the North-Maghrebic passive margin, related to the late Cretaceous initial Africa-Eurasia plate convergence (Dewey et al., 1989). Equivalent ages and metamorphic conditions were obtained for anchizonal rocks of the Ketama unit in the external Rif, interpreted as extension related metamorphism (Jabaloy et al., 2015; Vázquez et al., 2013).

The new rutile U-Pb c. 51 to 48 Ma age for metabasites of the Tellian Triassic may be related to palaeogene K-Ar ages obtained from K-feldspar, phlogopite and phengite, between  $45 \pm 2$  and  $25 \pm 0.9$  Ma in more internal Triassic outcrops, in a similar structural position (Bellon & Perthuisot, 1977). These ages may represent initial subduction of the Tethys oceanic crust and crustal thickening at the transition between the North Maghrebic passive margin and the Tethys ocean, producing the superposition of the Kabylia Cretaceous flysch over Tellian nappes (Figure 13a). This crustal thickening and related deformation favored the mineral blastesis in the Tellian metabasites producing rutile + chlorite paragenesis (Figures 9e and 9g). Between the Cretaceous and Eocene, subduction was active in the Alps (Malusà et al., 2015; Rubatto et al., 1998; Villa et al., 2014) and along the Apennine-Maghrebic subduction system (Martin et al., 2011). HP metamorphism in Corsica gives early Eocene  $54 \pm 8$  Ma rutile U-Pb ages (Maggi et al., 2012) that was followed by early to late Eocene 50–30 Ma  $^{39}\text{Ar}/^{40}\text{Ar}$  ages related to thrusting in the Corsica basement (Rossetti et al., 2022). Eocene HP/LT metamorphism was also registered in the AlKaPeKa upper-plate, for example, in the Alpujarride rocks of the Alboran domain (38 Ma  $^{39}\text{Ar}/^{40}\text{Ar}$  ages, Bessière et al., 2022; Marrone et al., 2021). Rutile blastesis in Northern Tunisia also coincides with shortening along the Atlas in the latest Cretaceous–Eocene (Frizon de Lamotte et al., 2009). Furthermore, Eocene shortening has also been invoked to explain the unconformity between metamorphic Cretaceous Kabylia flysch units outcropping in Northern Algeria and the overlying later Oligo-Miocene Numidian flysch (e.g., Wildi, 1983). Eocene to early Oligocene subduction is further supported by volcanic arc zircons within the Tethys flysch units ( $33 \pm 1$  Ma, Fornelli et al. (2020) and 40–28 Ma in the Rif, Abbassi et al. (2021)).

The Tellian metabasites crop out among anchizonal to epizonal Triassic evaporites at the base of the nappe stack, sandwiched between lower-grade Cretaceous or younger sediments. The underlying Cretaceous of the Atlas series reached conditions between immature and early to mid-mature oil generation according to Rock-Eval pyrolysis testing (Ben Ammar et al., 2020), implying temperatures probably below 150°C (e.g., Buller et al., 2005). Similar Cretaceous sediments overlie the Triassic evaporites. Thus, a double metamorphic gap occurs between the Tellian Triassic and its Cretaceous enveloping sediments that may be related either to older syn-orogenic extension, coeval to thrusting over the underlying Cretaceous, or to the late Miocene extensional phase overprinting the early Miocene nappe stack. In both cases, the early Eocene crustal thickening-related metamorphism occurred before the establishment of the present Tellian nappe stack, in a transitional region between the Tethys oceanic crust and the Maghrebic passive margin. Furthermore, the fact that Triassic outcrops, previously interpreted as Cretaceous salt glaciers, located to the south of the Tellian-Atlas boundary also contain Eocene metabasites (Bellon & Perthuisot, 1977) suggests that the Tellian nappe belt continued further South than presently acknowledged.

NW-directed subduction of the Tethys ocean was followed by continental subduction and collision producing UHP diamond growth in rocks of the Maghrebic lower crust, presently outcropping beneath the Kabylia Flysch and Tellian units at the Edough massif in NE Algeria (Caby et al., 2014; Caby et al., 2001). Rutile related to this UHP metamorphism was dated as early Oligocene ( $32.4 \pm 3.3$  Ma, Bruguier et al., 2017; Figure 13b). This age for



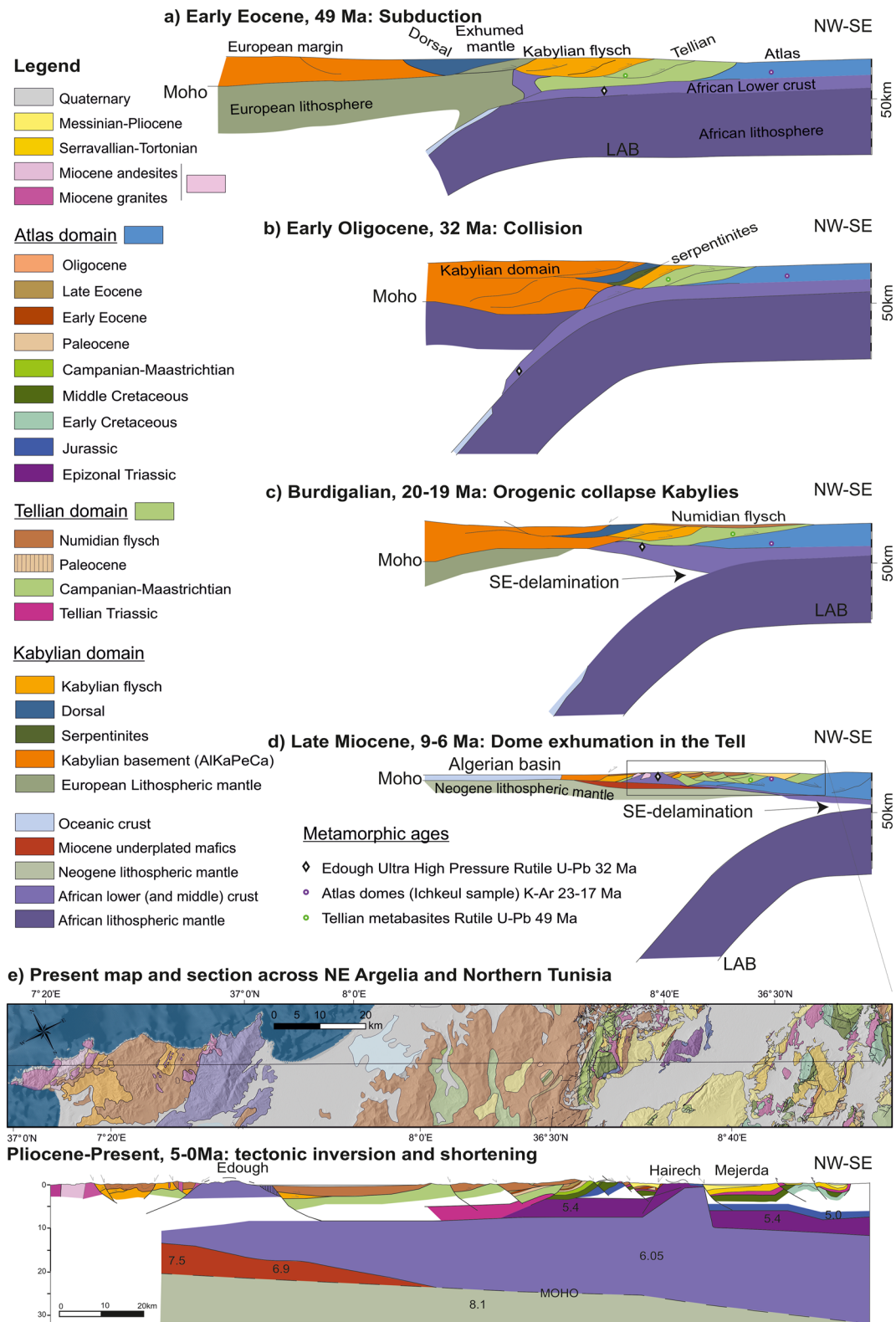


Figure 13.

continental collision in NE Algeria suggests the complete closure of the Tethys ocean in the central-western Mediterranean region at the time, implying that the later Oligocene to Early Miocene Numidian Flysch must have deposited upon the metamorphosed Kabylia Flysch and Tellian nappe domains, in a continental foredeep setting (Figure 13c).

The main phase of nappe stacking of the Tunisian Tell over the Atlas domain is dated as early Miocene by the overthrusting of the Oligocene to Burdigalian Numidian Flysch sandstones and their Tellian substrate over late Burdigalian to Langhian sediments of the Glauconite formation (Belayouni et al., 2013; Figure 3). Phlogopite in the Ichkeul marbles at the base of the Atlas domain gives  $23 \pm 1.2$  and  $17.6 \pm 0.9$  Ma ages (Bellon & Perthuisot, 1977), encompassing the early-Miocene nappe stack development (Figure 13c). However, the late-stage growth of biotite during heating and decompression suggests that the younger ages may reflect the initial extensional collapse of Northern Tunisia, which had already occurred in the internal Kabylies in Algeria, marked by late-stage K-rich magmatism intruding the nappe stack, dated at 17 Ma (Abbassene et al., 2016; Chazot et al., 2017) (Figures 3 and 13c). Early to middle Miocene magmatism in Northeastern Algeria and middle to late Miocene (12–6 Ma) in the Tunisian Tell was probably accompanied by important magmatic mafic underplating, evident from  $V_p$  velocities between 7.5 and 6.9 km/s at the base of the crust in the N-S EGT'85 line (Research Group for Lithospheric Structure in Tunisia, 1992) (Figures 13d and 13e).

Several domains of the Western Mediterranean underwent alternating extensional and shortening events in the Cenozoic including the Alboran domain (e.g., Balanyá et al., 1997; Booth-Rea et al., 2005; Hidas et al., 2013), the Valencia trough (Fontboté et al., 1990) and the Kabylies (Caby et al., 2001) (Figure 3). This may have occurred also in Northern Tunisia, with possible crustal extension occurring between the Eocene and early Miocene shortening events, or, being synorogenic, coeval to shortening in the footwall, and should be further studied in the future.

### 7.3. Halokinetic Structures in Northern Tunisia

We find two main types of Triassic outcrops, the shallower of which, develop halokinetic structures related mostly to late Neogene extension, and the deeper ones are represented by exhumed greenschist rocks of Triassic protoliths. The first type of Triassic bodies outcrop extensively in the Thibar, Lansarine or Bazina regions and have traditionally been interpreted as salt canopies or glaciers overlying the Atlas Cretaceous series (e.g., Amri et al., 2020; Ayed-Khaled et al., 2015; Masrouhi et al., 2014). However, these sheet-like bodies are not only overlain by Cretaceous sediments, but also by tilted extensional riders of Eocene Tellian limestones and late Miocene sediments. For example, in Ghzela, at the Jalta mine, and Mateur basin (Booth-Rea et al., 2018), in the Lansarine ridge (Gaidi et al., 2020; Figure 6e) or in the Mejerda basin (Seismic lines and cross section A-A', Figures 2 and 4). Moreover, the fact that the Triassic evaporites underwent early Eocene epizonal metamorphism means they juxtaposed the underlying Cretaceous sediments during a later thrusting stage.

We interpret that the shallower anchizonal to diagenetic Tellian evaporites and redbeds were originally located at the base of the Tellian nappes and were later reworked by the Mejerda and Ghzela extensional detachments and related normal faults, developing shallow-depth halokinetic structures rooting in the extensional LANFs. Thus, these Triassic outcrops are not salt glaciers nor are they sourced from the base of the underlying Atlas series as proposed by previous authors (e.g., Amri et al., 2020; Ayed-Khaled et al., 2015; Frifita et al., 2020; Masrouhi & Koyi, 2012; Rouvier, 1992, 1993). These evaporitic outcrops form salt walls along the main high-angle normal faults, define the main extensional detachments, and also form small diapiric bodies rooting in the LANFs

**Figure 13.** Schematic tectonic evolution of the Algerian-Tunisian Maghreb chain between the early Eocene and Present. Tectonic restoration does not preserve areas because of large displacements perpendicular to the chosen section, for example, by the E-W development of the Algerian basin (Haidar et al., 2022) and the orogenic collapse of Northern Tunisia (Booth-Rea et al., 2018). (a) Ypresian subduction of the Tethys oceanic crust and development of the Kabylia Flysch and Tellian margin orogenic wedge. Metamorphism of the Tellian Triassic metabasites dated by rutile U-Pb at  $49.78 \pm 1.28$  Ma. (b) Early Oligocene collision of the Kabylia and North Maghreb domains and UHP metamorphism in the African subducted lower crust dated by rutile U-Pb at  $32.3 \pm 3.3$  Ma (Bruguier et al., 2017). (c) Early Miocene orogenic collapse in the Kabylia domain of NE Algeria. Overthrusting of the Tell over the Atlas domain and metamorphism of the Atlas Triassic series. Dated by K-Ar at 23–17 Ma (Bellon & Perthuisot, 1977). Deposition of the Numidian Flysch over the Tell foredeep domain, which initiated in the Oligocene. (d) Late Miocene extensional collapse and dome exhumation in Northern Tunisia. Crustal thinning and magmatic intrusions, including underplating of mafic rocks at the base of the crust under Northeastern Algeria and Northern Tunisia initiated in the early-middle Miocene. Shortening at the time propagated southeastwards into the Central Tunisia. (e) Geological map and cross section through Northeastern Algeria and the Tunisian Tell. The geological base is taken from Wildi (1983) with modifications by Caby et al. (2001) and Marignac et al. (2016) on the Algerian side. The Tunisian segment of the map is based on 1:50,000 geological maps of the Office National des Mines (ONM), digitized in Gaidi et al. (2020).  $P$ -wave velocities plotted in the lower and middle crust across the section are projected from the N-S EGT'85 line, which cuts across the Hairech massif (Research Group for Lithospheric Structure in Tunisia, 1992).



(Figures 4 and 5). Moreover, these structures have been re-used and inverted during the later Plio-Quaternary shortening in the region (Gaidi et al., 2020).

The deeper Triassic bodies are found in antiformal dome-type outcrops, where epizonal and HP/LT orogenic crust has been exhumed from midcrustal depths in the Oued Belif, Ichkeul and Hairech massifs (cross sections A-A' and B-B', Figure 2). These metamorphic domes were produced by extensional exhumation of the North Tunisian orogenic middle crust during the middle to late Miocene and do not represent diapirs or salt domes as proposed by previous authors (e.g., Amiri et al., 2011, 2020; Ayed-Khaled et al., 2015; Frifita et al., 2020; Khelil et al., 2019) (Figures 13d and 13e).

#### 7.4. Extensional Exhumation in Northern Tunisia

Our field and geophysical evidence shows different systems of extensional faults that detach at two different structural levels within the Tell nappe stack (Booth-Rea et al., 2018). The shallower LANF, represented by the Ghzela and Mejerda detachments that show NE- and SW-directed extension, cut down into the Mesozoic Atlas sequence producing the Mateur and Mejerda basin depocenters. These faults exhume mostly the Eocene to Cretaceous Atlas sequence. The younger extensional structures produce mostly SE-directed extension and are formed by a system of high-angle listric faults that cut the above detachments and root at depths of approximately 3s TWT. These faults bound the Hairech (cross section A-A', Figures 2 and 13e) and Ichkeul massifs (Figures 7c and 7d) and outcrop along the Lansarine massif, where the Tellian Triassic and overlying early to late Miocene sediments are tilted over a low-angle normal fault with SE-transport cutting down into Cretaceous Atlas sediments (Gaidi et al., 2020; Figure 6e).

The extensional systems worked sequentially, the first system produced mostly E- to NE-directed extension during the Tortonian ( $\approx 11$ –8 Ma), and maybe including the Serravallian, with the development of brittle LANFs like the Mejerda, Ghzele and brittle-ductile shear zones like the Nefza detachment. The final exhumation of these midcrustal rocks to the surface was accomplished by a later orthogonal extensional system, producing mostly southwards-directed extension during the Tortonian to Messinian ( $\approx 8$ –6) Ma. High-angle normal faults, cutting LANFs of this later system are the structures that presently bound the Hairech and Ichkeul mid-crustal dome structures (Figures 5 and 7d, cross-sections in Figure 2).

This work shows that the main tectonic boundaries present in the Tunisian Tell were reworked during the late Miocene extensional collapse (Figures 13d and 13e). The remains of the original nappe pile are cut, tilted and displaced by LANF and extensional detachments that exhumed the Tunisian orogenic middle crust, producing tectonic omissions and metamorphic gaps in the lithological sequences, during the late Miocene (cross section A-A', Figures 2, 6f, 13d, and 13e). The exhumation of midcrustal domes is further supported by seismic-refraction EGT'85 North-South line that shows the high-velocity crustal material (6.05 km/s) reaching the surface at the Hairech ridge (Research Group for Lithospheric Structure in Tunisia, 1992) (Figure 13e). The late Miocene extension in Northern Tunisia propagated southeastwards during the Pliocene to Quaternary, affecting large regions of Central Tunisia, the Sicilian Channel and the Pelagian domain offshore (Arab et al., 2020; Belguith et al., 2011, 2013; Civile et al., 2010). This crustal thinning probably initiated in the middle Miocene concomitant to oceanic spreading of the easternmost Algerian basin (Haidar et al., 2022) (Figure 14).

#### 7.5. Extensional Tectonics and Related Geodynamic Features of Tunisia

This tectonic model for Tunisia explains many geophysical features of the region that are not explained by a model of protracted, only shortening, since the Cretaceous and has to be taken into consideration when restoring and defining the main orogenic belts in Northern Tunisia. Our work shows that allochthonous anchizonal Triassic rocks we have attributed to the Tellian domain crop out to the South of the classical Tell boundary, indicating that the Tell orogenic wedge originally occupied a larger region toward the south than presently considered. Actually, the boundaries established for this orogenic belt coincide with the Present position of active shortening structures that formed since the Pliocene, like the Alia-Thibar fault system (Gaidi et al., 2020), which produces the main seismicity in the area (Soumaya et al., 2015) and accommodates most of the GPS measured shortening of the region (Bougrine et al., 2019).

Heat flow in Tunisia shows present-day values around 80–90 mW/m<sup>2</sup> with higher values toward the E of Tunisia (Lucazeau & Dhia, 1989). This heat flow is higher than observed in typical active fold and thrust belts around

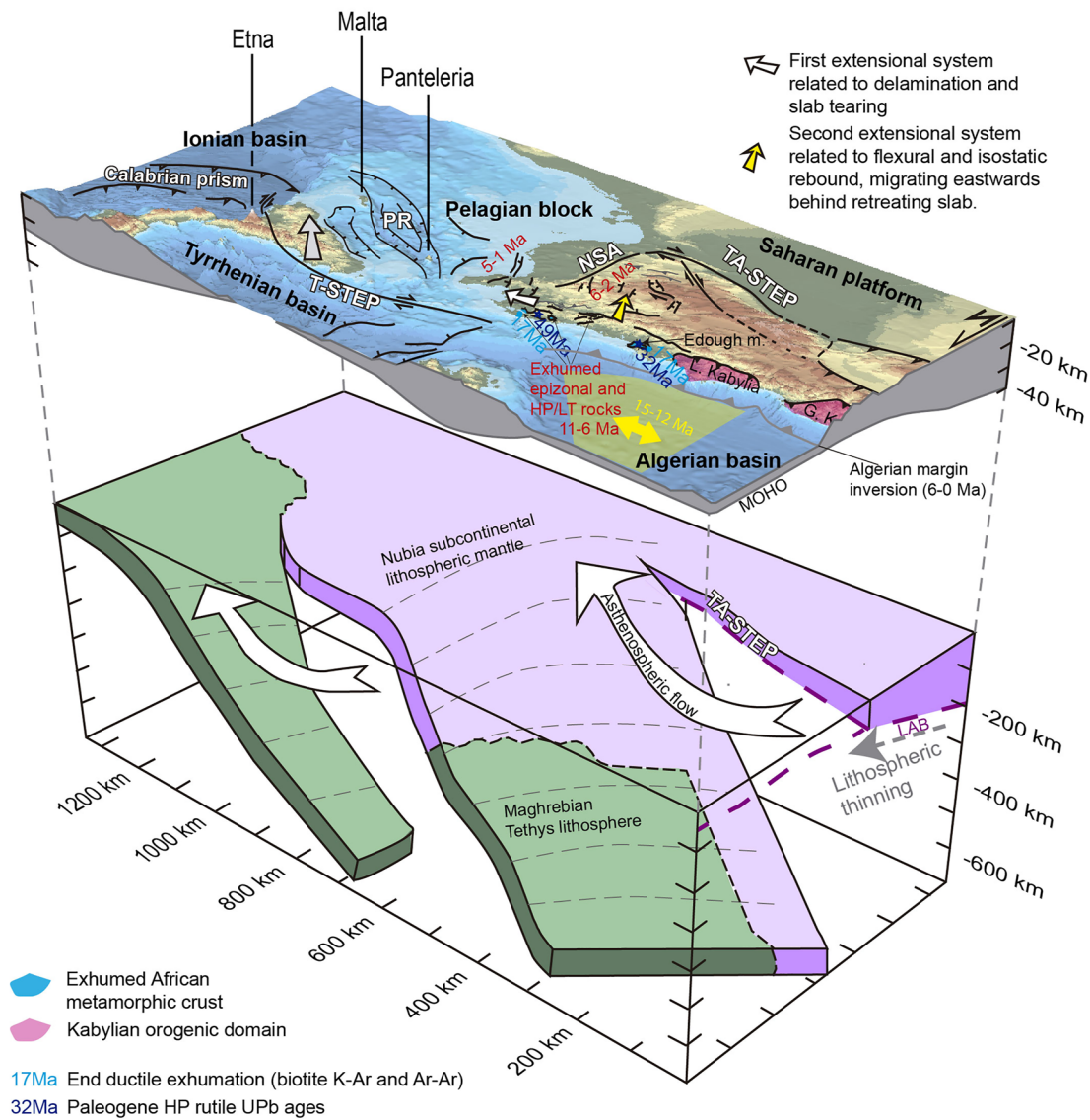


**Figure 14.** Cartoon of the tectonic mechanisms driving mid-crustal exhumation and the location of exhumed middle crust in Northern Tunisia (this work) and lower crust in the Edough massif, after Cabry et al. (2001). Notice the thinning of the Tunisian-Algerian lithosphere across the Tunisian Atlas STEP boundary (TA-STEP). NE-SW extension initiated in the middle Miocene coeval to the opening of the East Algerian Basin (Haidar et al., 2022) and propagated into Northern Tunisia in the Tortonian (approx. 11–8 Ma). Later SE-directed extension finally exhumed the Tunisian metamorphic domes, including the Ichkeul High-Pressure Low-Temperature (HP/LT) calcschist, in the late Tortonian-Messinian (approx. 8–5.3 Ma). Exhumed metamorphic rocks include early Eocene metabasites (Rutile U-Pb) and early Miocene HP/LT marbles and calcschist in the easternmost Ichkeul dome (23 and 17 Ma phlogopite K-Ar, Bellon and Perthuisot, 1977). UHP diamond bearing rocks with rutile dated at are exhumed in the Edough massif (Bruguier et al., 2017). Figure background, modified from Booth-Rea et al. (2018).

the world (Booth-Rea et al., 2008; Lucazeau, 2019; Morgan & James, 1989). Furthermore, lithospheric thickness shows a strong decrease from values above 180 km south of the Tunisian South Atlasic thrust and values around 140 (Globig et al., 2016) and probably less under the Southern Atlas STEP boundary where negative shear wave velocity anomalies are observed around 80–100 km depth (Radi et al., 2017). This relative thin lithospheric thickness in Tunisia is also accompanied by abundant hydrothermalism in the region (Dhia, 1987), mantle degassing (Fourré et al., 2011) and related high-temperature Fe-Zn-Pb mineralizations (>190°C) since the late Miocene (e.g., Ben Aïssa et al., 2018; Benchilla et al., 2003; Decrée et al., 2008; Jemmali et al., 2014). Data that suggests higher heat-flow values in the Tortonian for the whole region. Several geophysical studies support the existence of a mantle slab underlying central Tunisia (El-Sharkawy et al., 2020; Faccenna et al., 2014; Fichtner & Villaseñor, 2015; Jallouli & Mickus, 2000; Piromallo & Morelli, 2003; Research Group for Lithospheric Structure in Tunisia, 1992) (Figure 14).



Extension in Northern Tunisia has been related to the E to SE retreat and peeling-back of the slab body described above, under Tunisia since the late Miocene, which would include a strip of Nubian continental lithospheric mantle (Booth-Rea et al., 2018; Camafort et al., 2020; Roure et al., 2012) (Figures 13d and 14). The older extensional system migrated eastwards, toward the direction of slab retreat, and was thus, probably related to delamination of the lithospheric mantle inboard of the South Tunisian Atlas STEP boundary (Figure 14). The later southwards-directed extension was accompanied by topographic uplift that migrated toward the E-SE in the late Miocene (Salaj & Vanhouten, 1988), reaching the eastern coast of Tunisia in the Quaternary. This extension and the related topographic uplift we propose may be associated with flexural and isostatic rebound after the delamination under Northern and probably Central Tunisia (Booth-Rea et al., 2018; Roure et al., 2012). Slab retreat was favored by slab tearing along the Southern Tunisian Atlas thrust front that has been interpreted as a dextral STEP boundary (Booth-Rea et al., 2018; Camafort et al., 2020; Soumaya et al., 2020), which continues active at Present day favoring the southeastwards escape of the Tunisian Atlas, respect to the Saharan Atlas, according to GPS data (Bougrine et al., 2019) (Figure 14).

### 7.6. Nappe Belt Extensional Thinning in the Western Mediterranean

The structure of the Tell in Northern Tunisia resembles the one observed in other Western Mediterranean nappe belts, like the External Rif in Morocco, where greenschist rocks were exhumed in the Tamsame massif during the Tortonian (Booth-Rea et al., 2012; Negro et al., 2007; Figure 1). The Betics nappe belt also has metamorphic rocks that underwent pumpellyite-actinolite facies metamorphism under approximately 300°C and 4–5 kbar (Morata et al., 1994; Puga et al., 1988), which were probably exhumed through extensional tectonics (Azañón et al., 2012; Rodríguez-Fernández, Azor, & Azañón, 2011; Rodríguez-Fernández et al., 2013). At the same time, deeper HP/LT rocks from the subducted Iberian passive margin were exhumed from mid-crustal depths, under the allochthonous hinterland rocks, by ductile-brittle detachments in the Betics (e.g., Booth-Rea et al., 2005; Booth-Rea et al., 2015; Jabaloy et al., 1993; Martínez-Martínez & Azañón, 1997; Martínez-Martínez et al., 2002; Morales et al., 2022). In all cases, the extensional structures affect the nappe belt structure developed during the early Miocene in the Rif, Betics, and Tell orogenic belts (Figure 1). Extension propagated behind the nappe belt development, exhuming rocks from mid-crustal depths (Booth-Rea et al., 2012, 2020).

Abriding, the structure observed in Northern Tunisia is comparable to other nappe belts in the Western Mediterranean that were extended between the middle Miocene and Recent (e.g., Booth-Rea et al., 2012; Carmignani & Kligfield, 1990; Ghisetti & Vezzani, 2002; Moragues et al., 2021; Rodríguez-Fernández et al., 2013; Figure 1). Although, several works suggest that extension in these nappe belts is minor and related to the internal dynamics of the accretionary wedge (Balanya et al., 2012; Jimenez-Bonilla et al., 2016; Khelil et al., 2019), in Northern Tunisia and Algeria, the Eastern Betics and Eastern Rif, extension produced crustal thinning under the nappe belt, lithospheric rejuvenation and exhumation of metamorphic rocks (Azdimousa et al., 2019; Booth-Rea et al., 2012, 2018, 2020; Caby et al., 2001; Negro et al., 2007). In these later cases, where the crust shows thickness below 30 km (de Lis Mancilla and Díaz, 2015; de Lis Mancilla et al., 2015; Research Group for Lithospheric Structure in Tunisia, 1992) we suggest extension was related to the propagation of the edge of the subduction system under the nappe belt domain. Thus, slab tearing and subcontinental lithospheric delamination determined the extensional collapse of nappe belts all around the Western Mediterranean in the Betics, Rif and Tell, mostly during the late Miocene, and more recently under the Central Apennines (Figure 1).

Heating during decompression coeval to the development of late-stage L-S metamorphic fabrics is observed in the exhumed metapelites of the South Iberian subducted passive margin (Booth-Rea et al., 2015) and in Northern Tunisia. And may be a diagnostic feature of lithospheric mantle delamination and subsequent heating, together with K-Si-rich shoshonitic volcanism (Booth-Rea et al., 2007, 2018; Duggen et al., 2003) and mafic underplating at the base of the crust, as we interpret in the refraction line in Northern Tunisia (Figure 13d) and underlying coastal areas of SE Spain, adjacent to the Alboran magmatic arc (L. Gómez de la Peña, Grevemeyer, Kopp, et al., 2020).

Future work should further analyze the age and P-T conditions reached during the metamorphism of the Northern Tunisia extensional domes and the actual extent of the low-angle detachments described here, further south in the Atlas orogenic belt. Furthermore, deep geophysical soundings are necessary to understand the lithospheric structure of Tunisia and the existence or not of an attached lithospheric mantle slab under the region.

## 8. Conclusions

1. We present the first U-Pb ion-probe dating of early Eocene metamorphism related to Africa-Eurasia plate convergence along the North Maghreb passive margin, producing the blastesis of rutile at  $49.78 \pm 1.28$  Ma.
2. These new radiometric ages together with previously published K-Ar ages support a polymetamorphic evolution of Northern Tunisia with distinct metamorphic events in the Eocene and early Miocene.
3. The Ichkeul dome hosts HP/LT metamorphic rocks with high-Si K-white mica + chlorite + quartz and calcite + dolomite + talc + quartz paragenesis equilibrated at 0.8 Gpa under 350°C that were exhumed through heating and decompression in the biotite stability field to 400°C–440°C at 0.6–0.3 GPa.
4. Triassic outcrops in Northern Tunisia are made up by very low-grade and low-grade metamorphic rocks with three outcropping epizonal domes.
5. Most diapiric structures in Northern Tunisia are rooted in the Mejerda detachment and intruded the overlying sedimentary overburden during late Miocene extension. These include salt walls extruding through normal faults and small-scale diapirs. The evaporites have played an important role as decollement surfaces both during late Miocene extension and the later Plio-Quaternary shortening.
6. The mid-crustal exhumation observed in Northern Tunisia is analogous to the one described in other nappe belts of the Western Mediterranean like the Betics and Rif, where delamination and tearing of the lithospheric mantle propagated under the continental nappe belt domains.

## Data Availability Statement

Compositional analyses of different minerals and LA-ICP-MS data are available as Tables in Supporting Information S1 and Tables S2 and S4. The reflection seismic lines and the geological map used in this manuscript are archived in Booth-Rea (2023), available as data in Fighshare via <https://doi.org/10.6084/m9.figshare.22821974.v1> with open access conditions and license by CC BY 4.0.

## Acknowledgments

This study was supported by research projects financed by the Ministerio de Ciencia e innovación PID2019-107138RB-I00 and P18-RT-3632 of the Junta de Andalucía, Erasmus Mundus External Cooperation Window and by Scientific Cooperation Agreement 0534 between the Office National des Mines (ONM), the Tunis el Manar University and the Group for Relief and Active Processes Analysis (ARPA) from the University of Granada. We are grateful to the Tunisian Company of Petroleum Activities (ETAP) for sharing their Reflection Seismic Data. We appreciate the revisions by François Roure, Federico Rossetti and an anonymous reviewer that greatly improved the original manuscript. Funding for open access charge: Universidad de Granada / CBUA.

## References

- Abad, I., Nieto, F., Peacor, D. R., & Vellilla, N. (2003). Prograde and retrograde diagenetic and metamorphic evolution in metapelitic rocks of Sierra Espuña (Spain). *Clay Minerals*, 38, 1–23. <https://doi.org/10.1180/0009855033810074>
- Abbassene, F., Chazot, G., Bellon, H., Bruguier, O., Ouabadi, A., Maury, R. C., et al. (2016). A 17 Ma onset for the post-collisional K-rich calc-alkaline magmatism in the Maghrebides: Evidence from Bougaroun (northeastern Algeria) and geodynamic implications. *Tectonophysics*, 674, 114–134. <https://doi.org/10.1016/j.tecto.2016.02.013>
- Abbassi, A., Cipollari, P., Fellin, M. G., Zaghoul, M. N., Guillong, M., El Mourabet, M., & Cosentino, D. (2021). The Numidian sand event in the Burdigalian foreland basin system of the Rif, Morocco, in a source-to-sink perspective. *GSA Bulletin*, 134(9–10), 2280–2304. <https://doi.org/10.1130/B36136.1>
- Agard, P., Vidal, O., & Goffé, B. (2001). Interlayer and Si content of phengite in HP-LT carpholite-bearing metapelites. *Journal of Metamorphic Geology*, 19(5), 477–493. <https://doi.org/10.1046/j.0263-4929.2001.00322.x>
- Agostinetti, N. P., Levin, V., & Park, J. (2008). Crustal structure above a retreating trench: Receiver function study of the northern Apennines orogen. *Earth and Planetary Science Letters*, 275(3–4), 211–220. <https://doi.org/10.1016/j.epsl.2008.06.022>
- Aïdi, C., Beslier, M. O., Yelles-Chaouche, A. K., Klingelhoefer, F., Bracene, R., Galve, A., et al. (2018). Deep structure of the continental margin and basin off Greater Kabylia, Algeria—New insights from wide-angle seismic data modeling and multichannel seismic interpretation. *Tectonophysics*, 728–729, 1–22. <https://doi.org/10.1016/j.tecto.2018.01.007>
- Alyahyaoui, S., & Zouari, H. (2014). Synsedimentary folding process and transverse tectonic during Late Miocene to Quaternary in north-eastern Tunisia: Case of Mateur–Menzel Bourguiba region. *Arabian Journal of Geosciences*, 7(11), 4957–4973. <https://doi.org/10.1007/s12517-013-1111-2>
- Amiri, A., Chaqui, A., Nasr, I. H., Inoubli, M. H., Ayed, N. B., & Tlig, S. (2011). Role of preexisting faults in the geodynamic evolution of Northern Tunisia, insights from gravity data from the Medjerda valley. *Tectonophysics*, 506(1–4), 1–10. <https://doi.org/10.1016/j.tecto.2011.03.004>
- Amri, Z., Naji, C., Masrouhi, A., & Bellier, O. (2020). Interconnection salt diapir–allochthonous salt sheet in northern Tunisia: The Lansarine–Baoula case study. *Journal of African Earth Sciences*, 170, 103876. <https://doi.org/10.1016/j.jafrearsci.2020.103876>
- Arab, M., Maherssi, C. E., Granjeon, D., Roure, F., Déverchère, J., Cuilhé, L., et al. (2020). On the origin and consequences of crustal-scale extension between Africa and Sicily since Late Miocene: Insights from the Kaboudia area, western Pelagian Sea. *Tectonophysics*, 795, 228565. <https://doi.org/10.1016/j.tecto.2020.228565>
- Arab, M., Rabineau, M., Déverchère, J., Bracene, R., Belhai, D., Roure, F., et al. (2016). Tectonostratigraphic evolution of the eastern Algerian margin and basin from seismic data and onshore-offshore correlation. *Marine and Petroleum Geology*, 77, 1355–1375. <https://doi.org/10.1016/j.marpetgeo.2016.08.021>
- Ayed-Khaled, A., Zouaghi, T., Atawa, M., & Ghanmi, M. (2015). New evidence on the geologic setting of Medjerda Valley plain (northern Tunisia) from integrated geophysical study of Triassic evaporite bodies. *Annals of Geophysics*, 58(3), S0326. <https://doi.org/10.4401/ag-6567>
- Azañón, J. M., García-Dueñas, V., & Goffé, B. (1998). Exhumation of high-pressure metapelites and coeval crustal extension in the Alpujarride complex (Betic cordillera). *Tectonophysics*, 285(3–4), 231–252. [https://doi.org/10.1016/s0040-1951\(97\)00273-4](https://doi.org/10.1016/s0040-1951(97)00273-4)
- Azañón, J. M., Roldán, F. J., & Rodríguez Fernández, J. (2012). Fallas y despegues extensionales en el Subbético central: Implicaciones en la evolución Neógena de las Zonas externas de La cordillera Bética. *Geogaceta*, 52, 107–110.
- Azdimousa, A., Jabaloy-Sánchez, A., Münch, P., Martínez-Martínez, J. M., Booth-Rea, G., Vázquez-Vilchez, M., et al. (2019). Structure and exhumation of the Cap des Trois Fourches basement rocks (Eastern Rif, Morocco). *Journal of African Earth Sciences*, 150, 657–672. <https://doi.org/10.1016/j.jafrearsci.2018.09.018>



- Balanya, J. C., Crespo-Blanc, A., Díaz-Azpiroz, M., Expósito, I., Torcal, F., Pérez-Peña, V., & Booth-Rea, G. (2012). Arc-parallel vs back-arc extension in the Western Gibraltar arc: Is the Gibraltar forearc still active? *Geológica Acta: an international earth science journal*, 10(3), 249–263.
- Balanyá, J. C., García-Dueñas, V., Azañón, J. M., & Sánchez-Gómez, M. (1997). Alternating contractional and extensional events in the Alpujarride nappes of the Alboran domain (Betics, Gibraltar Arc). *Tectonics*, 16(2), 226–238. <https://doi.org/10.1029/96tc03871>
- Bedir, M., Boukadi, N., Ben Timzal, F., Zitouni, L., Alouani, R., Slimane, F., et al. (2001). Subsurface Mesozoic basins in the central Atlas of Tunisia: Tectonics, sequence deposit distribution, and hydrocarbon potential. *AAPG Bulletin*, 85(5), 885–907. <https://doi.org/10.1306/8626CA2D-173B-11D7-8645000102C1865D>
- Belayouni, H., Guerrero, F., Martín-Martín, M., & Serrano, F. (2013). Paleogeographic and geodynamic Miocene evolution of the Tunisian tell (Numidian and post-Numidian Successions): Bearing with the Maghreb chain. *International Journal of Earth Sciences*, 102(3), 831–855. <https://doi.org/10.1007/s00531-012-0824-x>
- Belguith, Y., Geoffroy, L., Mourgues, R., & Rigane, A. (2013). Analogue modelling of Late Miocene—Early Quaternary continental crustal extension in the Tunisia—Sicily channel area Tunisia. *Tectonophysics*, 608, 576–585. <https://doi.org/10.1016/j.tecto.2013.08.023>
- Belguith, Y., Geoffroy, L., Rigane, A., Gourmelen, C., & Ben, H. (2011). Neogene extensional deformation and related stress regimes in central Tunisia. *Tectonophysics*, 509(3–4), 198–207. <https://doi.org/10.1016/j.tecto.2011.06.009>
- Belhajtaher, I., Mattioli, E., Soussi, M., & Chaabane, N. B. (2023). Biostratigraphy of the Numidian Formation and its underlying Tellian unit, based on calcareous nannofossils in Northern Tunisia: Implication on their stratigraphic vs. tectonic relationships. *Journal of African Earth Sciences*, 201, 104896. <https://doi.org/10.1016/j.jafrearsci.2023.104896>
- Bellon, H., & Perthuisot, V. (1977). Ages radiométriques (K/Ar) de feldspaths potassiques et de micas neofomes dans le Trias de Tunisie septentrionale. *Bulletin de la Société Géologique de France*, 7(5), 1179–1184. <https://doi.org/10.2113/gssgfbull.s7-xix.5.1179>
- Ben Aïssa, L., Alouani, R., & Ben Aïssa, W. (2018). Tectono-magmatic events and Genesis of Fe-Pb-Zn resources in Nefza area, NW Tunisia. *Arabian Journal of Geosciences*, 11(20), 1–14. <https://doi.org/10.1007/s12517-018-3910-y>
- Ben Aïssa, R., Ben Aïssa, W., Ben Haj Amara, A., Ben Aïssa, L., & Tlig, S. (2021). The trace and rare Earth element contributions to the understanding of chouchia iron-copper deposits in Northern Tunisia: Metal sources interrelated with magmatism and metamorphism. *Arabian Journal of Geosciences*, 14(9), 1–18. <https://doi.org/10.1007/s12517-021-07095-2>
- Ben Ammar, S., Riahi, S., Belhadj Mohamed, A., & Layeb, M. (2020). Source rock characterization of the upper Barremian, Albian and cenomanian—Turonian organic-rich strata outcropping in Oued Bazina area, NE of Thibar diapir: Northern Tunisia. *Arabian Journal of Geosciences*, 13(24), 1–21. <https://doi.org/10.1007/s12517-020-06315-5>
- Benouali-Mebarek, N., Frizon de Lamotte, D. F., Roca, E., Bracene, R., Faure, J. L., Sassi, W., & Roure, F. (2006). Post-Cretaceous kinematics of the Atlas and Tell systems in central Algeria: Early foreland folding and subduction-related deformation. *Comptes Rendus Geoscience*, 338(1–2), 115–125. <https://doi.org/10.1016/j.crte.2005.11.005>
- Ben Chelbi, M., Melki, F., & Zargouni, F. (2006). Mode of salt bodies emplacement in Septentrional Atlas of Tunisia. Example of a Bir Afou salt body. *Comptes Rendus Geoscience*, 338(5), 349–358. <https://doi.org/10.1016/j.crte.2006.02.009>
- Benchilla, L., Guilhaumou, N., Mougou, P., Jaswal, T., & Roure, F. (2003). Reconstruction of palaeo-burial history and pore fluid pressure in foothill areas: A sensitivity test in the Hammam Zriba (Tunisia) and Koh-i-Maran (Pakistan) ore deposits. *Geofluids*, 3(2), 103–123. <https://doi.org/10.1046/j.1468-8123.2003.00053.x>
- Berman, R. G. (1991). Thermobarometry using multi-equilibrium calculations: A new technique, with petrological applications. *The Canadian Mineralogist*, 29, 833–855.
- Bessière, E., Scaillet, S., Augier, R., Jolivet, L., Miguel Azañón, J., Booth-Rea, G., et al. (2022). <sup>40</sup>Ar/<sup>39</sup>Ar age constraints on HP/LT metamorphism in extensively overprinted units: The example of the Alpujarride subduction complex (Betic Cordillera, Spain). *Tectonics*, 41(2), e2021TC006889. <https://doi.org/10.1029/2021tc006889>
- Bons, P. D., & den Brok, B. (2000). Crystallographic preferred orientation development by dissolution–precipitation creep. *Journal of Structural Geology*, 22(11), 1713–1722. [https://doi.org/10.1016/s0191-8141\(00\)00075-4](https://doi.org/10.1016/s0191-8141(00)00075-4)
- Booth-Rea, G. (2003). Geological map of Northern Tunisia and cross-sections through the studied region. Seismic cross-section composition using multichannel reflection seismic lines L1, L2 and L3. Seismic reflection line L4 across the Mejerda basin [Dataset]. Figshare. <http://doi.org/10.6084/m9.figshare.22821974.v1>
- Booth-Rea, G., Azañón, J. M., & García-Dueñas, V. (2004). Extensional tectonics in the northeastern Betics (SE Spain): Case study of extension in a multilayered upper crust with contrasting rheologies. *Journal of Structural Geology*, 26(11), 2039–2058. <https://doi.org/10.1016/j.jsg.2004.04.005>
- Booth-Rea, G., Azañón, J. M., Goffé, B., Vidal, O., & Martínez-Martínez, J. M. (2002). High-pressure, low-temperature metamorphism in Alpujarride units of southeastern Betics (Spain). *Comptes Rendus Geoscience*, 334(11), 857–865. [https://doi.org/10.1016/s1631-0713\(02\)01787-x](https://doi.org/10.1016/s1631-0713(02)01787-x)
- Booth-Rea, G., Azañón, J. M., Martínez-Martínez, J. M., Vidal, O., & García-Dueñas, V. (2005). Contrasting structural and P-T evolution of tectonic units in the southeastern Betics: Key for understanding the exhumation of the Alboran Domain HP/LT crustal rocks (western Mediterranean). *Tectonics*, 24(2), 1–23. <https://doi.org/10.1029/2004tc001640>
- Booth-Rea, G., Gaidi, S., Melki, F., Marzougui, W., Azañón, J. M., Galvé, J. P., et al. (2020). Comment on “How to build an extensional basin in a contractional setting? Numerical and physical modelling applied to the Mejerda basin at the front of the eastern tell of Tunisia” by Mannoubi Khelil et al. *Journal of Structural Geology*, 138, 103935. <https://doi.org/10.1016/j.jsg.2019.103935>
- Booth-Rea, G., Gaidi, S., Melki, F., Marzougui, W., Azañón, J. M., Zargouni, F., et al. (2018). Late Miocene extensional collapse of Northern Tunisia. *Tectonics*, 37(6), 1626–1647. <https://doi.org/10.1029/2017TC004846>
- Booth-Rea, G., Jabaloy-Sánchez, A., Azdimousa, A., Asebriy, L., Vilchez, M. V., & Martínez-Martínez, J. M. (2012). Upper-crustal extension during oblique collision: The Tamsame extensional detachment (eastern Rif, Morocco). *Terra Nova*, 24(6), 505–512. <https://doi.org/10.1111/j.1365-3121.2012.01089.x>
- Booth-Rea, G., Klaeschen, D., Grevemeyer, I., & Reston, T. (2008). Heterogeneous deformation in the Cascadia convergent margin and its relation to thermal gradient (Washington, NW USA). *Tectonics*, 27(4), 1–15. <https://doi.org/10.1029/2007TC002209>
- Booth-Rea, G., Martínez-Martínez, J. M., & Giacomini, F. (2015). Continental subduction, intracrustal shortening, and coeval upper-crustal extension: PT evolution of subducted south Iberian paleomargin metapelites (Betics, SE Spain). *Tectonophysics*, 663, 122–139. <https://doi.org/10.1016/j.tecto.2015.08.036>
- Booth-Rea, G., Ranero, C. R., Martínez-Martínez, J. M., & Grevemeyer, I. (2007). Crustal types and Tertiary tectonic evolution of the Alborán sea, western Mediterranean. *Geochemistry, Geophysics, Geosystems*, 8(10), Q10005. <https://doi.org/10.1029/2007GC001639>
- Bouaziz, S., Barrier, E., Soussi, M., Turki, M. M., & Zouari, H. (2002). Tectonic evolution of the northern African margin in Tunisia from paleostress data and sedimentary record. *Tectonophysics*, 357(1–4), 227–253. [https://doi.org/10.1016/S0040-1951\(02\)00370-0](https://doi.org/10.1016/S0040-1951(02)00370-0)

- Bougrine, A., Yelles-Chaouche, A. K., & Calais, E. (2019). Active deformation in Algeria from continuous GPS measurements. *Geophysics Journal International*, 217(1), 572–588. <https://doi.org/10.1093/gji/ggz035>
- Bouillin, J.-P., Durand Delga, M., & Olivier, P. (1986). Betic-rifian and Tyrrhenian Arcs: Distinctive features, Genesis and development stages. In F. Wezel (Ed.), *The origin of arcs. Developments in geotectonics* (Vol. 21, pp. 281–304). <https://doi.org/10.1016/B978-0-444-42688-8.50017-5>
- Boukaoud, E. H., Godard, G., Chabou, M. C., Bouftouha, Y., & Doukkari, S. (2021). Petrology and geochemistry of the Texenna ophiolites, northeastern Algeria: Implications for the Maghrebian flysch suture zone. *Lithos*, 390, 106019. <https://doi.org/10.1016/j.lithos.2021.106019>
- Boukhalfa, K., Soussi, M., Ozcan, E., Banerjee, S., & Tounekti, A. (2020). The Oligo-Miocene siliciclastic foreland basin deposits of northern Tunisia: Stratigraphy, sedimentology and paleogeography. *Journal of African Earth Sciences*, 170, 103932. <https://doi.org/10.1016/j.jafrearsci.2020.103932>
- Boutaleb, A., Afalfiz, A., Aïssa, D. E., Kolli, O., Marignac, C. H., & Belkacem, T. (2000). Métallogénie et évolution géodynamique de la chaîne tellienne en Algérie. *Bulletin du Service Géologique d'Algérie*, 11, 3–27.
- Bracène, R., & Frizon de Lamotte, D. F. (2002). The origin of intraplate deformation in the Atlas system of western and central Algeria: From Jurassic rifting to cenozoic–Quaternary inversion. *Tectonophysics*, 357(1–4), 207–226. [https://doi.org/10.1016/s0040-1951\(02\)00369-4](https://doi.org/10.1016/s0040-1951(02)00369-4)
- Broggi, A. (2008). Kinematics and geometry of Miocene low-angle detachments and exhumation of the metamorphic units in the hinterland of the Northern Apennines (Italy). *Journal of Structural Geology*, 30(1), 2–20. <https://doi.org/10.1016/j.jsg.2007.09.012>
- Bruguier, O., Bosch, D., Caby, R., Vitale-Brovarone, A., Fernandez, L., Hammor, D., et al. (2017). Age of UHP metamorphism in the Western Mediterranean: Insight from rutile and minute zircon inclusions in a diamond-bearing garnet megacryst (Edough massif, NE Algeria). *Earth and Planetary Science Letters*, 474, 215–225. <https://doi.org/10.1016/j.epsl.2017.06.043>
- Bucher, K., & Grapes, R. (2011). Metamorphism of dolomites and limestones. In *Petrogenesis of metamorphic rocks* (pp. 225–255). Springer.
- Bugini, R., Folli, L., & Marchisio, R. (2019). “Giallo Antico” in roman architecture of Lombardy: A preliminary survey. In *Conference of the Arabian journal of geosciences* (pp. 107–109). Springer.
- Buller, A. T., Bjørkum, P. A., Nadeau, P. H., & Walderhaug, O. (2005). *Distribution of hydrocarbons in sedimentary basins* (Vol. 15). Research & Technology Memoir.
- Caby, R., Bruguier, O., Fernandez, L., Hammor, D., Bosch, D., Mechat, M., et al. (2014). Metamorphic diamonds in a garnet megacryst from the Edough Massif (northeastern Algeria). Recognition and geodynamic consequences. *Tectonophysics*, 637, 341–353. <https://doi.org/10.1016/j.tecto.2014.10.017>
- Caby, R., Hammor, D., & Delor, C. (2001). Metamorphic evolution, partial melting and Miocene exhumation of lower crust in the Edough metamorphic core complex, west Mediterranean orogen, eastern Algeria. *Tectonophysics*, 342(3–4), 239–273. [https://doi.org/10.1016/s0040-1951\(01\)00166-4](https://doi.org/10.1016/s0040-1951(01)00166-4)
- Camafort, M., Pérez-Peña, J. V., Booth-Rea, G., Melki, F., Gràcia, E., Azañón, J. M., et al. (2020). Active tectonics and drainage evolution in the Tunisian Atlas driven by interaction between crustal shortening and mantle dynamics. *Geomorphology*, 351, 106954. <https://doi.org/10.1016/j.geomorph.2019.106954>
- Carmignani, L., & Kligfield, R. (1990). Crustal extension in the Northern Apennines: The transition from compression to extension in the Alpi Apuane core complex. *Tectonics*, 9(6), 1275–1303. <https://doi.org/10.1029/tc009i006p01275>
- Carminati, E., Wortel, M. J. R., Spakman, W., & Sabadini, R. (1998). The role of slab detachment processes in the opening of the western—Central Mediterranean basins: Some geological and geophysical evidence. *Earth and Planetary Science Letters*, 160(3–4), 651–665. [https://doi.org/10.1016/s0012-821x\(98\)00118-6](https://doi.org/10.1016/s0012-821x(98)00118-6)
- Chazot, G., Abbassene, F., Maury, R. C., Déverchère, J., Bellon, H., Ouabadi, A., & Bosch, D. (2017). An overview on the origin of post-collisional Miocene magmatism in the Kabylies (northern Algeria): Evidence for crustal stacking, delamination and slab detachment. *Journal of African Earth Sciences*, 125, 27–41. <https://doi.org/10.1016/j.jafrearsci.2016.10.005>
- Cherniak, D. J. (2000). Pb diffusion in rutile. *Contributions to Mineralogy and Petrology*, 139(2), 198–207. <https://doi.org/10.1007/pl00007671>
- Chertova, M. V., Spakman, W., Geenen, T., Van Den Berg, A. P., & Van Hinsbergen, D. J. J. (2014). Underpinning tectonic reconstructions of the western Mediterranean region with dynamic slab evolution from 3-D numerical modeling. *Journal of Geophysical Research: Solid Earth*, 119(7), 5876–5902. <https://doi.org/10.1002/2014jb011150>
- Civile, D., Lodolo, E., Accettella, D., Geletti, R., Ben-Avraham, Z., Deponte, M., et al. (2010). The Pantelleria graben (Sicily Channel, Central Mediterranean): An example of intraplate ‘passive’ rift. *Tectonophysics*, 490(3–4), 173–183. <https://doi.org/10.1016/j.tecto.2010.05.008>
- Cohen, C. R., Schamel, S., & Boyd-Kaygi, P. (1980). Neogene deformation in northern Tunisia: Origin of the eastern Atlas by microplate—Continental margin collision. *Geological Society of America Bulletin*, 91(4), 225–237. [https://doi.org/10.1130/0016-7606\(1980\)91<225:ndinto>2.0.co;2](https://doi.org/10.1130/0016-7606(1980)91<225:ndinto>2.0.co;2)
- Crespo-Blanc, A., & Campos, J. (2001). Structure and kinematics of the South Iberian paleomargin and its relationship with the flysch trough units: Extensional tectonics within the Gibraltar arc fold-and-thrust belt (western Betics). *Journal of Structural Geology*, 23(10), 1615–1630. [https://doi.org/10.1016/s0191-8141\(01\)00012-8](https://doi.org/10.1016/s0191-8141(01)00012-8)
- Crespo-Blanc, A., & Frizon de Lamotte, D. F. (2006). Structural evolution of the external zones derived from the flysch trough and the South Iberian and Maghrebian paleomargins around the Gibraltar arc: A comparative study. *Bulletin de la Société Géologique de France*, 177(5), 267–282. <https://doi.org/10.2113/gssgfbull.177.5.267>
- Daudet, M., Mouthereau, F., Bricchau, S., Crespo-Blanc, A., Gautheron, C., & Angrand, P. (2020). Tectono-stratigraphic and thermal evolution of the western Betic flysch: Implications for the geodynamics of South Iberian margin and Alboran domain. *Tectonics*, 39(7), e2020TC006093. <https://doi.org/10.1029/2020tc006093>
- Decrée, S., Marignac, C., Abidi, R., Jemmali, N., Deloué, E., & Souissi, F. (2016). Tectonomagmatic context of Sedex Pb–Zn and polymetallic Ore deposits of the Nappe zone Northern Tunisia, and comparisons with MVT deposits in the region. In *Mineral deposits of North Africa* (pp. 497–525). Springer.
- Decrée, S., Marignac, C., De Putter, T., Deloué, E., Liégeois, J. P., & Demaiffe, D. (2008). Pb–Zn mineralization in a Miocene regional extensional context: The case of the Sidi Driss and the Douahria ore deposits (Nefza mining district, northern Tunisia). *Ore Geology Reviews*, 34(3), 285–303. <https://doi.org/10.1016/j.oregeorev.2008.01.002>
- Decrée, S., Marignac, C., De Putter, T., Yans, J., Clauer, N., Dermech, M., et al. (2013). The Oued Belif hematite-rich breccia: A Miocene iron oxide Cu–Au–(U–REE) deposit in the Nefza mining district, Tunisia. *Economic Geology*, 108(6), 1425–1457. <https://doi.org/10.2113/econgeo.108.6.1425>
- Decrée, S., Marignac, C., Liégeois, J. P., Yans, J., Ben Abdallah, R., & Demaiffe, D. (2014). Miocene magmatic evolution in the Nefza district (Northern Tunisia) and its relationship with the Genesis of polymetallic mineralizations. *Lithos*, 192, 240–258. <https://doi.org/10.1016/j.lithos.2014.02.001>
- de Lis Mancilla, F., Booth-Rea, G., Stich, D., Pérez-Peña, J. V., Morales, J., Azañón, J. M., et al. (2015). Slab rupture and delamination under the Betics and Rif constrained from receiver functions. *Tectonophysics*, 663, 225–237. <https://doi.org/10.1016/j.tecto.2015.06.028>



- de Lis Mancilla, F., & Diaz, J. (2015). High resolution Moho topography map beneath Iberia and Northern Morocco from receiver function analysis. *Tectonophysics*, 663, 203–211. <https://doi.org/10.1016/j.tecto.2015.06.017>
- de Ruyg, M. J. (1995). Extensional diapirism in the eastern Prebetic foldbelt, southeastern Spain. In M. P. A. Jackson, D. G. Roberts, & S. Snelson (Eds.), *Salt tectonics: A global perspective: AAPG memoir* (Vol. 65, pp. 353–367).
- Dewey, J. F., Helman, M. L., Knott, S. D., Turco, E., Hutton, D. H. W., & Knott, S. D. (1989). *Kinematics of the western mediterranean* (Vol. 45, pp. 265–283). Geological Society London Special Publications. <https://doi.org/10.1144/GSL.SP.1989.045.01.15>
- Dhia, H. B. (1987). The geothermal gradient map of central Tunisia: Comparison with structural, gravimetric and petroleum data. *Tectonophysics*, 142(1), 99–109. [https://doi.org/10.1016/0040-1951\(87\)90297-6](https://doi.org/10.1016/0040-1951(87)90297-6)
- Dhifaoui, R., Strzeczynski, P., Mourgues, R., Rigane, A., Gourmelen, C., & Peigné, D. (2021). Accommodation of compression and lateral extension in a continental crust: Analogical modeling of the Central Atlas (eastern Algeria, Tunisia) and Pelagian Sea. *Tectonophysics*, 817, 229052. <https://doi.org/10.1016/j.tecto.2021.229052>
- Di Luzio, E., Mele, G., Tiberti, M. M., Cavinato, G. P., & Parotto, M. (2009). Moho deepening and shallow upper crustal delamination beneath the central Apennines. *Earth and Planetary Science Letters*, 280(1–4), 1–12. <https://doi.org/10.1016/j.epsl.2008.09.018>
- Duggen, S., Hoernle, K., van den Bogaard, P., Rüpke, L., & Phipps Morgan, J. (2003). Deep roots of the Messinian salinity crisis. *Nature*, 422(6932), 602–606. <https://doi.org/10.1038/nature01553>
- Durand-Delga, M. (1971). Les unités a Mésozoïque métamorphique d'El Milia a Texenna (Algérie) et leur cadre structural. *Bulletin de la Société Géologique de France*, 7(3–4), 328–337. <https://doi.org/10.2113/gssgfbull.s7-xiii.3-4.328>
- Eggert, R. G., & Kerrick, D. M. (1981). Metamorphic equilibria in the siliceous dolomite system: 6 kbar experimental data and geologic implications. *Geochimica et Cosmochimica Acta*, 45(7), 1039–1049. [https://doi.org/10.1016/0016-7037\(81\)90130-7](https://doi.org/10.1016/0016-7037(81)90130-7)
- El Ghali, A., Ayed, N. B., Bobier, C., Zargouni, F., & Krifa, A. (2003). Les manifestations tectoniques synsédimentaires associées à la compression éocène en Tunisie: Implications paléogéographiques et structurales sur la marge Nord-Africaine. *Comptes Rendus Geoscience*, 335(9), 763–771. [https://doi.org/10.1016/s1631-0713\(03\)00117-2](https://doi.org/10.1016/s1631-0713(03)00117-2)
- El-Sharkawy, A., Meier, T., Lebedev, S., Behrmann, J. H., Hamada, M., Cristiano, L., et al. (2020). The slab puzzle of the Alpine-Mediterranean region: Insights from a new, high-resolution, shear wave velocity model of the upper mantle. *Geochemistry, Geophysics, Geosystems*, 21(8), e2020GC008993. <https://doi.org/10.1029/2020gc008993>
- Faccenna, C., Becker, T. W., Auer, L., Billi, A., Boschi, L., Brun, J. P., et al. (2014). Mantle dynamics in the Mediterranean. *Reviews of Geophysics*, 52(3), 283–332. <https://doi.org/10.1002/2013rg000444>
- Faccenna, C., Piromallo, C., Crespo-Blanc, A., Jolivet, L., & Rossetti, F. (2004). Lateral slab deformation and the origin of the western Mediterranean arcs. *Tectonics*, 23(1). <https://doi.org/10.1029/2002tc001488>
- Fant, J. C. (2001). Rome's marble yards. *Journal of Roman Archaeology*, 14, 167–198. <https://doi.org/10.1017/s1047759400019875>
- Fernandez, L., Bosch, D., Bruguier, O., Hammor, D., Caby, R., Monié, P., et al. (2016). Permo-Carboniferous and early Miocene geological evolution of the internal zones of the Maghrebides—New insights on the western Mediterranean evolution. *Journal of Geodynamics*, 96, 146–173. <https://doi.org/10.1016/j.jog.2015.10.001>
- Fichtner, A., & Villaseñor, A. (2015). Crust and upper mantle of the western Mediterranean—Constraints from full-waveform inversion. *Earth and Planetary Science Letters*, 428, 52–62. <https://doi.org/10.1016/j.epsl.2015.07.038>
- Fontboté, J. M., Guimerà, J., Roca, E., Sàbat, F., Santanach, P., & Fernández-Ortigosa, F. (1990). The Cenozoic geodynamic evolution of the Valencia trough (western Mediterranean). *Revista de la Sociedad Geologica de Espana*, 3(3–4), 249–259.
- Fornelli, A., Gallicchio, S., Micheletti, F., & Langone, A. (2020). Preliminary U-Pb detrital zircon ages from Tufiti di Tusa formation (Lucanian Apennines, Southern Italy): Evidence of rupelian volcanoclastic supply. *Minerals*, 10(9), 786. <https://doi.org/10.3390/min10090786>
- Fourré, E., Di Napoli, R., Aiuppa, A., Parello, F., Gaubi, E., Jean-Baptiste, P., et al. (2011). Regional variations in the chemical and helium-carbon isotope composition of geothermal fluids across Tunisia. *Chemical Geology*, 288(1–2), 67–85. <https://doi.org/10.1016/j.chemgeo.2011.07.003>
- Frey, M. (1987). Very low-grade metamorphism of clastic sedimentary rocks. In M. Frey (Ed.), *Low temperature metamorphism* (pp. 9–58). Blackie.
- Frifita, N., Mickus, K., & Gharbi, M. (2020). Gravity contribution to the Mejerda foreland basin, Northwestern region of Tunisia. *Journal of African Earth Sciences*, 171, 103956. <https://doi.org/10.1016/j.jafrearsci.2020.103956>
- Frizon de Lamotte, D., Andrieux, J., & Guezou, J. C. (1991). Cinématique des chevauchements neogènes dans l'Arc bético-rifain; discussion sur les modèles géodynamiques. *Bulletin de la Société Géologique de France*, 162(4), 611–626. <https://doi.org/10.2113/gssgfbull.162.4.611>
- Frizon de Lamotte, D., Saint Bezar, B., Bracène, R., & Mercier, E. (2000). The two main steps of the Atlas building and geodynamics of the western Mediterranean. *Tectonics*, 19(4), 740–761. <https://doi.org/10.1029/2000tc900003>
- Frizon de Lamotte, D. F., Leturmy, P., Missenard, Y., Khomsi, S., Ruiz, G., Saddiqi, O., et al. (2009). Mesozoic and cenozoic vertical movements in the Atlas system (Algeria, Morocco, Tunisia): An overview. *Tectonophysics*, 475(1), 9–28. <https://doi.org/10.1016/j.tecto.2008.10.024>
- Gaidi, S., Booth-Rea, G., Melki, F., Marzougui, W., Ruano, P., Pérez-Peña, J. V., et al. (2020). Active fault segmentation in Northern Tunisia. *Journal of Structural Geology*, 139, 104146. <https://doi.org/10.1016/j.jsg.2020.104146>
- Gao, X. Y., Zheng, Y. F., Xia, X. P., & Chen, Y. X. (2014). U–Pb ages and trace elements of metamorphic rutile from ultrahigh-pressure quartzite in the Sulu orogen. *Geochimica et Cosmochimica Acta*, 143, 87–114. <https://doi.org/10.1016/j.gca.2014.04.032>
- García-Dueñas, V., Balanyá, J. C., & Martínez-Martínez, J. M. (1992). Miocene extensional detachments in the outcropping basement of the northern Alboran basin (Betics) and their tectonic implications. *Geo-Marine Letters*, 12(2), 88–95. <https://doi.org/10.1007/bf02084917>
- Gartrell, A. P. (1997). Evolution of rift basins and low-angle detachments in multilayer analog models. *Geology*, 25(7), 615–618. [https://doi.org/10.1130/0091-7613\(1997\)025<0615:eorbal>2.3.co;2](https://doi.org/10.1130/0091-7613(1997)025<0615:eorbal>2.3.co;2)
- Gelabert, B., Sabat, F., & Rodríguez-Perea, A. (1992). A structural outline of the Serra de Tramuntana of Mallorca (Balearic Islands). *Tectonophysics*, 203(1–4), 167–183. [https://doi.org/10.1016/0040-1951\(92\)90222-r](https://doi.org/10.1016/0040-1951(92)90222-r)
- Ghanmi, M., Youssef, M. B., Jouirou, M., Zargouni, F., & Vila, J. M. (2001). “Glacier de sel” du Jebel Kebbouch (NW Tunisie). *Eclogae Geologicae Helveticae*, 94, 153–160.
- Ghisetti, F., & Vezzani, L. (2002). Normal faulting, extension and uplift in the outer thrust belt of the central Apennines (Italy): Role of the caranico fault. *Basin Research*, 14(2), 225–236. <https://doi.org/10.1046/j.1365-2117.2002.00171.x>
- Ghorabi, M., & Henry, B. (1992). Magnetic fabric of rock from Jebel Hairech (Northern Tunisia) and its structural implications. *Journal of African Earth Sciences*, 14(2), 267–274. [https://doi.org/10.1016/0899-5362\(92\)90103-J](https://doi.org/10.1016/0899-5362(92)90103-J)
- Gimeno-Vives, O., Mohn, G., Bosse, V., Haissen, F., Zaghloul, M. N., Atouabat, A., & Frizon de Lamotte, D. (2019). The Mesozoic margin of the Maghrebian Tethys in the Rif belt (Morocco): Evidence for polyphase rifting and related magmatic activity. *Tectonics*, 38(8), 2894–2918. <https://doi.org/10.1029/2019tc005508>

- Globig, J., Fernández, M., Torne, M., Vergés, J., Robert, A., & Faccenna, C. (2016). New insights into the crust and lithospheric mantle structure of Africa from elevation, geoid, and thermal analysis. *Journal of Geophysical Research: Solid Earth*, *121*(7), 5389–5424. <https://doi.org/10.1002/2016jb012972>
- Gómez de la Peña, L., Grevemeyer, I., Kopp, H., Díaz, J., Gallart, J., Booth-Rea, G., et al. (2020). The lithospheric structure of the Gibraltar Arc System from wide-angle seismic data. *Journal of Geophysical Research: Solid Earth*, *125*(9), e2020JB019854. <https://doi.org/10.1029/2020jb019854>
- Gómez de la Peña, L. G., Ranero, C. R., Gràcia, E., & Booth-Rea, G. (2020). The evolution of the westernmost Mediterranean basins. *Earth-Science Reviews*, *214*, 103445. <https://doi.org/10.1016/j.earscirev.2020.103445>
- Govers, R., & Wortel, M. J. R. (2005). Lithosphere tearing at STEP faults: Response to edges of subduction zones. *Earth and Planetary Science Letters*, *236*(1–2), 505–523. <https://doi.org/10.1016/j.epsl.2005.03.022>
- Granado, P., Ruh, J. B., Santolaria, P., Strauss, P., & Muñoz, J. A. (2021). Stretching and contraction of extensional basins with pre-rift salt: A numerical modeling approach. *Frontiers of Earth Science*, *9*, 648937. <https://doi.org/10.3389/feart.2021.648937>
- Guerrera, F., Martín-Martín, M., Perrone, V., & Tramontana, M. (2005). Tectono-sedimentary evolution of the southern branch of the Western Tethys (Maghrebian flysch Basin and Lucanian Ocean): Consequences for Western Mediterranean geodynamics. *Terra Nova*, *17*(4), 358–367. <https://doi.org/10.1111/j.1365-3121.2005.00621.x>
- Guidotti, C. V., & Sassi, F. P. (1986). Classification and correlation of metamorphic facies series by means of Muscovite b (o) data from low-grade metapelites. *Neues Jahrbuch für Mineralogie. Abhandlungen*, *153*, 363–380.
- Haidar, S., Déverchère, J., Graindorge, D., Arab, M., Medaouri, M., & Klingelhoefer, F. (2022). Back-Arc dynamics controlled by slab rollback and tearing: A reappraisal of Seafloor spreading and kinematic evolution of the eastern Algero-Balearic Basin (Western Mediterranean) in the middle-Late Miocene. *Tectonics*, *41*(2), e2021TC006877. <https://doi.org/10.1029/2021tc006877>
- Halloul, N., & Gourgaud, A. (2012). The post-collisional volcanism of northern Tunisia: Petrology and evolution through time. *Journal of African Earth Sciences*, *63*, 62–76. <https://doi.org/10.1016/j.jafrearsci.2011.10.004>
- Hidas, K., Booth-Rea, G., Garrido, C. J., Martínez-Martínez, J. M., Padrón-Navarta, J. A., Konc, Z., et al. (2013). Backarc basin inversion and subcontinental mantle emplacement in the crust: Kilometre-scale folding and shearing at the base of the proto-Alborán lithospheric mantle (Betic cordillera, southern Spain). *Journal of the Geological Society*, *170*(1), 47–55. <https://doi.org/10.1144/jgs2011-151>
- Hippert, J. F. (1994). Microstructures and c-axis fabrics indicative of quartz dissolution in sheared quartzites and phyllonites. *Tectonophysics*, *229*(3–4), 141–163. [https://doi.org/10.1016/0040-1951\(94\)90026-4](https://doi.org/10.1016/0040-1951(94)90026-4)
- Hirth, G., & Tullis, J. (1992). Dislocation creep regimes in quartz aggregates. *Journal of Structural Geology*, *14*(2), 145–159. [https://doi.org/10.1016/0191-8141\(92\)90053-y](https://doi.org/10.1016/0191-8141(92)90053-y)
- Jabaloy, A., Galindo-Zaldívar, J., & González-Lodeiro, F. (1993). The Alpujárride-Nevado-Fibabride extensional shear zone, Betic Cordillera, SE Spain. *Journal of Structural Geology*, *15*(3–5), 555–569. [https://doi.org/10.1016/0191-8141\(93\)90148-4](https://doi.org/10.1016/0191-8141(93)90148-4)
- Jabaloy-Sánchez, A., Azdimousa, A., Booth-Rea, G., Asebriy, L., Vázquez-Víchez, M., Martínez-Martínez, J. M., & Gabites, J. (2015). The structure of the Tensamane fold-and-thrust stack (eastern Rif, Morocco): Evolution of a transpressional orogenic wedge. *Tectonophysics*, *663*, 150–176. <https://doi.org/10.1016/j.tecto.2015.02.003>
- Jallouli, C., & Mickus, K. (2000). Regional gravity analysis of the crustal structure of Tunisia. *Journal of African Earth Sciences*, *30*(1), 63–78. [https://doi.org/10.1016/S0899-5362\(00\)00008-7](https://doi.org/10.1016/S0899-5362(00)00008-7)
- Jemali, N., Souissi, F., Carranza, E. J. M., Vennemann, T. W., & Bogdanov, K. (2014). Geochemical constraints on the Genesis of the Pb–Zn deposit of Jalta (northern Tunisia): Implications for timing of mineralization, sources of metals and relationship to the Neogene volcanism. *Geochemistry*, *74*(4), 601–613. <https://doi.org/10.1016/j.chemer.2014.01.002>
- Jimenez-Bonilla, A., Torvela, T., Balanyá, J. C., Expósito, I., & Díaz-Azpiroz, M. (2016). Changes in dip and frictional properties of the basal detachment controlling orogenic wedge propagation and frontal collapse: The external central Betics case. *Tectonics*, *35*(12), 3028–3049. <https://doi.org/10.1002/2016tc004196>
- Jolivet, L., Faccenna, C., Goffé, B., Burov, E., & Agard, P. (2003). Subduction tectonics and exhumation of high-pressure metamorphic rocks in the Mediterranean orogens. *American Journal of Science*, *303*(5), 353–354. <https://doi.org/10.2475/ajs.303.5.353>
- Jolivet, L., Faccenna, C., Goffé, B., Mattei, M., Rossetti, F., Brunet, C., et al. (1998). Midcrustal shear zones in postorogenic extension: Example from the northern Tyrrhenian Sea. *Journal of Geophysical Research*, *103*(B6), 12123–12160. <https://doi.org/10.1029/97jb03616>
- Jolivet, L., Faccenna, C., & Piromallo, C. (2009). From mantle to crust: Stretching the Mediterranean. *Earth and Planetary Science Letters*, *285*(1–2), 198–209. <https://doi.org/10.1016/j.epsl.2009.06.017>
- Jolivet, L., Trotet, F., Monié, P., Vidal, O., Goffé, B., Labrousse, L., et al. (2010). Along-strike variations of P–T conditions in accretionary wedges and syn-orogenic extension, the HP–LT Phyllite–Quartzite Nappe in Crete and the Peloponnese. *Tectonophysics*, *480*(1–4), 133–148. <https://doi.org/10.1016/j.tecto.2009.10.002>
- Khelil, M., Khomsi, S., Roure, F., Vergés, J., & Zargouni, F. (2021). Structural styles of the Tellian fold-and-thrust belt of Tunisia based on structural transects: Insights on the subsurface oil and gas pre-salt plays. *Arabian Journal of Geosciences*, *14*(19), 1985. <https://doi.org/10.1007/s12517-021-08308-4>
- Khelil, M., Souloumiac, P., Maillot, B., Khomsi, S., & Frizon de Lamotte, D. (2019). How to build an extensional basin in a contractional setting? Numerical and physical modelling applied to the Mejerda Basin at the front of the eastern tell of Tunisia. *Journal of Structural Geology*, *129*, 103887. <https://doi.org/10.1016/j.jsg.2019.103887>
- Kherroubi, A., Déverchère, J., Yelles, A., Mercier de Lépinay, B., Domzig, A., Cattaneo, A., et al. (2009). Recent and active deformation pattern off the easternmost Algerian margin, Western Mediterranean Sea: New evidence for contractional tectonic reactivation. *Marine Geology*, *261*(1–4), 17–32. <https://doi.org/10.1016/j.margeo.2008.05.016>
- Khomsi, S., Frizon de Lamotte, D., Bédir, M., & Echihi, O. (2016). The Late Eocene and Late Miocene fronts of the Atlas Belt in eastern Maghreb: Integration in the geodynamic evolution of the Mediterranean domain. *Arabian Journal of Geosciences*, *9*(15), 650. <https://doi.org/10.1007/s12517-016-2609-1>
- Khomsi, S., Ghazi, M., Jemia, B., Frizon de Lamotte, D., Maherssi, C., Echihi, O., et al. (2009). An overview of the Late Cretaceous–Eocene positive inversions and Oligo-Miocene subsidence events in the foreland of the Tunisian Atlas: Structural style and implications for the tectonic agenda of the Maghrebian Atlas system. *Tectonophysics*, *475*(1), 38–58. <https://doi.org/10.1016/j.tecto.2009.02.027>
- Khomsi, S., Khelil, M., Roure, F., & Zargouni, F. (2021). Surface and subsurface architecture of the Kasseb structures: Implications for petroleum exploration beneath the Tellian allochthon, the easternmost portion of the Maghrebides. *Arabian Journal of Geosciences*, *14*(3), 1–20. <https://doi.org/10.1007/s12517-020-06401-8>
- Khomsi, S., Roure, F., & Vergés, J. (2022). Hinterland and foreland structures of the eastern Maghreb tell and Atlas thrust belts: Tectonic controlling factors, pending questions, and oil/gas exploration potential of the pre-Triassic traps. *Arabian Journal of Geosciences*, *15*(6), 1–11. <https://doi.org/10.1007/s12517-022-09707-x>



- Kilian, R., Heilbronner, R., & Stünitz, H. (2011). Quartz grain size reduction in a granitoid rock and the transition from dislocation to diffusion creep. *Journal of Structural Geology*, 33(8), 1265–1284. <https://doi.org/10.1016/j.jsg.2011.05.004>
- Kooijman, E., Mezger, K., & Berndt, J. (2010). Constraints on the U–Pb systematics of metamorphic rutile from in situ LA-ICP-MS analysis. *Earth and Planetary Science Letters*, 293(3–4), 321–330. <https://doi.org/10.1016/j.epsl.2010.02.047>
- Kübler, B., & Jaboyedoff, M. (2000). Illite crystallinity. *Comptes Rendus de l'Académie des Sciences-Series IIA-Earth and Planetary Science*, 331(2), 75–89. [https://doi.org/10.1016/s1251-8050\(00\)01395-1](https://doi.org/10.1016/s1251-8050(00)01395-1)
- Kurtz, J. (1983). Geochemistry of early Mesozoic basalts from Tunisia. *Journal of African Earth Sciences*, 1(2), 113–125. [https://doi.org/10.1016/0899-5362\(83\)90003-9](https://doi.org/10.1016/0899-5362(83)90003-9)
- Lamont, T. N., Searle, M. P., Waters, D. J., Roberts, N. M., Palin, R. M., Smye, A., et al. (2020). Compressional origin of the Naxos metamorphic core complex, Greece: Structure, petrography, and thermobarometry. *GSA Bulletin*, 132(1–2), 149–197. <https://doi.org/10.1130/b31978.1>
- Lanari, P., Wagner, T., & Vidal, O. (2014). A thermodynamic model for di-trioctahedral chlorite from experimental and natural data in the system MgO–FeO–Al<sub>2</sub>O<sub>3</sub>–SiO<sub>2</sub>–H<sub>2</sub>O: Applications to P–T sections and geothermometry. *Contributions to Mineralogy and Petrology*, 167(2), 1–19. <https://doi.org/10.1007/s00410-014-0968-8>
- Law, R. D. (2014). Deformation thermometry based on quartz c-axis fabrics and recrystallization microstructures: A review. *Journal of Structural Geology*, 66(0), 129–161. <https://doi.org/10.1016/j.jsg.2014.05.023>
- Leoni, L., Sartori, F., & Tamponi, M. (1998). Composition variation in K-white micas and chlorites coexisting in Al-saturated metapelites under late diagenetic to low grade metamorphic conditions (Internal Liguride Units, Northern Apennines, Italy). *European Journal of Mineralogy*, 10(6), 1321–1339. <https://doi.org/10.1127/ejm/10/6/1321>
- Leprêtre, R., Frizon de Lamotte, D., Combier, V., Gimeno-Vives, O., Mohn, G., & Eschard, R. (2018). The Tell-Rif orogenic system (Morocco, Algeria, Tunisia) and the structural heritage of the southern Tethys margin. *BSGF-Earth Sciences Bulletin*, 189(2), 10. <https://doi.org/10.1051/bsgf/2018009>
- Letargo, C. M., Lamb, W. M., & Park, J. S. (1995). Comparison of calcite + dolomite thermometry and carbonate + silicate equilibria: Constraints on the conditions of metamorphism of the Llano uplift, central Texas, USA. *American Mineralogist*, 80(1–2), 131–143. <https://doi.org/10.2138/am-1995-1-213>
- Levander, A., Bezada, M. J., Niu, F., Humphreys, E. D., Palomeras, I., Thurner, S. M., et al. (2014). Subduction-driven recycling of continental margin lithosphere. *Nature*, 515(7526), 253–256. <https://doi.org/10.1038/nature13878>
- Li, Q., Palomeras, I., & Meng, X. (2021). Lithospheric structure beneath southern Iberia and northern Morocco constrained by 3D Kirchhoff-approximate GRT imaging. *Journal of Geophysics and Engineering*, 18(2), 268–281. <https://doi.org/10.1093/jge/gxab012>
- Loneragan, L., & Platt, J. P. (1995). The Malaguide-Alpujarride boundary: A major extensional contact in the internal zone of the eastern Betic Cordillera, SE Spain. *Journal of Structural Geology*, 17(12), 1655–1671. [https://doi.org/10.1016/0191-8141\(95\)00070-t](https://doi.org/10.1016/0191-8141(95)00070-t)
- Loneragan, L., & White, N. (1997). Origin of the Betic-Rif mountain belt. *Tectonics*, 16(3), 504–522. <https://doi.org/10.1029/96TC03937>
- Lucazeau, F. (2019). Analysis and mapping of an updated terrestrial heat flow data set. *Geochemistry, Geophysics, Geosystems*, 20(8), 4001–4024. <https://doi.org/10.1029/2019gc008389>
- Lucazeau, F., & Dhia, H. B. (1989). Preliminary heat-flow density data from Tunisia and the Pelagian Sea. *Canadian Journal of Earth Sciences*, 26(5), 993–1000. <https://doi.org/10.1139/e89-080>
- Luvizotto, G. L., Zack, T., Triebold, S., & Von Eynatten, H. (2009). Rutile occurrence and trace element behavior in medium-grade metasedimentary rocks: Example from the erzgebirge, Germany. *Mineralogy and Petrology*, 97(3), 233–249. <https://doi.org/10.1007/s00710-009-0092-z>
- Maggi, M., Rossetti, F., Corfu, F., Theye, T., Andersen, T. B., & Faccenna, C. (2012). Clinopyroxene–rutile phyllonites from the East Tenda shear zone (Alpine Corsica, France): Pressure–temperature–time constraints to the Alpine reworking of Variscan Corsica. *Journal of the Geological Society*, 169(6), 723–732. <https://doi.org/10.1144/jgs2011-120>
- Mahdi, D., Abdallah, R. B., Hatira, N., Tlili, A., Chaftar, H. R., & Jamoussi, F. (2013). Burial history determination of the Triassic succession of Central and Northern Tunisia using clay minerals. *Arabian Journal of Geosciences*, 6(11), 4347–4355. <https://doi.org/10.1007/s12517-012-0699-y>
- Malusà, M. G., Faccenna, C., Baldwin, S. L., Fitzgerald, P. G., Rossetti, F., Balestrieri, M. L., et al. (2015). Contrasting styles of (U) HP rock exhumation along the cenozoic Adria-europe plate boundary (Western Alps, Calabria, Corsica). *Geochemistry, Geophysics, Geosystems*, 16(6), 1786–1824. <https://doi.org/10.1002/2015gc005767>
- Marignac, C., Aïssa, D. E., Cheilletz, A., & Gasquet, D. (2016). Edough-cap de Fer polymetallic district, northeast Algeria: II. Metallogenic evolution of a late Miocene metamorphic core complex in the Alpine Maghrebide belt. In *Mineral deposits of North Africa* (pp. 167–199). Springer.
- Marmi, R., & Guiraud, R. (2006). End Cretaceous to recent polyphased compressive tectonics along the “Mole Constantinois” and foreland (NE Algeria). *Journal of African Earth Sciences*, 45(1), 123–136. <https://doi.org/10.1016/j.jafrearsci.2006.01.009>
- Marrone, S., Monie, P., Rossetti, F., Aldega, L., Bouybououene, M., Charpentier, D., et al. (2021). Timing of Alpine orogeny and postorogenic extension in the Alboran Domain, inner Rif chain, Morocco. *Tectonics*, 40(7), e2021TC006707. <https://doi.org/10.1029/2021tc006707>
- Martin, L. A., Rubatto, D., Brovarone, A. V., & Hermann, J. (2011). Late Eocene lawsonite-eclogite facies metasomatism of a granulite sliver associated to ophiolites in Alpine Corsica. *Lithos*, 125(1–2), 620–640. <https://doi.org/10.1016/j.lithos.2011.03.015>
- Martínez-Martínez, J. M., & Azañón, J. M. (1997). Mode of extensional tectonics in the southeastern Betics (SE Spain): Implications for the tectonic evolution of the peri-Alborán orogenic system. *Tectonics*, 16(2), 205–225. <https://doi.org/10.1029/97tc00157>
- Martínez-Martínez, J. M., Booth-Rea, G., Azañón, J. M., & Torcal, F. (2006). Active transfer fault zone linking a segmented extensional system (Betics, southern Spain): Insight into heterogeneous extension driven by edge delamination. *Tectonophysics*, 422(1–4), 159–173. <https://doi.org/10.1016/j.tecto.2006.06.001>
- Martínez-Martínez, J. M., Soto, J. I., & Balanyá, J. C. (2002). Orthogonal folding of extensional detachments: Structure and origin of the Sierra Nevada elongated dome (Betics, SE Spain). *Tectonics*, 21, 1–3. <https://doi.org/10.1029/2001tc001283>
- Masrouhi, A., Bellier, O., & Koyi, H. (2014). Geometry and structural evolution of Lorbeus diapir, northwestern Tunisia: Polyphase diapirism of the North African inverted passive margin. *International Journal of Earth Sciences*, 103(3), 881–900. <https://doi.org/10.1007/s00531-013-0992-3>
- Masrouhi, A., Ghanmi, M., Slama, M. M. B., Youssef, M. B., Vila, J. M., & Zargouni, F. (2008). New tectono-sedimentary evidence constraining the timing of the positive tectonic inversion and the Eocene Atlantic phase in northern Tunisia: Implication for the North African paleo-margin evolution. *Comptes Rendus Geoscience*, 340(11), 771–778. <https://doi.org/10.1016/j.crte.2008.07.007>
- Masrouhi, A., & Koyi, H. A. (2012). Submarine ‘salt glacier’ of Northern Tunisia, a case of Triassic salt mobility in North African Cretaceous passive margin (Vol. 363, pp. 579–593). Geological Society of London Special Publications. <https://doi.org/10.1144/sp363.29>
- Massonne, H. J., & Schreyer, W. (1987). Phengite geobarometry based on the limiting assemblage with K-feldspar, phlogopite and quartz. *Contributions to Mineralogy and Petrology*, 96(2), 214–224. <https://doi.org/10.1007/bf00375235>
- Massonne, H. J., & Szpurka, Z. (1997). Thermodynamic properties of white micas on the basis of high-pressure experiments in the systems K<sub>2</sub>O–MgO–Al<sub>2</sub>O<sub>3</sub>–SiO<sub>2</sub>–H<sub>2</sub>O. *Lithos*, 41(1–3), 229–250. [https://doi.org/10.1016/s0024-4937\(97\)82014-2](https://doi.org/10.1016/s0024-4937(97)82014-2)

- Melki, F., Zouaghi, T., Ben Chelbi, M., Bédir, M., & Zargouni, F. (2012). Role of the NE-SW Hercynian master fault systems and associated lineaments on the structuring and evolution of the Mesozoic and Cenozoic basins of the Alpine Margin, northern Tunisia. In E. Sharkov (Ed.), *Tectonics-recent advances: IntechOpen* (pp. 131–168). <https://doi.org/10.5772/50145>
- Melki, F., Zouaghi, T., Chelbi, M. B., Bédir, M., & Zargouni, F. (2010). Tectono-sedimentary events and geodynamic evolution of the Mesozoic and Cenozoic basins of the Alpine margin, Gulf of Tunis, north-eastern Tunisia offshore. *Comptes Rendus Geoscience*, 342(9), 741–753. <https://doi.org/10.1016/j.crte.2010.04.005>
- Melki, F., Zouaghi, T., Harrab, S., Sainz, A. C., Bédir, M., & Zargouni, F. (2011). Structuring and evolution of Neogene transcurent basins in the Tellian foreland domain, north-eastern Tunisia. *Journal of Geodynamics*, 52(1), 57–69. <https://doi.org/10.1016/j.jog.2010.11.009>
- Merriman, R. J., & Peacor, D. R. (1998). Very low-grade metapelites: Mineralogy, microfabrics and measuring reaction progress. *Low-grade Metamorphism*, 10–60. <https://doi.org/10.1002/9781444313345.ch2>
- Merriman, R. J., & Roberts, B. (1985). A survey of white mica crystallinity and polytypes in pelitic rocks of Snowdonia and Llŷn, North Wales. *Mineralogical Magazine*, 49(352), 305–319. <https://doi.org/10.1180/minmag.1985.049.352.02>
- Miller, M. S., & Agostinetti, N. P. (2012). Insights into the evolution of the Italian lithospheric structure from S receiver function analysis. *Earth and Planetary Science Letters*, 345, 49–59. <https://doi.org/10.1016/j.epsl.2012.06.028>
- Molli, G., Carlini, M., Vescovi, P., Artoni, A., Balsamo, F., Camurri, F., et al. (2018). Neogene 3-D structural architecture of the north-west Apennines: The role of the low-angle normal faults and basement thrusts. *Tectonics*, 37(7), 2165–2196. <https://doi.org/10.1029/2018tc005057>
- Monié, P., Maluski, H., Saadallah, A., & Gaby, R. (1988). New <sup>39</sup>Ar-<sup>40</sup>Ar ages of Hercynian and Alpine thermotectonic events in Grande Kabylie (Algeria). *Tectonophysics*, 152(1–2), 53–69. [https://doi.org/10.1016/0040-1951\(88\)90029-7](https://doi.org/10.1016/0040-1951(88)90029-7)
- Moragues, L., Ruano, P., Azañón, J. M., Garrido, C. J., Hidas, K., & Booth Rea, G. (2021). Two Cenozoic extensional phases in Mallorca and their bearing on the geodynamic evolution of the western Mediterranean. *Tectonics*, 40(11), e2021TC006868. <https://doi.org/10.1029/2021tc006868>
- Morales, J., Molina-Aguilera, A., de Lis Mancilla, F., Stich, D., Azañón, J. M., Teixidó, T., et al. (2022). Preservation of the Iberian Tethys paleomargin beneath the eastern Betic mountain range. *Gondwana Research*, 106, 237–246. <https://doi.org/10.1016/j.gr.2022.01.015>
- Morata, D., Aguirre, L., & Puga, E. (1994). Na-Metamorphic pyroxenes in low-grade metabasites from the external zones of the Betic cordilleras (southern Spain): Influence of rock chemical composition on their formation. *Andean Geology*, 21, 269–283.
- Morgan, P., & James, D. E. (1989). Heat flow in the Earth. In *Encyclopedia of solid earth geophysics* (pp. 634–646). Van Nostrand Reinhold.
- Morley, C. K. (1988). Out-of-sequence thrusts. *Tectonics*, 7(3), 539–561. <https://doi.org/10.1029/tc007i003p00539>
- Negredo, A. M., Mancilla, F. D. L., Clemente, C., Morales, J., & Fullea, J. (2020). Geodynamic modeling of edge-delamination driven by subduction-transform edge propagator faults: The Westernmost Mediterranean margin (Central Betic Orogen) case study. *Frontiers of Earth Science*, 8, 533392. <https://doi.org/10.3389/feart.2020.533392>
- Negro, F., Agard, P., Goffe, B., & Saddiqui, O. (2007). Tectonic and metamorphic evolution of the Tamsamane units, external Rif (northern Morocco): Implications for the evolution of the Rif and the Betic–Rif arc. *Journal of the Geological Society*, 164(4), 829–842. <https://doi.org/10.1144/0016-76492006-112>
- Nieto, F. (1997). Chemical composition of metapelitic chlorites; X-ray diffraction and optical property approach. *European Journal of Mineralogy*, 9(4), 829–841. <https://doi.org/10.1127/ejm/9/4/0829>
- Nieto, F., Mata, M. P., Bauluz, B., Giorgetti, G., Arkai, P., & Peacor, D. R. (2005). Retrograde diagenesis, a widespread process on a regional scale. *Clay Minerals*, 40(1), 93–104. <https://doi.org/10.1180/0009855054010158>
- Nocquet, J. (2012). Present-day kinematics of the Mediterranean: A comprehensive overview of GPS results. *Tectonophysics*, 579, 220–242. <https://doi.org/10.1016/j.tecto.2012.03.037>
- Palomas, I., Thurner, S., Levander, A., Liu, K., Villaseñor, A., Carbonell, R., & Harnafi, M. (2014). Finite-frequency Rayleigh wave tomography of the western Mediterranean: Mapping its lithospheric structure. *Geochemistry, Geophysics, Geosystems*, 15(1), 140–160. <https://doi.org/10.1002/2013gc004861>
- Parra, T., Vidal, O., & Agard, P. (2002). A thermodynamic model for Fe–Mg dioctahedral K white micas using data from phase-equilibrium experiments and natural pelitic assemblages. *Contributions to Mineralogy and Petrology*, 143(6), 706–732. <https://doi.org/10.1007/s00410-002-0373-6>
- Pedraza, A., Ruiz-Constán, A., García-Senz, J., Azor, A., Marín-Lechado, C., Ayala, C., et al. (2020). Evolution of the South-Iberian paleomargin: From hyperextension to continental subduction. *Journal of Structural Geology*, 138, 104122. <https://doi.org/10.1016/j.jsg.2020.104122>
- Perthuisot, V. (1981). Diapirism in northern Tunisia. *Journal of Structural Geology*, 3, 231–235. [https://doi.org/10.1016/0191-8141\(81\)90019-5](https://doi.org/10.1016/0191-8141(81)90019-5)
- Petit, C., Le Pourhiet, L., Scalabrino, B., Corsini, M., Bonnin, M., & Romagny, A. (2015). Crustal structure and gravity anomalies beneath the Rif, northern Morocco: Implications for the current tectonics of the Alboran region. *Geophysical Journal International*, 202(1), 640–652. <https://doi.org/10.1093/gji/ggv169>
- Peucat, J. J., Mahdjoub, Y., & Drareni, A. (1996). UPb and RbSr geochronological evidence for late Hercynian tectonic and Alpine overthrusting in Kabylean metamorphic basement massifs (northeastern Algeria). *Tectonophysics*, 258(1–4), 195–213. [https://doi.org/10.1016/0040-1951\(95\)00197-2](https://doi.org/10.1016/0040-1951(95)00197-2)
- Piana Agostinetti, N., Lucente, F. P., Selvaggi, G., & Di Bona, M. (2002). Crustal structure and Moho geometry beneath the Northern Apennines (Italy). *Geophysical Research Letters*, 29(20), 60-1–60-4. <https://doi.org/10.1029/2002gl015109>
- Piomallo, C., & Morelli, A. (2003). P wave tomography of the mantle under the Alpine-Mediterranean area. *Journal of Geophysical Research: Solid Earth*, 108(B2), 1–23. <https://doi.org/10.1029/2002JB001757>
- Platt, J. P. (1986). Dynamics of orogenic wedges and the uplift of high-pressure metamorphic rocks. *Geological Society of America Bulletin*, 97(9), 1037–1053. [https://doi.org/10.1130/0016-7606\(1986\)97<1037:doowat>2.0.co;2](https://doi.org/10.1130/0016-7606(1986)97<1037:doowat>2.0.co;2)
- Platt, J. P., Allerton, S., Kirker, A., Mandeville, C., Mayfield, A., Platzman, E. S., & Rimi, A. (2003). The ultimate arc: Differential displacement, oroclinal bending, and vertical axis rotation in the External Betic-Rif arc. *Tectonics*, 22(3), TC1005. <https://doi.org/10.1029/2001tc001321>
- Platt, J. P., Kelley, S. P., Carter, A., & Orozco, M. (2005). Timing of tectonic events in the Alpujarride complex, Betic cordillera, southern Spain. *Journal of the Geological Society*, 162(3), 451–462. <https://doi.org/10.1144/0016-764903-039>
- Platt, J. P., Whitehouse, M. J., Kelley, S. P., Carter, A., & Hollick, L. (2003). Simultaneous extensional exhumation across the Alboran Basin: Implications for the causes of late orogenic extension. *Geology*, 31(3), 251–254. [https://doi.org/10.1130/0091-7613\(2003\)031<0251:seeata>2.0.co;2](https://doi.org/10.1130/0091-7613(2003)031<0251:seeata>2.0.co;2)
- Puga, E., de Fliert, V., Torres-Roldán, R. L., & Sanz de Galdeano, C. (1988). Attempts of whole-rock K/Ar dating of Mesozoic volcanic and hypabyssal igneous rocks from the central Subbetic (southern Spain): A case of differential argon loss related to very low-grade metamorphism. *Estudios Geológicos*, 44(1–2), 47–59.
- Rabaute, A., & Chamot-Rooke, N. (2014). *Active tectonics of the Africa–Eurasia boundary from Algiers to Calabria, map at 1:1500 000 scale with GIS database*. Geosublight.
- Radi, Z., Yelles-Chaouche, A., Corchete, V., & Guettouche, S. (2017). Crust and upper mantle shear wave structure of Northeast Algeria from Rayleigh wave dispersion analysis. *Physics of the Earth and Planetary Interiors*, 270, 84–89. <https://doi.org/10.1016/j.pepi.2017.06.013>



- Ramzi, A., & Lassaad, C. (2017). Superposed folding in the Neogene series of the northeastern Tunisia: Precision of the upper Miocene compression and geodynamic significance. *International Journal of Earth Sciences*, 106(6), 1905–1918. <https://doi.org/10.1007/s00531-016-1394-0>
- Research Group for Lithospheric Structure in Tunisia. (1992). The EGT'85 seismic experiment in Tunisia: A reconnaissance of the deep structures. *Tectonophysics*, 207, 245–267.
- Riahi, S., Soussi, M., Kamel, B., Kmar, B. I. L., Stow, D., Sami, K., & Mourad, B. (2010). Stratigraphy, sedimentology and structure of the Numidian Flysch thrust belt in northern Tunisia. *Journal of African Earth Sciences*, 57(1–2), 109–126. <https://doi.org/10.1016/j.jafrearsci.2009.07.016>
- Riahi, S., Soussi, M., & Stow, D. (2021). Sedimentological and stratigraphic constraints on Oligo–Miocene deposition in the Mogod mountains, northern Tunisia: New insights for paleogeographic evolution of North Africa passive margin. *International Journal of Earth Sciences*, 110(2), 653–688. <https://doi.org/10.1007/s00531-020-01980-z>
- Ring, U., Glodny, J., Will, T., & Thomson, S. (2010). The Hellenic subduction system: High-pressure metamorphism, exhumation, normal faulting, and large-scale extension. *Annual Review of Earth and Planetary Sciences*, 38(1), 45–76. <https://doi.org/10.1146/annurev.earth.050708.170910>
- Ring, U., Will, T., Glodny, J., Kumerics, C., Gessner, K., Thomson, S., et al. (2007). Early exhumation of high-pressure rocks in extrusion wedges: Cycladic blueschist unit in the eastern Aegean, Greece, and Turkey. *Tectonics*, 26(2), TC2001. <https://doi.org/10.1029/2005tc001872>
- Roca, E., Sans, M., & Koyi, H. A. (2006). Polyphase deformation of diapiric areas in models and in the eastern Prebetics (Spain). *AAPG Bulletin*, 90(1), 115–136. <https://doi.org/10.1306/07260504096>
- Röder, G. (1988). Numidian marble and some of its Specialities. In N. Herz & M. Waelkens (Eds.), *Classical marble: Geochemistry, technology, trade* (pp. 91–96). Springer Netherlands. [https://doi.org/10.1007/978-94-015-7795-3\\_10](https://doi.org/10.1007/978-94-015-7795-3_10)
- Rodríguez-Fernández, J., Azor, A., & Miguel Azañón, J. (2011). The Betic intramontane basins (SE Spain): Stratigraphy, subsidence, and tectonic history. In C. Busby & A. Azor (Eds.), *Tectonics of sedimentary basins: Recent advances* (pp. 461–479). <https://doi.org/10.1002/9781444347166.ch23>
- Rodríguez-Fernández, J., Roldán, F. J., Azañón, J. M., & García-Cortés, A. (2013). El colapso gravitacional del frente orogénico alpino en el Dominio Subbético durante el Mioceno medio-superior: El Complejo Extensional Subbético. *Boletín Geológico y Minero*, 124, 477–504.
- Romagny, A., Jolivet, L., Menant, A., Bessière, E., Maillard, A., Canva, A., et al. (2020). Detailed tectonic reconstructions of the Western Mediterranean region for the last 35 Ma, insights on driving mechanisms Reconstructions détaillées de la Méditerranée occidentale depuis 35 Ma, implications en terme de mécanismes moteur. *BSGF-Earth Sciences Bulletin*, 191(1), 37. <https://doi.org/10.1051/bsgf/2020040>
- Rossetti, F., Cavazza, W., Di Vincenzo, G., Lucci, F., & Theye, T. (2022). Alpine tectono-metamorphic evolution of the Corsica basement. *Journal of Metamorphic Geology*, 41(2), 299–326. <https://doi.org/10.1111/jmg.12696>
- Rossetti, F., Faccenna, C., Jolivet, L., Funicello, R., Tecce, F., & Brunet, C. (1999). Syn-versus post-orogenic extension: The case study of Giglio Island (Northern Tyrrhenian Sea, Italy). *Tectonophysics*, 304(1–2), 71–93. [https://doi.org/10.1016/s0040-1951\(98\)00304-7](https://doi.org/10.1016/s0040-1951(98)00304-7)
- Roure, F., Casero, P., & Addoum, B. (2012). Alpine inversion of the North African margin and delamination of its continental lithosphere. *Tectonics*, 31(3), 1–28. <https://doi.org/10.1029/2011TC002989>
- Rouvier, H. (1977). *Géologie de l'Extreme-Nord tunisien: Tectoniques et paleogeographies superposees a l'extremite orientale de la chaîne nord-maghrébine. These Dr. es Sc.* Univ. Pierre Marie Curie.
- Rouvier, H. (1992). *Carte géologique de la Tunisie au 1/50.000, la feuille n° 19 d'Ain Drahem*. Office National des Mines.
- Rouvier, H. (1993). *Carte géologique de la Tunisie au 1/50.000, la feuille n° 24 de Fernena*. Office National des Mines.
- Rubatto, D., Gebauer, D., & Fanning, M. (1998). Jurassic formation and Eocene subduction of the Zermatt–Saas-Fee ophiolites: Implications for the geodynamic evolution of the central and Western Alps. *Contributions to Mineralogy and Petrology*, 132(3), 269–287. <https://doi.org/10.1007/s004100050421>
- Ryan, E., Papeschi, S., Viola, G., Musumeci, G., Mazzarini, F., Torgersen, E., et al. (2021). Syn-orogenic exhumation of high-P units by upward extrusion in an accretionary wedge: Insights from the Eastern Elba nappe stack (Northern Apennines, Italy). *Tectonics*, 40(5), e2020TC006348. <https://doi.org/10.1029/2020tc006348>
- Saadallah, A., & Caby, R. (1996). Alpine extensional detachment tectonics in the Grande Kabylie metamorphic core complex of the Maghrebides (northern Algeria). *Tectonophysics*, 267(1–4), 257–273. [https://doi.org/10.1016/s0040-1951\(96\)00101-1](https://doi.org/10.1016/s0040-1951(96)00101-1)
- Saadi, J., Karoui-Yaakoub, N., Doha, F., Zarghbib-Turki, D., Grira, C., & Sahli, W. (2023). Sedimentary evolution of the late Cretaceous-Eocene deep carbonates series of the foreland Maghrebian chain. The Tellian domain of northern Tunisia. *Journal of African Earth Sciences*, 200, 104879. <https://doi.org/10.1016/j.jafrearsci.2023.104879>
- Sábat, F., Gelabert, B., Rodríguez-Perea, A., & Giménez, J. (2011). Geological structure and evolution of Majorca: Implications for the origin of the Western Mediterranean. *Tectonophysics*, 510(1–2), 217–238. <https://doi.org/10.1016/j.tecto.2011.07.005>
- Saïd, A., Baby, P., Chardon, D., & Ouali, J. (2011). Structure, paleogeographic inheritance, and deformation history of the southern Atlas foreland fold and thrust belt of Tunisia. *Tectonics*, 30(6), TC6004. <https://doi.org/10.1029/2011TC002862>
- Salaj, J., & Vanhouten, F. B. (1988). Cenozoic Paleogeographic development of northern Tunisia, with special reference to the stratigraphic record in the Miocene trough. *Palaeogeography, Palaeoclimatology, Palaeoecology*, 64(1–2), 43–57. [https://doi.org/10.1016/0031-0182\(88\)90141-1](https://doi.org/10.1016/0031-0182(88)90141-1)
- Sani, F., Del Ventisette, C., Montanari, D., Coli, M., Nafissi, P., & Piazzini, A. (2004). Tectonic evolution of the internal sector of the Central Apennines, Italy. *Marine and Petroleum Geology*, 21(10), 1235–1254. <https://doi.org/10.1016/j.marpetgeo.2004.09.004>
- Searle, M. P., & Lamont, T. N. (2020). Compressional metamorphic core complexes, low-angle normal faults and extensional fabrics in compressional tectonic settings. *Geological Magazine*, 157(1), 101–118. <https://doi.org/10.1017/s0016756819000207>
- Simpson, G. D. H., Thompson, A. B., & Connolly, J. A. D. (2000). Phase relations, singularities and thermobarometry of metamorphic assemblages containing phengite, chlorite, biotite, K-feldspar, quartz and H<sub>2</sub>O. *Contributions to Mineralogy and Petrology*, 139(5), 555–569. <https://doi.org/10.1007/s004100000154>
- Soumaya, A., Ben Ayed, N., Delvaux, D., & Ghanmi, M. (2015). Spatial variation of present-day stress field and tectonic regime in Tunisia and surroundings from formal inversion of focal mechanisms: Geodynamic implications for central Mediterranean. *Tectonics*, 34(6), 1154–1180. <https://doi.org/10.1002/2015TC003895>
- Soumaya, A., Kadri, A., Ben Ayed, N., Kim, Y.-S., Dooley, T. P., Rajabi, M., & Braham, A. (2020). Deformation styles related to intraplate strike-slip fault systems of the Saharan-Tunisian Southern Atlas (North Africa): New kinematic models. *Journal of Structural Geology*, 140, 104175. <https://doi.org/10.1016/j.jsg.2020.104175>
- Stipp, M., Stünitz, H., Heilbronner, R., & Schmid, S. M. (2002). The eastern Tonale fault zone: A 'natural laboratory' for crystal plastic deformation of quartz over a temperature range from 250 to 700°C. *Journal of Structural Geology*, 24(12), 1861–1884. [https://doi.org/10.1016/s0191-8141\(02\)00035-4](https://doi.org/10.1016/s0191-8141(02)00035-4)
- Trincal, V., Lanari, P., Buatier, M., Lacroix, B., Charpentier, D., Labaume, P., & Muñoz, M. (2015). Temperature micro-mapping in oscillatory-zoned chlorite: Application to study of a green-schist facies fault zone in the Pyrenean Axial Zone (Spain). *American Mineralogist*, 100(11–12), 2468–2483. <https://doi.org/10.2138/am-2015-5217>

- Troudi, H., Tari, G., Alouani, W., & Cantarella, G. (2017). Styles of salt tectonics in Central Tunisia: An overview. In *Permo-triassic salt provinces of Europe, North Africa and the Atlantic margins: Tectonics and hydrocarbon potential*. Elsevier Inc. <https://doi.org/10.1016/B978-0-12-809417-4.00026-4>
- Van Hinsbergen, D. J. J., Vissers, R. L. M., & Spakman, W. (2014). Origin and consequences of western Mediterranean subduction, rollback, and slab segmentation. *Tectonics*, 33(4), 393–419. <https://doi.org/10.1002/2013TC003349>
- Vázquez, M., Asebriy, L., Azimousa, A., Jabaloy, A., Booth-Rea, G., Barbero, L., et al. (2013). Evidence of extensional metamorphism associated to Cretaceous rifting of the North-Maghrebian passive margin: The Tanger-Ketama Unit (External Rif, northern Morocco). *Geológica Acta*, 11(3), 277–293.
- Vermeesch, P. (2018). IsoplotR: A free and open toolbox for geochronology. *Geoscience Frontiers*, 9(5), 1479–1493. <https://doi.org/10.1016/j.gsf.2018.04.001>
- Vidal, O., Goffé, B., Bousquet, R., & Parra, T. (1999). Calibration and testing of an empirical chloritoid-chlorite Mg-Fe exchange thermometer and thermodynamic data for daphnite. *Journal of Metamorphic Geology*, 17(1), 25–40. <https://doi.org/10.1046/j.1525-1314.1999.00174.x>
- Vidal, O., Goffé, B., & Theye, T. (1992). Experimental study of the stability of sudoite and magnesiocorphyolite and calculation of a new petrogenetic grid for the system FeO–MgO–Al<sub>2</sub>O<sub>3</sub>–SiO<sub>2</sub>–H<sub>2</sub>O. *Journal of Metamorphic Geology*, 10(5), 603–614. <https://doi.org/10.1111/j.1525-1314.1992.tb00109.x>
- Vidal, O., Lanari, P., Muñoz, M., Bourdelle, F., & de Andrade, V. (2016). Deciphering temperature, pressure and oxygen-activity conditions of chlorite formation. *Clay Minerals*, 51(4), 615–633. <https://doi.org/10.1180/claymin.2016.051.4.06>
- Vidal, O., & Parra, T. (2000). Exhumation paths for high pressure metapelites obtained from local equilibria for chlorite–phengite assemblages. *Geological Journal*, 35(3–4), 139–161. <https://doi.org/10.1002/gj.856>
- Vidal, O., Parra, T., & Trotet, F. (2001). A thermodynamic model for Fe-Mg aluminous chlorite using data from phase equilibrium experiments and natural pelitic assemblages in the 100–600°C, 1–25 kbar P-T range. *American Journal of Science*, 301(6), 557–592. <https://doi.org/10.2475/ajs.301.6.557>
- Vidal, O., Parra, T., & Vieillard, P. (2005). Thermodynamic properties of the Tschermak solid solution in Fe-chlorite: Application to natural examples and possible role of oxidation. *American Mineralogist*, 90(2–3), 347–358. <https://doi.org/10.2138/am.2005.1554>
- Vignaroli, G., Faccenna, C., Rossetti, F., & Jolivet, L. (2009). Insights from the Apennines metamorphic complexes and their bearing on the kinematics evolution of the orogen. *Geological Society, London, Special Publications*, 311(1), 235–256. <https://doi.org/10.1144/sp311.9>
- Vila, J. M. (1970). Le Djebel Edough; un massif cristallin externe du Nord-Est de la Berberie. *Bulletin de la Société Géologique de France*, 7(5), 805–812. <https://doi.org/10.2113/gssgfbull.s7-xii.5.805>
- Vila, J. M. (1995). First terrestrial study of a Large submarine salt glacier - The eastern part of the Ouenza-Ladjabel-Meridef structure (Algerian Tunisian confines)—Proposal for an emplacement scenario and comparisons. *B Soc Geol Fr*, 166(2), 149–167.
- Vila, J. M., BenYoussef, M., Chikhaoui, M., & Ghanmi, M. (1996). A large submarine middle Albian “salt glacier” in north-western Tunisia (250 km(2)): The Triassic rocks of Ben Gasseur “diapir” and of El Kef anticline. *Comptes Rendus de l'Académie des Sciences Serie II A*, 322(3), 221–227.
- Villa, I. M., Bucher, S., Bousquet, R., Kleinhanns, I. C., & Schmid, S. M. (2014). Dating polygenetic metamorphic assemblages along a transect across the Western Alps. *Journal of Petrology*, 55(4), 803–830. <https://doi.org/10.1093/ptrology/egy007>
- Warr, L. N., & Ferreiro-Mahmann, R. (2015). Recommendations for Kübler index standardization. *Clay Minerals*, 50(3), 283–286. <https://doi.org/10.1180/claymin.2015.050.3.02>
- Wernicke, B. (1981). Low-angle normal faults in the Basin and range province: Nappe tectonics in an extending orogen. *Nature*, 291(5817), 645–648. <https://doi.org/10.1038/291645a0>
- Wernicke, B., & Burchfiel, B. C. (1982). Modes of extensional tectonics. *Journal of Structural Geology*, 4(2), 105–115. [https://doi.org/10.1016/0191-8141\(82\)90021-9](https://doi.org/10.1016/0191-8141(82)90021-9)
- Wildi, W. (1983). La chaîne tello-rifaine (Algérie, Maroc, Tunisie): Structure, stratigraphie et évolution du Trias au Miocène. *Revue de Géographie Physique et de Géologie Dynamique*, 24(3), 201–297.
- Wortel, M. J. R., & Spakman, W. (2000). Subduction and slab detachment in the Mediterranean-Carpathian region. *Science*, 290(5498), 1910–1917. <https://doi.org/10.1126/science.290.5498.1910>
- Yans, J., Verhaert, M., Gautheron, C., Antoine, P. O., Moussi, B., Dekoninck, A., et al. (2021). (U-Th)/He dating of supergene iron (oxyhydr-) oxides of the Nefza-Sejnane district (Tunisia): New insights into mineralization and mammalian Biostratigraphy. *Minerals*, 11(3), 260. <https://doi.org/10.3390/min11030260>
- Zouaghi, T., Bédir, M., Ayed-Khaled, A., Lazzez, M., Soua, M., Amri, A., & Inoubli, M. H. (2013). Autochthonous versus allochthonous upper Triassic evaporites in the Sbiba graben, central Tunisia. *Journal of Structural Geology*, 52, 163–182. <https://doi.org/10.1016/j.jsg.2013.03.011>

## References From the Supporting Information

- Axelsson, E., Pape, J., Berndt, J., Corfu, F., Mezger, K., & Raith, M. M. (2018). Rutile R632—A new natural reference material for U-Pb and Zr determination. *Geostandards and Geoanalytical Research*, 42(3), 319–338. <https://doi.org/10.1111/ggr.12213>
- Bracciali, L., Parrish, R. R., Horstwood, M. S. A., Condon, D. J., & Najman, Y. (2013). UPb LA-(MC)-ICP-MS dating of rutile: New reference materials and applications to sedimentary provenance. *Chemical Geology*, 347, 82–101. <https://doi.org/10.1016/j.chemgeo.2013.03.013>
- Bunge, H. J. (1982). *Texture analysis in materials sciences* (p. 593). Butterworth.
- Hielscher, R., & Schaab, H. (2008). A novel pole figure inversion method: Specification of the MTEX algorithm. *Journal of Applied Crystallography*, 41(6), 1024–1037. <https://doi.org/10.1107/s0021889808030112>
- Kisch, H. J. (1991). Illite crystallinity: Recommendations on sample preparation, X-ray diffraction settings, and interlaboratory samples. *Journal of Metamorphic Geology*, 9(6), 665–670. <https://doi.org/10.1111/j.1525-1314.1991.tb00556.x>
- Neumann, B. (2000). Texture development of recrystallised quartz polycrystals unravelled by orientation and misorientation characteristics. *Journal of Structural Geology*, 22(11), 1695–1711. [https://doi.org/10.1016/s0191-8141\(00\)00060-2](https://doi.org/10.1016/s0191-8141(00)00060-2)
- Paton, C., Hellstrom, J., Paul, B., Woodhead, J., & Hergt, J. (2011). Iolite: Freeware for the visualisation and processing of mass spectrometric data. *Journal of Analytical Atomic Spectrometry*, 26(12), 2508–2518. <https://doi.org/10.1039/c1ja10172b>
- Sassi, F. P., & Scolari, A. (1974). The *b<sub>0</sub>* value of the potassium white micas as a barometric indicator in low-grade metamorphism of pelitic schists. *Contributions to Mineralogy and Petrology*, 45(2), 143–152. <https://doi.org/10.1007/bf00371166>
- Santamaría-López, Á., Abad, I., Nieto, F., & Sanz de Galdeano, C. (2023). Early Mylonitization in the Nevado-Filábride complex (Betic cordillera) during the high-pressure episode: Petrological, Geochemical and thermobarometric data. *Minerals*, 13(1), 24. <https://doi.org/10.3390/min13010024>



- Schmitz, M. D., & Schoene, B. (2007). Derivation of isotope ratios, errors, and error correlations for U-Pb geochronology using  $^{205}\text{Pb}$ - $^{235}\text{U}$ -( $^{233}\text{U}$ )-spiked isotope dilution thermal ionization mass spectrometric data. *Geochemistry, Geophysics, Geosystems*, 8, Q08006. <https://doi.org/10.1029/2006GC001492>
- Warr, L. N., & Rice, A. H. N. (1994). Interlaboratory standardization and calibration of clay mineral crystallinity and crystallite size data. *Journal of Metamorphic Geology*, 12(2), 141–152. <https://doi.org/10.1111/j.1525-1314.1994.tb00010.x>